

WALL COMPENSATION FOR HIGH RESOLUTION  
ULTRA-WIDEBAND OBSTRUCTED LOCALIZATION

BY  
**NURUDDEEN MOHAMMED IYA**

A Thesis Presented to the  
DEANSHIP OF GRADUATE STUDIES

**KING FAHD UNIVERSITY OF PETROLEUM & MINERALS**  
DHAHRAN, SAUDI ARABIA

In Partial Fulfillment of the  
Requirements for the Degree of

**MASTER OF SCIENCE**

In

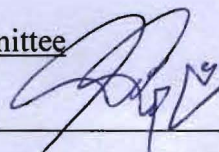
TELECOMMUNICATION ENGINEERING

December 2010

KING FAHD UNIVERSITY OF PETROLEUM AND MINERALS  
DHAHRAN 31261, SAUDI ARABIA  
DEANSHIP OF GRADUATE STUDIES

The thesis, written by NURUDDEEN MOHAMMED IYA  
under the direction of his thesis advisor and approved by his thesis committee members,  
has been presented to and accepted by Dean of Graduate Studies, in partial fulfillment  
of the requirements for the degree of **MASTER OF SCIENCE IN**  
**TELECOMMUNICATION ENGINEERING.**

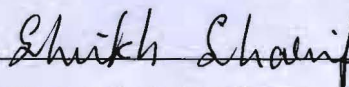
Thesis Committee



Dr. ALI HUSSEIN MUQAIBEL  
(Advisor)



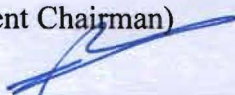
Dr. MOHAMED ADNAN LANDOLSI  
(Member)



Dr. SHEIK SHARIF IQBAL (Member)

  
Dr. SAMIR H. ABDUL-JAUWAD

(Department Chairman)

  
Dr. SALAM A. ZUMMO

(Dean of Graduate Studies)

3/1/11

Date



## DEDICATION

All praises be to Allah, the Creator and Lord of the Universe.

O' Allah,

Have mercy and accept it as a dedication to you

O' Allah,

Show it to me in the last day with the good deeds

O' Allah,

Great thanks to you for this accomplishment.

Your bounties;

my mother,

my father,

a lovely wife,

a great family,

and special friends,

I cannot deny, led to this accomplishment

## **ACKNOWLEDGEMENT**

All praise is to Allah (SWT), Lord of the Heavens and the Earths, and what they contain; Most Beneficial, Most Merciful. I seek His benediction on our beloved Prophet, the best of mankind, Muhammad (SAW), his household and his companions, till the Day of Judgment. I thank Allah for His infinite bounties on me, one of which is the completion of this work; I seek His mercy and forgiveness, and indeed, I fear His wrath.

My gratitude, without reservation, goes to my parents for their unrelented support and prayers throughout my life. I will forever remain grateful.

I would like to convey my sincere gratitude to my thesis advisor Dr. Ali Hussein Muqaibel for his exceptional support and guidance, thesis-wise and otherwise. I thank him for being available whenever I needed his assistance. It is my pleasure working with him.

Special thanks to distinguished members of my thesis committee Dr. Adnan Al-Andalusi and Dr. Sharif Iqbal first, for accepting to be on my thesis committee, further, for their useful guidance, motivation, and professional contribution to my success and that of this work.

I acknowledge the contribution of Mr. Umar M. Johar who was instrumental in carrying out the experimental part of this work. I also thank him for been patient with me throughout this period. I also extend my appreciation to the UWB High Resolution Positioning group for their support and motivation.

I acknowledge my wife, for her patience; my son, for his innocence; my family for their support; my friends for their best wishes; and KFUPM, for the opportunity it gave me to study and accomplish this work. To all, I remain grateful.

## TABLE OF CONTENTS

<b>DEDICATION .....</b>	<b>III</b>
<b>ACKNOWLEDGEMENT .....</b>	<b>IV</b>
<b>LIST OF TABLES.....</b>	<b>VII</b>
<b>LIST OF FIGURES.....</b>	<b>VIII</b>
<b>ABSTRACT .....</b>	<b>X</b>
<b>ABSTRACT (ARABIC).....</b>	<b>XI</b>
<b>1 INTRODUCTION.....</b>	<b>1</b>
1.1 OVERVIEW .....	1
1.2 LITERATURE SURVEY.....	4
1.2.1 Wall Modeling.....	6
1.2.2 Simulation of Through-the-Wall Propagation.....	8
1.2.3 Measurements of Through-the-Wall Propagation .....	9
1.2.4 Existing Systems and Applications .....	11
1.3 MOTIVATION .....	12
1.4 OBJECTIVES.....	15
1.5 THESIS STRUCTURE.....	16
<b>2 THEORY OF UWB THROUGH-WALL PROPAGATION AND CHARACTERIZATION.....</b>	<b>17</b>
2.1 DIELECTRIC PROPERTIES OF MATERIALS .....	17
2.2 WALL ATTENUATION AND DISPERSION.....	23
2.3 TECHNIQUES FOR MEASURING ATTENUATION AND DISPERSION THROUGH WALLS .....	26
2.3.1 Time Domain Technique .....	26
2.3.2 Frequency Domain Technique.....	29
<b>3 UWB CHARACTERIZATION OF OBSTRUCTED PROPAGATION .....</b>	<b>32</b>
3.1 INTRODUCTION.....	32
3.2 THE MEASUREMENT SETUP.....	34
3.2.1 Component Selection.....	34
3.2.2 Calibration .....	44
3.2.3 The Sample Materials.....	44
3.3 MEASUREMENT PROCEDURE .....	45
3.3.1 Transmission Measurements .....	46
3.3.2 Reflection Measurements .....	50
3.4 ANALYSIS METHOD .....	50
3.4.1 Single-Pass Technique.....	52
3.4.2 Multiple-Pass Technique .....	53
3.5 WALL PARAMETER CALCULATION.....	59

3.5.1	Data Acquisition .....	59
3.5.2	Un-gated Insertion Transfer Function, Time delay and Initial guess of permittivity .....	59
3.5.3	Time Gating .....	60
3.5.4	Wall (material) Parameters .....	66
3.6	MEASUREMENT RESULTS.....	66
3.6.1	Transmission Measurements Results.....	66
3.6.2	Reflection Measurements Results.....	74
3.6.3	Between Transmission and Reflection .....	76
3.7	COMPARISON WITH LITERATURE.....	80
3.8	MULTIPLE WALLS.....	82
3.8.1	Double Layer .....	82
3.8.2	Three Layer.....	86
3.9	ACCURACY RELATED ISSUES.....	88
3.9.1	Sources of Error.....	88
3.9.2	Repeatability and Variability Analysis.....	90
<b>4</b>	<b>WALL COMPENSATION .....</b>	<b>92</b>
4.1	INTRODUCTION.....	92
4.2	MEASUREMENT SETUP AND PROCEDURE .....	93
4.3	WALL COMPENSATION METHODS .....	95
4.3.1	Constant Amplitude and Delay Compensation.....	95
4.3.2	Frequency Dependent Data Method .....	98
4.3.3	Data Fitting Method.....	104
4.4	CONCLUSION .....	113
<b>5</b>	<b>CONCLUSIONS AND RECOMMENDATIONS .....</b>	<b>114</b>
5.1	SUMMARY AND CONCLUSIONS .....	114
5.2	RECOMMENDATIONS FOR FUTURE RESEARCH .....	116
<b>A</b>	<b>APPENDIX A .....</b>	<b>117</b>
I.	ANTENNA TEST RESULTS .....	117
	<b>NOMENCLATURE .....</b>	<b>119</b>
	<b>REFERENCES .....</b>	<b>123</b>
	<b>VITA .....</b>	<b>136</b>

## LIST OF TABLES

TABLE 3.1: Measurement setup equipment description .....	35
TABLE 3.2: Network analyzer specifications .....	37
TABLE 3.3: Antenna specification .....	38
TABLE 3.4: Amplifier specifications .....	40
TABLE 3.5: Length of cables used in the measurement.....	40
TABLE 3.6: General cable characteristics .....	41
TABLE 3.7: Wall materials showing dimensions.....	45
TABLE 3.8: Coefficients of linear and quadratic fit for the extracted parameters .....	69
TABLE 3.9: Results comparison with literature .....	81
TABLE 4.1: Showing constant amplitude and constant delay values used .....	98
TABLE 4.2: Target position errors due to the walls .....	107
TABLE 4.3: Percentage similarity of wall compensation results to ‘No Wall’ results ...	110
TABLE A.1: Antenna test results.....	118

## LIST OF FIGURES

Figure 1.1: Summary of research activities in the area of through-wall propagation .....	5
Figure 2.1: Time domain measurement setup .....	27
Figure 2.2: Frequency domain setup .....	30
Figure 3.1: Measurement equipment.....	36
Figure 3.2: Losses in the cables used .....	42
Figure 3.3: Transmission measurements, (a) Picture, (b) Schematic.....	48
Figure 3.4: Reflection measurements, (a) Picture, (b) Schematic.....	51
Figure 3.5: Chart for characterizing obstructed measurements.....	61
Figure 3.6: Frequency domain measurements (a) measured magnitude, (b) measured Phase, (c) filter and filtered un-gated insertion transfer function, (d) impulse responses..	63
Figure 3.7: The gating window .....	64
Figure 3.8: (a) Un-gated time domain signal with window, (b) gated time domain signal	65
Figure 3.9: Transmission: Insertion transfer function versus frequency for different walls .....	68
Figure 3.10: Transmission: dielectric constant versus frequency for different walls .....	70
Figure 3.11: Transmission: Loss tangents versus frequency for various walls.....	71
Figure 3.12: Transmission: attenuation constant for the different walls.....	72
Figure 3.13: Showing Erroneous data points for; (a) Transmission-insertion transfer function, (b) Transmission-dielectric constant, (c) Reflection-insertion transfer function, (d) Reflection-dielectric constant .....	73
Figure 3.14: Reflection: Dielectric constant versus frequency for the three materials .....	75
Figure 3.15: Comparing transmission and reflection results for wood; (a) insertion transfer function, (b) dielectric constant, (c) attenuation constant, (d) loss tangent.....	77
Figure 3.16: Comparing transmission and reflection results for glass; (a) insertion transfer function, (b) dielectric constant, (c) attenuation constant, (d) loss tangent.....	78
Figure 3.17: Comparing transmission and reflection results for a gypsum (a) insertion transfer function, (b) dielectric constant, (c) attenuation constant, (d) loss tangent .....	79



Figure 3.18: Wall configurations.....	83
Figure 3.19: Results for double walls showing (a) magnitude of received signal (b) impulse response and (c) insertion transfer function for wood relative to free-space.....	84
Figure 3.20: Effect of inter-wall spacing – (a) magnitude, (b) impulse response for wood .....	85
Figure 3.21: Block diagram of single layer and three layer insertion transfer functions ...	86
Figure 3.22: Three layer measurements .....	87
Figure 3.23: Effect of connector mismatch.....	89
Figure 3.24: Repeatability and variability analysis.....	91
Figure 4.1: Target measurements - (a) ‘Target Only’ (No Wall) (b) ‘Target + Wall’ .....	94
Figure 4.2: Reflections from target object with and without obstruction .....	96
Figure 4.3: Illustrating compensation using constant amplitude and constant delay, (a) wood, (b) glass, (c) gypsum .....	97
Figure 4.4: Transfer function of the localization scene.....	99
Figure 4.5: Wall compensation using raw data for wood sample in (a) frequency domain, (b) time domain .....	101
Figure 4.6: Wall compensation using raw data for glass sample in (a) frequency domain, (b) time domain .....	102
Figure 4.7: Wall compensation using raw data for gypsum sample in (a) frequency domain, (b) time domain .....	103
Figure 4.8: Wall Compensation using fit to data for (a) wood, (b) glass, and (c) gypsum .....	105
Figure 4.9: Compensation using the three methods for wood wall.....	111
Figure 4.10: Wall compensation for double wall (wood-gypsum) .....	112
Figure A.1: Antenna physical dimensions, gain and VSWR .....	117
Figure A.2: Antenna pattern at various frequencies.....	118

## ABSTRACT

**Name:** Nuruddeen Mohammed Iya

**Title:** Wall Compensation for High Resolution Ultra-wideband Obstructed Localization

**Major Field:** Telecommunication Engineering

**Date of Degree:** December 2010

One of the interesting properties of an Ultra-wideband (UWB) signal is its ability to penetrate walls and obstacles which comes from the lower frequency components of the signal. However, as the signal propagates through these obstacles, it gets attenuated, slows down, and gets dispersed, which indicates the effect of the propagating medium. In this work we demonstrate wall compensation for through-wall imaging, localization and communication receiver design purposes by first characterizing wave propagation through various building materials in UWB frequency range. Frequency-domain transmission and reflection measurements are performed using a Vector Network Analyzer over a frequency range of 1 – 18 GHz to examine wall effects. This is done by measuring the insertion transfer function given as the ratio of two signals measured in presence and absence of the wall. The dielectric constant and propagation loss are extracted from the measured insertion transfer function using signal processing techniques. The work considers typical indoor walls like glass, wood, and gypsum. Double layer walls and three layer walls are also investigated. Results from transmission and reflection measurements are compared with each other and with literature. The results obtained are then further used to estimate and correct the position accuracy of a target object located behind the walls using three proposed methods namely; constant amplitude and delay, frequency dependent data, and data fitting methods. The obtained results indicated relatively acceptable measure of wall compensation for the three methods. Results from such work provide insight on how to develop algorithms for effective target position estimation in imaging and localization applications. They are also useful data for channel modeling and link budget analysis.

## ABSTRACT (ARABIC)

### خلاصة الرسالة

الاسم الكامل: نور الدين محمد أيا

عنوان الرسالة: تعويض تأثير الجدار للتحديد عالي الدقة للمواقع المحجوزة باستخدام تقنية التردد الطيفي فائق الاتساع (UWB)

التخصص: هندسة الاتصالات.

تاريخ الشهادة: ديسمبر ٢٠١٠

من أفضل خصائص الإشارة ذات التردد الطيفي فائق الاتساع (UWB) هو قدرتها على اختراق الجدران والحواجز وهذه القدرة تأتي من الجزء ذي التردد الطيفي الأقل من الإشارة. على الرغم من ذلك إلا إن مرور هذه الإشارة (UWB) من خلال هذه الحواجز ينتج عنه اضمحلال وبطء وتشتت للإشارة وهذا يدل على تأثير المرور من خلال المواد. في هذا العمل سنعرض تعويض الجدار وذلك للتصوير من خلال الجدار وتحديد المواقع وتصميم جهاز الاستقبال، وذلك من خلال تمييز مرور الموجة ذات التردد المماثل ل (UWB) من خلال العديد من مواد البناء. قياسات الإرسال والانعكاس في نطاق التردد (Frequency domain) ستنفذ باستخدام محلل أنظمة متجه ( Vector Network Analyzer) في النطاق الترددي من 1-1٨ جيجا هرتز لدراسة تأثير الجدار من خلال قياس دالة النقل نتيجة لادخال الحاجز (insertion transfer function) والمعطاة كنسبة الموجتين المقاستين في وجود وعدم وجود الجدار. تم قياس معامل العزل (dielectric constant) و خسارة النشر (propagation loss) من (insertion transfer function) وذلك باستخدام تقنيات تحليل الإشارة. في هذا العمل تم اعتبار جدران داخلية نموذجية مصنوعة من الزجاج والخشب والجبس. تم أيضا اعتبار جدران من طبقتين ومن ثلاث طبقات. تم مقارنة النتائج من الإرسال والانعكاس مع تلك الموجودة في البحوث السابقة. علاوة على ذلك فقد استخدمت النتائج في تقدير الموقع الدقيق والصحيح لهدف ما يقع خلف الجدار وذلك باستخدام ثلاث طرق وتحديدا (constant amplitude and delay) و (frequency dependent data) و (data fitting). وقد أشارت النتائج لقبول نسبي للتعويض الناتج عن تأثير الجدار للثلاث طرق. يمكن استخدام النتائج المستخلصة من هذا العمل في تصميم خوارزمية فعالة لتقدير موقع الهدف أو للتصوير أو لتطبيقات تحديد المواقع من خلال الحواجز. أيضا هذه المعلومات مفيدة لنمذجة القناة (channel modeling) وتحليل ميزانية الرابط (link budget analysis).

# CHAPTER 1

## 1 INTRODUCTION

### 1.1 Overview

Recently, ultra-wideband (UWB) systems have been a subject of increasing interest. UWB systems are formally defined by the FCC as any radio whose bandwidth is at least 20% its centre frequency or a signal whose bandwidth is 500 MHz or more [FCC02]. UWB signals have the unique capabilities of extra-wide bandwidth, low power and multipath immunity. In addition, they are promised to have the ability to penetrate walls and obstacles, which addresses a variety of applications ranging from indoor wireless communications, through-wall imaging, detection and localization, where there is a desire to see into obscured areas. The study of radio signal propagation through walls is useful in that it shows the effect of the obstacle on the propagating signal or in other words, shows the behavior of the signal as it propagates through the material. This is usually achieved by investigating the interaction of the electromagnetic wave incident on the wall sample and extracting its electrical properties. In this work however, special consideration is given to UWB signals and their behavior when propagating through these obstacles.

Electromagnetic waves passing through a medium are subject to amplitude and phase distortions. These distortions are categorically attributed to dispersive and attenuative properties of the medium of propagation. There is an increasing need to understand and model these impairing effects in order to find better ways of mitigating them. In the context of through-the-wall detection, the ultimate objective is to use the dispersion and attenuation models in developing algorithms for detection, classification, and localization of objects behind walls. This, in turn, necessitates accurate modeling of electromagnetic effects associated with wave propagation and scattering, in pursuit of devising credible solutions. Ignoring the propagation effects limits the scope of our understanding of the sensed data, decreases resolution, and reduces the effective depth for which accurate results can be obtained.

A propagation path obstruction is defined as a man-made or natural physical object that lies close enough to a radio wave path to cause a measurable effect on the path loss exclusive of reflection effects [TIA96]. Thus, electrical properties of the materials that make up these obstructions are important data for indoor radio communication planning and modeling, in addition to imaging and detection [Hua96]. It is, therefore, of paramount importance to study the electromagnetic properties of these materials for examining through-the-wall detection and *imaging* issues and devising the desired solutions.

In addition to materials that make the wall, the shape of the wall and its composition also influence the propagation effects. Another effect is caused by multiple reflections within the wall. This impact becomes more pronounced if the wall is

heterogeneous. The dielectric constants of obstructions and their thicknesses introduce variable delays in the propagation path. The travel time through the thickness of an object on the signal path is critical to the delay measurement when high accuracy is desired. The problem becomes more severe in typical localization applications, where transmit and receive antennas are collocated on the same side of the wall. This requires the transmitted signal to propagate through the wall twice. Another important challenge is associated with angles of incidence of the wave on the wall or from (to) the transmit (receive) antenna. Furthermore, in practical situations, coupling effects, radiation pattern, input impedance, and polarization of transmit and receive antennas are important factors that need to be taken into consideration.

In an effort to address these problems, this work investigates propagation through different building walls in order to characterize them over a wide range of frequency. This is the first step in the wall compensation process. Wood, Glass and Gypsum walls were examined over a frequency range of 1 – 18 GHz. To the best of our knowledge, this wide frequency range has not been studied for wall characterization. Most of the studies are at specific frequencies, lower frequency range or the X – Band. The characterization method is based on measuring the *insertion transfer function*, defined as the ratio of two signals measured in the presence and in the absence of the wall. The dielectric constant of the wall material is related to the measured insertion transfer function through a complex transcendental equation that can be solved using an approximate one-dimensional root search. Transmission and reflection measurements were carried out in frequency domain using a vector network analyzer and a pair of wideband antennas to extract the insertion

loss and dielectric constant for each wall material. Results obtained are in agreement with those presented in literature. Multiple walls were also considered and the effect of spacing between walls was investigated.

In imaging and localization applications, the presence of the wall and its effect on the target's position cannot be ignored. The wall is mostly there and the perceived target position is usually shifted due to the wall characteristics. This problem is investigated and we sought to use information about the wall obtained from the wall characterization study to correct the position estimation of the target object by de-embedding the wall and thus, removing its effect from the process.

## **1.2 Literature Survey**

This section provides a literature review of the recent works on electromagnetic wave propagation through obstacles. It will be seen that much has been done to characterize obstacles for propagation effects in narrowband frequencies using simulations, theoretical models, and experimental techniques for various materials. However, more study is required on wideband characterization of these materials, particularly for through-the-wall detection and communication purposes. Figure 1.1 classifies the work of different authors for wall material characterization based on different criteria. These are types of building material (wood, glass); conditions and structure of materials like wetness, and moisture content; methods used to extract wall characteristics, whether through experimentation or simulation; parameters used to characterize various walls, e.g reflection coefficient, dielectric constant, etc; and frequencies at which the parameters are extracted. This classification as well as the list of authors, however, is not exhaustive.

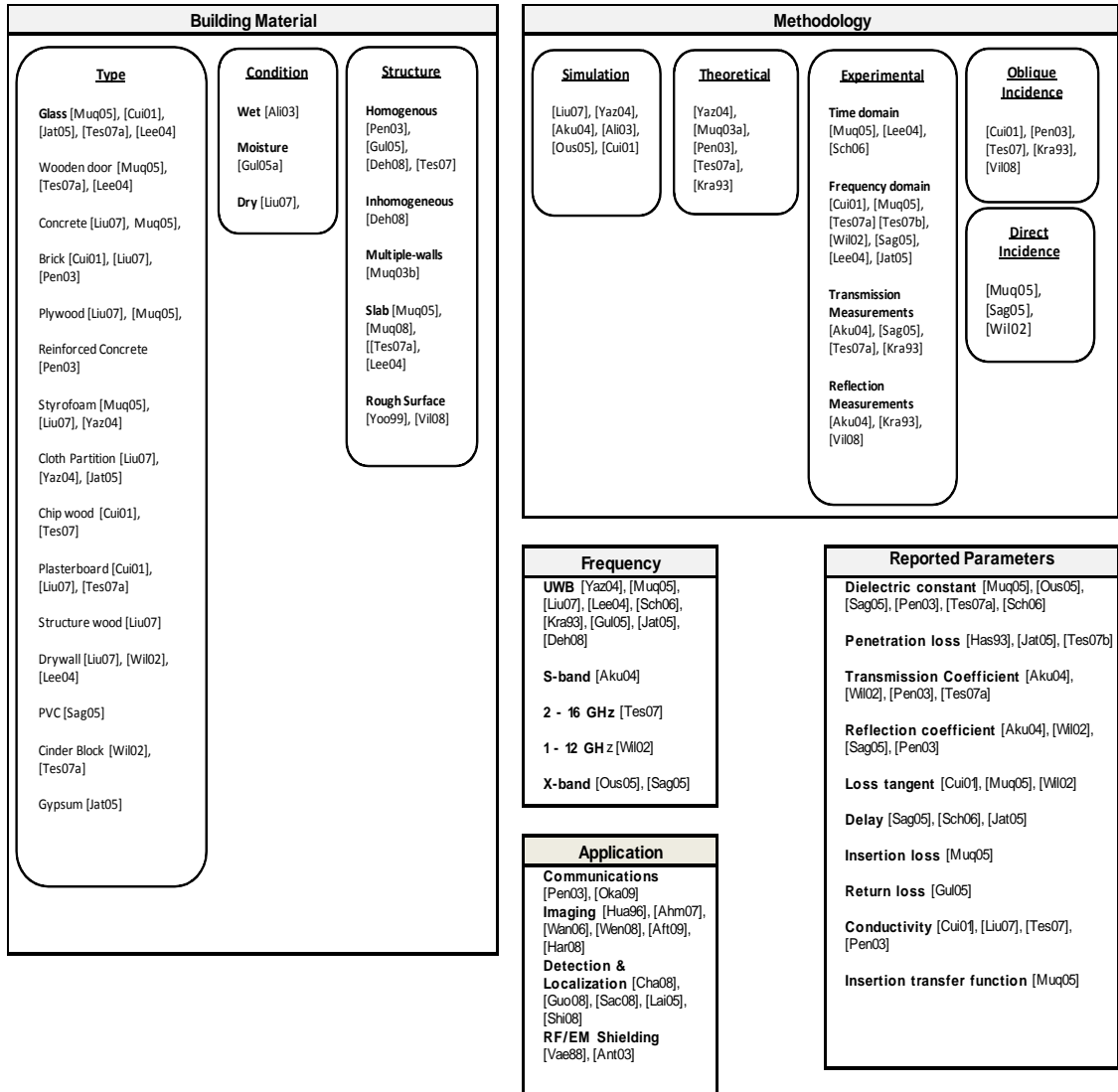


Figure 1.1: Summary of research activities in the area of through-wall propagation



Several studies have been conducted on the electromagnetic characterization of building materials, and various techniques were proposed both in the narrowband and wideband ranges of frequencies. For instance, 433 MHz, 868 MHz, 2.4 GHz, and 5 GHz [Ali03]; 2.6–3.9 GHz [Aku04]; 5.8 GHz [Cui01]; 1–6 GHz [Lee04]; 8–12 GHz [Ous05]; and 900 MHz [Pen03] are example frequencies or frequency ranges used. More recently, studies were conducted on the UWB characterization of building materials [Muq03b], [Lee04], [Muq05], [Liu07].

Electromagnetic parameters, including dielectric constant [Muq05], [Ous05], [Tes07b], [Yaz04], loss tangent [Muq05], [Wil02], conductivity [Cui01], [Tes07b], insertion loss [Muq05], return loss, path loss or propagation loss [Jat05], [Pen03], delay spread [Jat05], [Sag04], reflection coefficients [Aku04], [Sag05], [Wil02], and transmission coefficients [Aku04], [Tes07a], [Cui01], [Wil02], are commonly used to characterize the materials for propagation effects. These parameters are usually extracted through various theoretical and experimental methods. It should also be noted that all these authors reported the thickness of a wall as a critical parameter in characterizing the wall material when subjected to electromagnetic signals. Literature on various aspects of through wall propagation is reviewed in the sub-sections that follow.

### **1.2.1 Wall Modeling**

Many theoretical models, both statistical and analytical, have been proposed to extract wall parameters at various frequencies. Earlier investigations on such characterization were summarized in a comprehensive review by Hashemi [Has93]. More recently, on a more statistical note, Liu et al. [Liu07] analyzed channel capacity for seven different

building materials and their effects on a MIMO UWB system. Akuthota et al. [Aku04] developed an electromagnetic model to determine the dielectric property profile of cement-based materials. Their model was based on determining the effective propagation constant from the transmission and reflection properties, and it is useful in predicting changes in the dielectric properties of materials. In another development, Cuinas and Sanchez [Cui01] proposed an internal multi-reflection model that takes into account the material thickness's effect on phase measurements. The model was further used to augment experimental results obtained from studying electromagnetic properties of six typical building materials to determine their amplitude and phase responses. Pena et al. [Pen03] used two ray-tracing models to estimate attenuation, permittivity, and conductivity of a brick and concrete wall at 900 MHz. Sagnard and El Zein [Sag04], [Sag05] presented a high-resolution method based on the Matrix Pencil algorithm to reconstruct the impulse response by identifying individual multipath components within a material sample. This method utilizes the fact that each path is characterized by its own complex delay and amplitude.

Other theoretical approaches are available in [Muq03a], [Yaz04], and [Tes07a]. In [Muq03a], Muqaibel and Safaai-Jazi proposed a simplified model that uses a one-dimensional search algorithm for determining the complex dielectric constant for wall materials. This was obtained by analyzing the transfer function of the wall. Yazdandoost and Kohno [Yaz04] provided a compact analytical form of computing the complex relative permittivity of building materials from fundamental principles of electromagnetic waves for the UWB characterization of materials. Their results for the complex dielectric

constant of Styrofoam with 10 cm thickness and cloth partition with 6 cm thickness closely match those of [Muq03a]. Noori et al. [Noo08] obtained an analytical model to predict the impulse responses of the wall material from transmission coefficients assuming oblique wave incidence, and studied their effect on UWB transmission.

### **1.2.2 Simulation of Through-the-Wall Propagation**

Simulation tools also play important roles in studying propagation effects. Ali-Rantala et al. [Ali03] studied how different walls and wall materials affect the attenuation of electromagnetic waves using an advanced computer simulation tool. In addition, [Ous05] developed two algorithms using theoretical formulas from [Muq03a] to extract material characteristics using Ansoft's High Frequency Structure Simulator (HFSS) software.

These models alone, however, are inadequate in providing a comprehensive description of the system propagation behavior. To effectively characterize electromagnetic wave propagation through obstacles, accurate measurements are required to augment the theoretical modeling. The major difficulty facing measurement accuracy is that of adequately taking into consideration all effects, including antenna, cable, connectors, and multipath effects, and their interaction with the complex indoor environment. Although antenna effects had been studied [Ada08], multipath effects were reduced through time-domain gating [Muq03b], [Muq08] or anechoic chamber measurements [Sag04], [Sag05], [Jat05], and calibration was performed to take care of cable errors, measurements still have to be repeated several times to ensure accuracy and repeatability of the results. Therefore, the theoretical and experimental approaches are complementary and should be used together.

### 1.2.3 Measurements of Through-the-Wall Propagation

Measurements for characterizing through-the-wall propagation effects can be conducted in the time domain or in the frequency domain. Time-domain measurements on samples of brick and concrete were carried out in the UWB range of frequencies [Nem06], [Sch06], and wall parameters of thickness, permeability, and permittivity were estimated at 900 MHz [Pen03]. In [Muq05], it is observed that significant distortions occur when a bipolar Gaussian pulse is passed through a brick wall as compared to a wooden door. Gulck et al. [Gul05a] demonstrated a non-contacting determination of moisture content in bulk materials using sub-nanosecond UWB pulses. In another development, Gulck et al. [Gul05b] characterized materials using UWB pulses for the purpose of localization. Attiya et al. [Att04] used the time-domain technique to examine the potentials and limitations of through-the-wall human body detection.

A reasonable amount of work has been carried out using the frequency domain technique [Muq05], [Tes07b], [Jat05], [Lee04]. In a thorough investigation, Muqaibel et al. [Muq05] performed a UWB characterization of ten commonly used building material samples. The results obtained for the dielectric constants of these materials were found to be in agreement with those reported in the literature. Although there are significant differences and inaccuracies in the values of loss tangents for different materials at different frequencies obtained by different researchers, these discrepancies are largely attributed to the difference in material composition. It is also observed that the dielectric constants of uniform materials like wood and drywall, on an average, tend to decrease

with frequency, while those with nonuniform structures like brick and concrete block exhibit a more complex behavior.

Tesserault et al. [Tes07b] based their through-the-wall measurements on transmission power for door, chipboard and wall bearing. Results indicate a slight decrease of permittivity with frequency, while conductivity, which was calculated from the imaginary part of the complex permittivity, shows a more sensitive variation with frequency for the chipboard. Jaturatussani et al. [Jat05] used biconical antennas to find the dispersion and the penetration loss for four different materials. Lee et al. [Lee04] made obstructed LoS measurements on samples of drywall, wooden door, and glass door. Frequency responses showed a marked signal loss in the case of drywall, and the impulse response showed signal distortion and considerable delay. It is also observed in [Hua96] that for walls constructed from composite materials, the theoretical material constants are approximations and, therefore, wall parameters including the thickness can be estimated from the reflected (or transmitted) signal. In [Vil08], reflection measurements were performed at different angles where an aluminum plate was used as a reflection reference, large enough to cover an antenna beam footprint at any incident angle. However, the scattering effects of the wall surface caused by any surface roughness were not considered because these effects were very weak according to the estimated standard deviation of surface roughness of 0.05 mm that is small compared to a wavelength of 5.66 cm at 5.3 GHz.

#### 1.2.4 Existing Systems and Applications

A good understanding of the wall effect has allowed for better imaging systems because getting information on the internal features of a structure makes it much easier for activities in surveillance, rescue and military applications [Sin07]. It is also useful in manufacturing to detect unwanted objects in a production line. A typical example of a real life application of through wall imaging is Prism 200<sup>TM</sup> [Cam60] used by tactical operators which indicates the location and number of people behind a wall or barrier and is capable of penetrating concrete, reinforced concrete, cinder block, brick, drywall and other common wall types, with a range of up to 20 m.

Methods on how to accurately detect a target behind walls have been proposed by a number of researchers. Chandra et al. [Cha08] applied a singular value decomposition algorithm to minimize clutter and detect a metallic target behind plywood and brick wall in the UWB frequency range. Guolong et al. [Guo08] illustrated the impact of delay in position accuracy and used a through-the-wall compensation algorithm to correct the position of the located human to within 24 cm. Rovnakova et al [Rov09] proposed two methods to correctly trace moving targets behind walls and compensate for the ‘wall effect’. Imaging accuracy, however, is not only dependent on signal processing but also on the availability of detailed information about buildings, which includes material constants (permittivity and conductivity), thicknesses of walls, as well as the structures of the buildings themselves [Hua96].

Recently, information on propagation effects is also used to reconstruct buildings for imaging and localization purposes [Bar08], [Bar06]. In [Bar08], model-based

reasoning architectures are developed to estimate structural details and correctly model a building and its contents. This type of approach obtains image information and, using propagation information, predicts a three-dimensional building model that best matches the obtained information. [Ahm07], [Wan06], and [Wen08] also demonstrated the imaging problem with practical assumptions of unknown wall parameters.

Understanding the wall effect also helps in the development of RF/EM shielding for important building locations. Vaessen et al. [Vae88] investigated RF shielding properties of low-cost building materials where grids were embedded in addition to coating, and both were examined theoretically and experimentally. Results illustrated that unlike metal coating, wire grids exhibit significant frequency dependence.

There is no doubt that the study of through-obstacle propagation has led to interesting developments in wireless radio systems particularly in receiver design and link budget analysis. However, as research on propagation through different materials continues in order to cover more grounds, more possibilities emerge providing new directions for study, and thus, applications like through-wall imaging and localization create motives for further research.

### **1.3 Motivation**

Advances in communications and military have led to increased interest in the field of through the wall propagation. One interesting aspect of this is the detection of objects or humans behind obstacles, which has found applications in rescue missions, surveillance, and reconnaissance efforts. Electromagnetic waves traveling through an obstacle are subject to amplitude and phase distortion which is brought about by many

factors including the shape and composition of the wall. These factors play important roles in finding the exact position of a target behind a wall. Uncertainties in wall parameters blur and defocus target images causing them to shift away from their true positions [Ahm07]. It is therefore essential to study these adverse effects with the aim of finding reliable solutions. A considerable amount of research has been done to study the effect of wall composition on wave propagation [Tes07a], [Vil08], [Cui01] and consequently its effect on target detection [Ahm07]. However, most of these studies are in the narrowband frequency ranges or at specific frequencies. Furthermore, little has been done to develop solutions to correct the wall effects.

One of the main objectives of this work is to investigate the interaction of an ultra-wideband signal incident on the wall sample and extracting its electrical characteristics using frequency domain radiated techniques. Ultra-wideband signals are known to have high penetration capability and they provide high resolution. The second major objective is to use the information obtained about the wall to correct the adverse effect of the wall on the position accuracy of an object located behind it. Radiated methods, unlike cavity or waveguide methods, lend themselves to nondestructive and broadband applications. Performing measurements in the frequency domain allows for the application of a wide variety of noise reduction techniques. The information obtained from such investigation is useful to the following applications:

1. Designing a wireless communication system to suit the application needed and thus, the antennas [Yan08], pulse shape [Foo04], and receiver can be tailored to improve system performance.



2. Develop through-wall imaging and localization systems. These systems are particularly important in surveillance, rescue [Sin07], and military applications. These systems are based on short-pulse waveforms which can penetrate materials and provide precise ranging information [Mah05]. Ultra wideband has emerged as an excellent candidate for such applications [Aft09], and [Har08].

3. Designing building structures to withstand RF and EM wave penetration [Ant03], [Vae88] commonly known as EM/RF Shielding. Indoor wireless networks transmit RF signals that often propagate outside the physically controlled area of a building posing a security risk to sensitive data. Telecommunication [Lem02], medical, research, and military installations located near AM, FM and TV stations are subjected to RF ingress, equipment malfunction, test procedure difficulties, worker health problems, and compromised security situations particularly at defense facilities. Since short-pulse waveform systems like UWB radar can be used in imaging applications to locate humans or objects behind obstacles [Sac08], [Shi08], and [Lai05], ‘*anti-imaging*’ walls can also be designed to hinder radar penetration particularly in security situations, and in providing privacy.

4. *Modeling the obstacle* for communication purposes as in office (industrial and hospital) buildings [Pen03]. Information on building material properties like attenuation and insertion loss will be useful in choice of material for constructing say a radio research facility for example.

Additionally, modeling the obstacle can be used in healthcare, where the human body is envisioned as a frequency-dependent, irregular, lossy, and inhomogeneous

dielectric material [For07], and therefore EM wave propagation through it is greatly influenced. An example of this can be seen in wireless body area networks (WBAN) [For07], [Dib06].

While many studies had been carried out on characterization of obstacles for propagation effects, it is worthy of note that most of them relate only to certain applications, like radar, or at specific frequencies, or for indoor propagation, etc, and therefore cover only a sub-group of the numerous research areas. Thus, many issues are still subject to further research.

## **1.4 Objectives**

In the course of performing this work, the objectives are as follows:

1. Develop a test-bed for obstructed UWB localization. The system is a frequency domain setup based on a Vector Network Analyzer. This task includes choosing and acquiring material samples, wideband antennas, low noise amplifiers, wall mount for easy movement of wall samples, and appropriate cables.
2. Conduct transmission and reflection measurements to characterize some typical indoor walls (wood, glass, gypsum). The characterized walls should be presented in terms of the insertion loss function (magnitude and phase) providing information about the impact of the specific thickness and how the retrieved data can be further generalized. Parameters like dielectric constant and loss tangent are also obtained. Different scenarios (different distance from the wall, multiple walls, space between wall, etc) are considered and study the impact of on the waveform.

3. Demonstrate wall compensation by using the prior knowledge of the wall to correct the position estimation and perform error analysis. This is achieved using three methods namely; Constant Amplitude and Delay, Frequency Dependent Raw Data Method, and Data Fitting Method.

## **1.5 Thesis Structure**

After having an introduction which includes a review of literature and an insight on the objectives and motivation behind this thesis work, Chapter 2 gives a theoretical background on through-wall propagation. This includes an overview of EM wave propagation in dielectric media, various methods used in wall characterization, including the frequency domain technique we used. Chapter 3 details the description of our measurement setup for this work including the equipment, accessories and materials used. Experiments for studying UWB signal propagation through typical walls are also presented there. Conducted transmission and reflection measurements for wood, glass and gypsum are described and the results are presented. Repeatability and variability analysis are also covered. In chapter 4, wall compensation is demonstrated by using results obtained from chapter 3. The experiment done to determine an object behind the wall is described and the methods used to correct its position are discussed. Chapter 5 concludes the work with a summary and gives suggestions for future research. This thesis also includes an appendix and a nomenclature list. The appendix provides the manufacturers test results for the antenna used in the measurements. The Nomenclature provides a list of all symbols used in the text with their meanings.

## CHAPTER 2

### 2 THEORY OF UWB THROUGH-WALL PROPAGATION AND CHARACTERIZATION

#### 2.1 Dielectric Properties of Materials

The propagation characteristics of electromagnetic waves traveling through walls are largely determined by the type of material composing these walls. Wall compositions are, in general, dielectric and nonmagnetic in nature. Thus, they exhibit no response to magnetic fields. However, when such materials are subjected to electric fields, numerous electric dipoles are created within their molecular structures. These dipoles tend to align along the direction of the external electric field,  $E$ . The cumulative effect of the localized shift between bound positive and negative charges is called polarization,  $P$ . It corresponds to a state of stress within the material, which gives rise to potential energy storage. This energy is released when the external electric field is removed. The ability of a material to be polarized or “stressed” by external fields is a property determined by its molecular structure. Within the wall material, the density of electric field lines (i.e., the electric flux density,  $D$ ) is enhanced due to polarization, such that

$$D = D_o + P \quad (2.1)$$

where  $D_o$  is the free-space electric flux density. The ratio of the number of field lines inside the material to that in free space (absence of material) is called *dielectric constant* or *relative permittivity* of the material:

$$\epsilon_r = 1 + \frac{P}{\epsilon_o E} \quad (2.2)$$

The dielectric constant is, thus, a measure of the energy storage capability of the material. The permittivity of a material,  $\epsilon$ , is that of free space,  $\epsilon_o$ , multiplied by the dielectric constant.

The time-varying (or ac) nature of the external field has profound effects on the polarization of the material and its permittivity. These effects translate into frequency-dependent behaviors and incremental changes in the material conductivity. The materials' frequency dependence gives rise to the phenomenon of dispersion, a subject that is addressed later in this section.

To study the effects of time variations on electric properties of materials, it is customary to represent the electric dipole by the harmonic oscillator model or the classical mass-spring system. More sophisticated models exist but are beyond the scope of this work. The following differential equation governs the displacement  $l$  of an electric dipole

with charge  $q$  and mass  $m$  in response to a time-harmonic applied electric field with angular frequency  $\omega$  [Bal89]:

$$m \frac{\partial^2 l}{\partial t^2} + k \frac{\partial l}{\partial t} + sl = qE_o e^{j\omega t} \quad (2.3)$$

where  $k$  is the damping coefficient (friction),  $s$  is the tension parameter (spring),  $E_o$  is the amplitude of the applied electric field.

The steady-state solution for the displacement is readily obtained by using  $\partial/\partial t = j\omega$  in (2.3) and solving for  $l$ . The result is [Bal89]

$$l(t) = \frac{qE_o e^{j\omega t}}{m \left( \left( \frac{s}{m} - \omega^2 \right) + j\omega \left( \frac{k}{m} \right) \right)} \quad (2.4)$$

The polarization due to  $N$  similar electric dipoles per unit volume within the material is given by

$$P = Nql(t) \quad (2.5)$$

Accordingly, the relative permittivity is obtained as

$$\varepsilon_r = 1 + \frac{\frac{Nq^2}{\varepsilon_o m}}{\left(\frac{s}{m} - \omega^2\right) + j\omega\left(\frac{k}{m}\right)} = \varepsilon_r' - j\varepsilon_r'' \quad (2.6)$$

which is, in general, a complex quantity. The real and imaginary parts of  $\varepsilon_r$  are given by

$$\varepsilon_r' = 1 + \frac{\frac{Nq^2\left(\frac{s}{m} - \omega^2\right)}{\varepsilon_o m}}{\left(\frac{s}{m} - \omega^2\right) + \left(\frac{\omega k}{m}\right)^2} \quad (2.7)$$

$$\varepsilon_r'' = \frac{\frac{Nq^2\left(\frac{\omega k}{m}\right)}{\varepsilon_o m}}{\left(\frac{s}{m} - \omega^2\right) + \left(\frac{\omega k}{m}\right)^2} \quad (2.8)$$

The real part of the relative permittivity accounts for the energy storing capability of the material, while its imaginary part gives rise to an incremental change in the material conductivity. Thus, the *effective conductivity* of the material becomes

$$\sigma_e = \sigma_s + \sigma_a = \sigma_s + \omega\varepsilon_o\varepsilon_r'' \quad (2.9)$$

where  $\sigma_s$  is the static conductivity (sometimes called the *dc conductivity*) responsible for the ohmic losses inside the dielectric material; it is very small for good dielectrics. The ac

field conductivity,  $\sigma_a$ , gives rise to heating of the dielectric material due to its dipole oscillations. The ratio of the two energies, namely, the stored (displacement) energy and the energy lost due to conductivity, defines the *loss tangent* of the material. Including ac variations, the loss tangent,  $\tan \delta$ , is given by

$$\tan \delta = \frac{\sigma_s + \sigma_a}{\omega \epsilon_0 \epsilon_r'} + \frac{\epsilon_r''}{\epsilon_r'} \quad (2.10)$$

The determination of the electrical properties of the wall materials is essential, as these properties affect a variety of applications including through-the-wall imaging. The ability of walls to alter the propagation of ultra-wideband (UWB) signals is largely attributed to the real part of the complex permittivity and the effective conductivity of the wall material. These quantities can, in fact, be design parameters for better localization. In the light of the above discussion, the total electric current density within the material can be expressed as

$$J = \sigma_e E + j\omega \epsilon_0 \epsilon_r' E = j\omega \epsilon_0 \epsilon_r' (1 - j \tan \delta) E \quad (2.11)$$

The time-harmonic wave equation becomes

$$\nabla^2 E = j\omega \mu \sigma_e E - \omega^2 \mu \epsilon_0 \epsilon_r' E = \gamma^2 E \quad (2.12)$$



where  $\mu = \mu_o \mu_r$  is the permeability of the material and  $\mu_r$  is unity for non-magnetic materials. Also,  $\gamma$  is the *complex propagation constant* defined as

$$\gamma = \alpha + j\beta = \sqrt{j\omega\mu(\sigma_e + j\omega\epsilon_o\epsilon_r')} \quad (2.13)$$

The parameters  $\alpha$  and  $\beta$  are best known as the *attenuation* and *phase* constants, respectively. They can be expressed in terms of the material properties and frequency as

$$\alpha = \omega \sqrt{\frac{\mu\epsilon_o\epsilon_r'}{2}} \left[ \sqrt{1 + \left(\frac{\sigma_e}{\omega\epsilon_o\epsilon_r'}\right)^2} - 1 \right]^{\frac{1}{2}} \quad \text{Np/m,} \quad (2.14)$$

and

$$\beta = \omega \sqrt{\frac{\mu\epsilon_o\epsilon_r'}{2}} \left[ \sqrt{1 + \left(\frac{\sigma_e}{\omega\epsilon_o\epsilon_r'}\right)^2} + 1 \right]^{\frac{1}{2}} \quad \text{rad/m} \quad (2.15)$$

The attenuation suffered by a signal impinging on a wall can be, in general, attributed to conductivity loss, reflection loss, and multiple reflections within the wall. The conductivity loss may be a significant attenuation factor especially at higher frequencies and in the presence of liquids. However, most dry wall materials do not

exhibit significant ohmic losses. The losses due to reflections depend on the degree of contrast in the dielectric constant between the wall material and free space and the angle of incidence. Effects of multiple reflections inside the wall structure become significant when inhomogeneities are present and when the wall thickness is much larger than the signal wavelength. The realization of an object's position behind the wall requires the correct building up of the signal phase. Walls can contribute significantly to the alteration of the signal phase. While the signal attenuation due to through-the-wall propagation can be easily compensated, say, by increasing the level of transmit power, the treatment of the signal phase requires more elaborate schemes.

## **2.2 Wall Attenuation and Dispersion**

As mentioned earlier, UWB systems promise excellent wall penetration abilities. The propagation depth of an electromagnetic wave is proportional to its wavelength [Lee04]. The fine time resolution (fraction of a nanosecond) achieved by UWB systems makes it a candidate for precise ranging and localization of persons or objects behind walls and obstacles. This is unlike the narrowband systems that achieve high resolution using shortwave radio which in effect does not provide good penetration capabilities.

Consequently, the propagation of UWB signals is significantly affected by the frequency-dependent properties of materials comprising the propagation medium. Over such a wide range of frequencies, materials exhibit diverse behaviors when interacting with electromagnetic waves. As the frequency of the interacting field increases, the molecular dipoles of the material subjected to the field cannot respond instantaneously.

The result of this sluggish response of the material to electromagnetic waves is dispersion. This phenomenon causes different spectral components of a UWB signal to travel at different speeds. The attenuation caused by reactive losses (dipole oscillation) is also frequency dependent, implying that different components of the signal are attenuated by different amounts. The most important manifestation of these effects is in pulse broadening, loss of amplitude, and, generally, signal distortions. The direct consequences amount to the loss of all or some of the following: bandwidth, accuracy, and identification capability. In impulse radio UWB systems, narrow time-domain pulses are used. The pulse propagation characteristics are best explained by the group velocity concept. The group velocity, denoted as  $v_g$ , is the velocity with which the electromagnetic energy travels, and is determined from

$$v_g = \frac{d\omega}{d\beta} \quad (2.16)$$

In nondispersive media, the group velocity is the same as the phase velocity,  $v_p = \omega/\beta$  and is constant at all frequencies. In dispersive media, the group velocity is a function of frequency; thus, a delay difference develops between the travel times of different spectral components of a pulse. This delay difference causes pulse broadening, that is, the time width of the pulse is increased and hence assumes a narrower bandwidth (loss of bandwidth). The pulse broadening phenomenon is more pronounced for very short pulses.

Dispersion theories predict that, away from the resonance regions, the dielectric constant of a material increases with frequency [Hay06]. In fact, it has been shown that the dispersion curves of most materials follow a few well-known classical models, such as Debye and Lorentz models. In the Debye model, a relaxation time is defined to account for how electric dipoles follow the behavior of the applied electric field. At low frequencies, the dipoles can follow the field closely, resulting in strong polarization. However, as the frequency of oscillation of the applied field increases, the dipoles start to lose track of field variations and weaker polarization is expected. Thus, materials with long relaxation times exhibit weak polarizability, while those with short relaxation times show high degrees of polarization. For dielectric materials, the dispersion relation in (2.6) is rewritten as

$$\epsilon_r = \epsilon_\infty + \frac{\epsilon_s - \epsilon_\infty}{1 + j\omega\tau} \quad (2.17)$$

where  $\epsilon_\infty$  is the optical dielectric constant,  $\epsilon_s$  is the static dielectric constant and  $\tau$  is the material relaxation time.

The Debye model in (2.17) is a mathematical expression that can be fitted to experimental data. Once the fit is attained, the model can be used in analytical or numerical simulations. The Lorentz model takes into account multiple resonances of the material as well as dipole coupling effects. It is directly derived from the motion Equation (2.3). Introducing  $\omega_p^2 = Nq/\epsilon_0 m$  and  $\omega_o^2 = s/m$ , (2.6) is expressed as

$$\varepsilon_r = \varepsilon_\infty + \frac{(\varepsilon_s - \varepsilon_\infty)\omega_p^2}{\omega_o^2 + 2j\omega\Gamma + \omega^2} \quad (2.18)$$

where  $\omega_o$  is the material resonance frequency and  $\Gamma$  is the damping factor. For frequencies well below the resonance frequency of the material, the dielectric constant is real and independent of frequency, and hence there is no dispersion. As the frequency nears resonance, the dielectric constant increases and attenuation also becomes significant.

### **2.3 Techniques for Measuring Attenuation and Dispersion through Walls**

Unlike narrowband wireless systems, in which signal distortion is essentially caused by multipath components, in UWB wireless systems, signals may suffer significant distortions due to the dispersive properties of wall materials in the propagation path, multipath components, and also bandwidth limitations of transmit and receive antennas. In this section, techniques for the wideband measurement of attenuation and dispersion of signals propagating through walls are discussed. In particular, time-domain as well as frequency-domain free-space radiated measurement techniques, which lend themselves to in situ and nondestructive applications, are discussed.

#### **2.3.1 Time Domain Technique**

The time-domain technique consists of a pair of transmit and receive UWB antennas such as TEM horns, a pulse generator, a digital sampling oscilloscope, and a triggering signal generator as shown in Figure 2.1. Very short-duration Gaussian-like pulses are radiated by

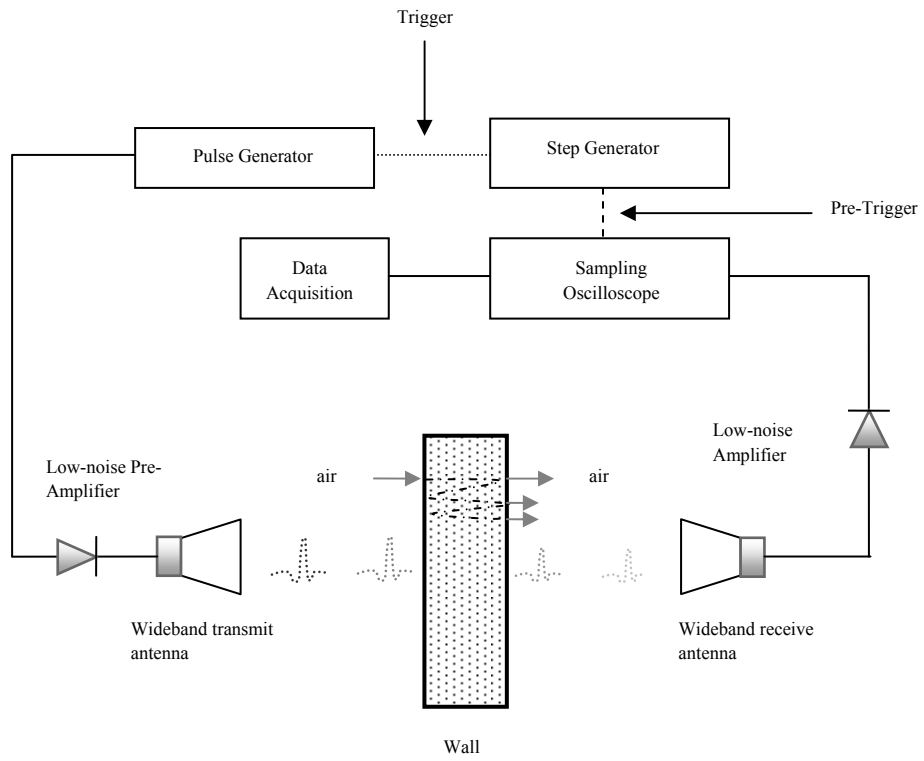


Figure 2.1: Time domain measurement setup

an antenna whose bandwidth is sufficiently large that it causes negligible signal distortions. The signal is received by another antenna and detected by means of a wideband detector such as a digital sampling oscilloscope. An ultra-wideband power amplifier may be used at the feed point of the transmit antenna if higher radiated power is needed.

The synchronization of both transmit and receive sides of the propagation channel is an important requirement in time-domain measurements. To maintain synchronization, a low jitter triggering signal is established between the pulse generator and the digital sampling oscilloscope. The sampling oscilloscope requires a pre-trigger. This is achieved by using a step generator driver that can supply the required trigger and pre-trigger signals. The time delay introduced by the triggering cables and the propagation path of the pulse is compensated by adjusting the time delay between the pre-trigger and the delayed trigger signals.

Calibration and noise are two other important issues that need to be addressed. The purpose of calibration is to eliminate the effects of non-ideal characteristics of the measurement instruments from the measured data. Also, received signals may suffer degradation due to the interference and noise from various sources. The narrowband noise is usually due to electromagnetic interference from nearby narrowband systems, and often takes the form of a sinusoidal waveform added to the received signal. This type of noise can be eliminated through bandpass filtering. The wideband noise, on the other hand, refers to the thermal noise in the receiver. The wideband noise typically appears in the

form of random short pulses and can be significantly reduced through multiple signal averaging, a feature generally available in sampling oscilloscopes.

### **2.3.2 Frequency Domain Technique**

The frequency domain technique uses network analyzers to perform swept frequency measurements within the intended bandwidth. Network analyzers can provide a wealth of knowledge about a device under test, including its magnitude, phase, and group-delay response. To accomplish this, a network analyzer must provide a source for stimulus, signal-separation devices, receivers for signal detection, and display/processing circuitry for reviewing results. The source is usually a built-in phase-locked (synthesized) voltage-controlled oscillator. Signal-separation hardware allows measurements of a portion of the incident signal to provide a reference for ratio measurements, and it separates the incident (forward) and reflected (reverse) signals present at the input of the device under test [Pac97]. The frequency domain setup also consist of a two port S-parameter test set that provides both forward and reverse measurements. The RF power is available from either port 1 or port 2, and either test port can be connected to the vector network analyzer's receiver inputs. Such test sets allow the use of full two-port error correction techniques for the highest measurement accuracy.

A pair of horn antennas is used with one of them as the transmitter connected to port 1 and the other as the receiver connected to port 2 of the S-parameter test set as indicated in Figure 2.2. The network analyzer performs a swept frequency measurement within the required frequency band. Each data point obtained from the measurement is in



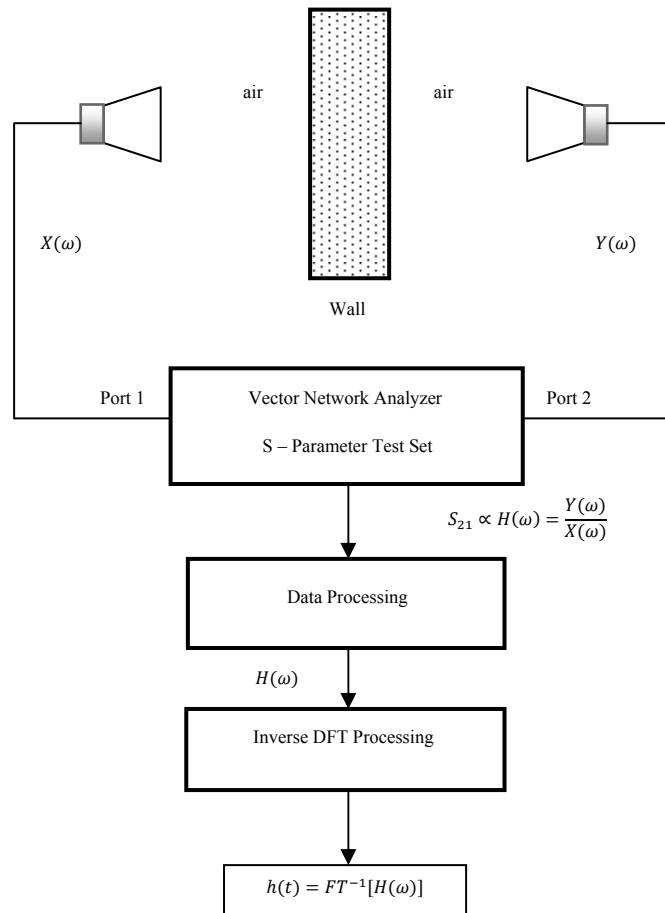


Figure 2.2: Frequency domain setup

a complex form represented by a magnitude and a phase term. Thus, the frequency band and required number of points has to be specified. For wideband characterization, where a wide frequency range needs to be swept, one has to make a trade-off between the frequency resolution and the required number of measurements that is directly proportional to the time it takes to perform the experiment as well as data storage requirements.

Direct phase measurements in wideband through-the-wall propagation over long distances should be dealt with very carefully, as available VNAs are generally designed for the measurement of complex S-parameters of small two-port networks rather than long propagation distances. Errors in direct phase measurements occur due to the difference between the measured frequency and the frequency of the received signal caused by the propagation delay time through the wall. In the sweep mode operation, the VNA frequency changes linearly with the sweep time. With long propagation paths, the frequency of the signal at the end of the channel would be different from that at the beginning, resulting in errors in both magnitude and phase measurements. To avoid sweep mode errors, frequency stepping instead of frequency sweeping may be used. In the frequency stepping mode of operation, the duration of the frequency step should be larger than the time delay between transmit and receive antennas. It is emphasized that the measured signal is the one recorded at the end of the step rather than the average of measured signals received during the time step.

In the next chapter, a detailed description of the experimental setup used in this work for characterizing UWB propagation through walls is given.

## CHAPTER 3

### 3 UWB CHARACTERIZATION OF OBSTRUCTED PROPAGATION

#### 3.1 Introduction

In communication and radar systems, the effect of signal distortion needs to be equalized. Obstructions with linear properties as well as those with non-linear properties introduce distortion in both magnitude and phase to signals passing through them. Linear effects impose changes in the time waveform of signals by altering the amplitude or phase relationships of the spectral components that make up the signal. No new signals are created. On the other hand non-linear effects can shift an incident signal in frequency or add other frequency components resulting in a modified pulse shape or frequency content.

Measuring both magnitude and phase components are important in that they are needed to fully characterize the obstruction and understand its effect on the signal. In addition, impulse response characterization requires magnitude and phase information of the transfer function in order to perform IFFT. Calibration, which uses vector error

correction, improves measurement accuracy and needs magnitude and phase data to build an effective error model.

Measurements are important in obstructed propagation studies because they provide a direct way of extracting obstacle properties and present a clear understanding of its effects on signal propagation. Measurements can be performed using both time domain and frequency domain techniques. In the time-domain method, a periodic train of pulses is applied to a material sample of known thickness using an antenna connected to a pulse generator and is received by an identical antenna connected to a digital sampling oscilloscope. While in the frequency domain, sinusoidal signals are used instead of pulses and a Vector Network Analyzer (VNA) with an antenna connected to each of its two ports is used to perform sweep frequency measurements. Additionally, when extracting wall parameters like dielectric constant and loss tangent, a variety of methods are employed together with the time domain or the frequency domain techniques. Such methods can be sampled methods like coaxial or transmission line methods or they can be in-situ methods (e.g free-space radiated measurements).

In this work, a free-space radiation frequency domain technique is employed. The VNA provides higher dynamic range than time domain equipment and also there is no need for synchronization between transmitter and receiver as is the case with the time domain technique. Also, the frequency domain technique allows for ease of application of a wide variety of noise reduction schemes. We performed the free-space radiated measurements for both transmission and reflection. There are several reasons for this: 1. Measurements using free-space procedures are contactless and nondestructive. 2. Cavity

and wave guide methods require that sample materials be machined properly to fit the cavity and/or waveguide cross-sections with negligible air-gaps. This requirement affects the accuracy of measurements for materials that cannot be machined precisely. 3. Some materials are inhomogeneous in structure due to variation in manufacturing processes. Because of this, unwanted higher order modes can be excited at the air-dielectric interface in the waveguide and cavities. 4. Characterization using free-space radiated measurements matches the configuration of the final application for which the experiments are carried out, which is communications and radar.

## **3.2 The Measurement Setup**

This section details the description, the experimental setup (including accessories) for both transmission and reflection measurements, and the contribution of each to the measurement results.

### **3.2.1 Component Selection**

Table 3.1 summarizes the hardware used to build the through-wall UWB localization setup and Figure 3.1 shows their pictures. Each of these components is then further described in the following headings.

#### *The Vector Network Analyzer System*

Vector network analyzer systems measure the magnitude and phase characteristics of networks and of components. The system consists of the source, the s-parameter test set, the vector signal processor display. Together these comprise a complete response system

TABLE 3.1: Measurement setup equipment description

<b>Equipment</b>	<b>Description</b>
<b>Network Analyzer System</b>	HP 8510C Network Analyzer with 83621B RF source and 8514B S-parameter test set
<b>Antenna</b>	Pair of broadband horn antennas (1 – 18 GHz) JXTXLB – 10180
<b>Amplifier</b>	Low-noise amplifier (1 -18 GHz) with SMA female LA1018N3209
<b>Cables</b>	Times Microwave StripFlex low loss high performance coaxial cable (1 – 18 GHz)
<b>Tripod</b>	Tripod for broadband horn antennas
<b>Connectors</b>	Two N-Type female to SMA male for connecting to amplifier ports



(a) antenna



ectors



Figure 3.1: Measurement equipment

that provides stimulus to the device under test and measures the signal transmitted through the device or reflected from its input.

The Network Analyzer System we used operates between 45 GHz and 20 GHz. The dynamic range is given in Table 3.2 below

TABLE 3.2: Network analyzer specifications [Agi00]

	0.045 – 2 (GHz)	2 – 8 (GHz)	8 – 20 (GHz)
<b>Maximum power (at port 2)</b>	+20dBm	+11 dBm	+10 dBm
<b>Reference power (at port 1)</b>	+2 dBm	-2 dBm	-6 dBm
<b>Minimum power (at port 2)</b>	-66 dBm	-95 dBm	-95 dBm

### *Antenna*

The antennas used were a pair of broadband TEM horn antennas operating between 1 – 18 GHz. The specifications are shown in the Table 3.3 below. A TEM horn uses TEM wave propagation having a velocity that is constant for all frequencies. At the horn throat, all frequencies generated arrive at the aperture together, and a wideband pulse is transmitted from the aperture. An antenna aperture is a measure of how big a piece of an incoming wave front an antenna can intercept. Horns are regarded as constant aperture antennas because the aperture remains fixed with frequency, thus the transfer function in transmit will be linear with frequency, while the transfer function on receive is constant. As frequency  $f$  increases, the size of this aperture in units of wavelength increases as  $f^2$ . This narrows the pattern and increases the antenna gain as  $f^2$ . This is particularly desired on the receiver side as it adds directly to link performance [Gre03].



Wideband antennas provide propagation information over a wide bandwidth, making it easy to identify and eliminate effects of unwanted reflections in time domain by way of time gating. Horn antennas are directional and are therefore useful in clutter reduction and enhancing overall system performance. This also, makes them useful in time domain gating.

TABLE 3.3: Antenna specification

<b>Manufacturer</b>	<b>Chengdu Ainfo Inc. China</b>
<b>Part Number</b>	JTXLB – 10180
<b>Frequency range</b>	1 – 18 GHz
<b>Gain (Typical)</b>	11 dBi
<b>Polarization</b>	Linear
<b>VSWR (Typical)</b>	2.0:1
<b>Size</b>	241mm x 160mm x 240mm
<b>Net Weight</b>	1.38 kg

The manufacturer test results for the antenna showing the gain and VSWR are shown in Appendix A-I.

### *Amplifier*

The maximum output at the port of the HP8510C network analyzer is +17 dBm. Using path loss formula free space measurements with the wideband horn antenna at 18 GHz and antenna separation of 1.8 m, we have

$$\begin{aligned}
 pathloss &= \left[ \frac{\lambda}{4\pi R} \right]^2 & (3.1) \\
 &= 20 \log(0.0167) - 20 \log(4\pi) - 20 \log(1.8) \\
 &= -62.6 \text{ dB}
 \end{aligned}$$

There is a maximum cable insertion loss of 2.2 dB per meter [Dyn05] at 18 GHz giving 16.5 dB for total length of our cables (7.5 m). The loss was computed to be around 79.1 dB. Therefore, an amplifier on the transmitter was required to have sufficient gain and input power levels to achieve a reasonably high transmit power. Based on these requirements and limitations, a low noise amplifier with specifications given in Table 3.4 was used. The amplifier is required to exhibit constant good gain and phase responses over the band of interest.

### *Cables*

Long cables connecting the S-parameter test set ports to the transmitter and/or receiver generally create a major limitation, because at high frequencies cable losses increase exponentially, causing a significant reduction in the dynamic range. The cables used for the measurement are labelled and the lengths are indicated in Table 3.5 below. The cable losses are also measured and the plots are shown in Figure 3.2. Table 3.6 also summarizes the general characteristics of the cables.

TABLE 3.4: Amplifier specifications [A-INF]

<b>Manufacturer</b>	Chengdu Ainfo Inc. China
<b>Part Number</b>	LA1018N3209
<b>Frequency range</b>	1 – 18 GHz
<b>Gain</b>	Min: 28 dB, Max: 36 dB
<b>Noise Figure</b>	Max: 4.5 dB
<b>P<sub>out</sub> @ 1 dB</b>	Min: +9 dBm
<b>Flatness</b>	Max: +/- 2.2 dB
<b>IP3</b>	18 dB (typical)
<b>VSWR</b>	2.2
<b>Current (+12V)</b>	250 mA (typical)
<b>Connector</b>	SMA female
<b>Net Weight</b>	0.075 kg

TABLE 3.5: Length of cables used in the measurement

<b>Cable Label</b>	<b>Length (meters)</b>
<b>A</b>	1.5
<b>B</b>	1.5
<b>C</b>	4.5

TABLE 3.6: General cable characteristics

<b>Manufacturer</b>	Times Microwave
<b>Catergory</b>	Stripflex
<b>Model</b>	SF-142B
<b>Description</b>	Flexible
<b>Impedance</b>	50 Ohms
<b>Max. Operating Frequency</b>	18 GHz
<b>Cut-Off Frequency</b>	34.1 GHz
<b>Nominal Impedance</b>	50 Ohms
<b>Nominal Velocity Of Propagation</b>	70.7 %
<b>Nominal Delay</b>	1.44 Ns / feet
<b>Maximum Operating Voltage</b>	1,879 VRMS
<b>Maximum CW Power Rating</b>	85 Watts at 18.0 GHz
<b>Maximum Return Loss</b>	-20 dB at 18.0 GHz
<b>Maximum Insertion Loss</b>	75.1 dB / 100 feet at 18.0 GHz
<b>Nominal Insertion Loss</b>	68.3 dB / 100 feet at 18.0 GHz

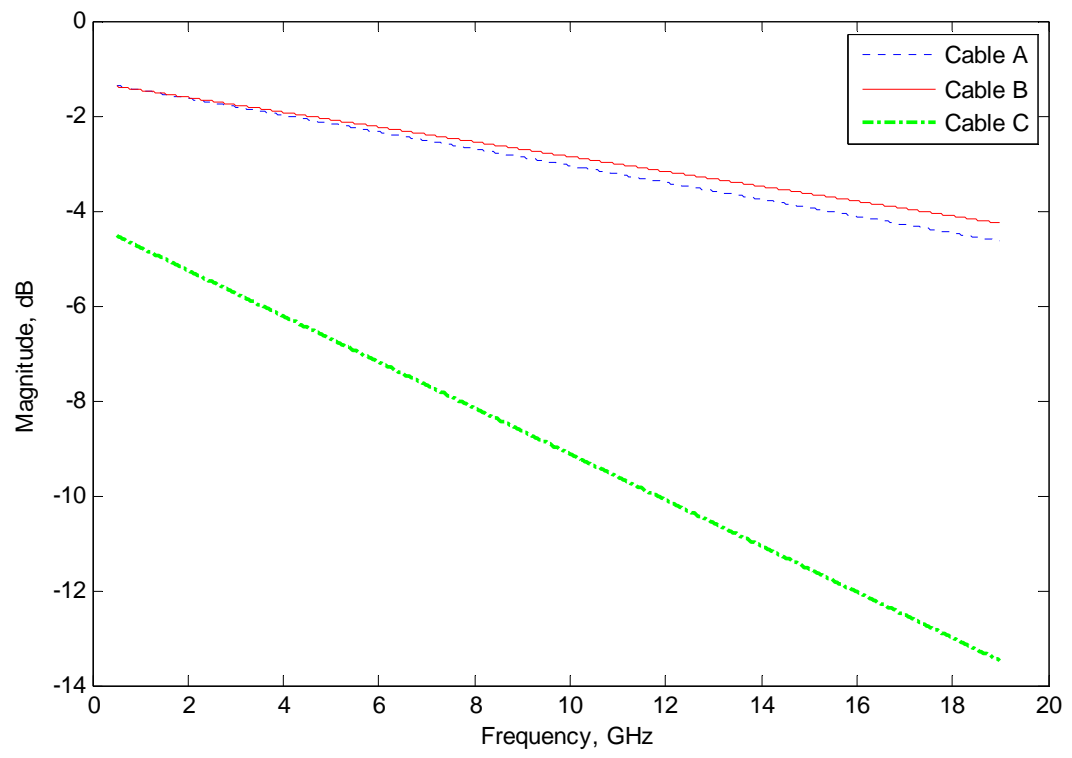


Figure 3.2: Losses in the cables used

### *Connectors*

The frequency range of any connector is limited by the excitation of the first circular waveguide propagation mode in the coaxial structure. Decreasing the diameter of the outer conductor increases the highest usable frequency; filling the air space with dielectric lowers the highest usable frequency and increases system loss. Performance of all connectors is affected by the quality of the interface for the mated pair. If the diameters of the inner and outer conductors vary from the nominal design, if plating quality is poor, or if contact separation at the junction is excessive, then the reflection coefficient and resistive loss at the interface will be degraded. As the interface between instruments, cable, DUT, test fixture, the connector is a critical element in achieving good measurement results. Connectors may look mundane, but they are fragile, precision-machined components and are highly sensitive to care in handling [Hie08].

An adapter with N – Type-to-SMA connector was used to connect the cables to the amplifier. N – Type is one of the most common RF connectors in use around today. It is a high performance connector designed by Bell Labs in the 1940's. The N connector is rugged, relatively inexpensive and the standard version is capable of mode-free operation to 11 GHz with precision versions supporting up to 18 GHz. The SMA was originally intended for use on semi-rigid coaxial cable and later for flexible cable. SMA operates up to 18 GHz with the precision versions extending the upper frequency limit to 26.5 GHz [Han09].

### 3.2.2 Calibration

A measurement calibration procedure transfers the accuracy of the calibration standards (Open, Short, and Load) to the measurement of the device. Since the response of the standards is known to a high degree of accuracy, the system can measure one or more standards, then use the results of these measurements to provide data to algorithms which process the measured data for display. This process is called measurement calibration, accuracy enhancement, or error correction [Agi01].

A Full 2-port measurement calibration was performed in our case because it provides the best magnitude and phase measurement accuracy. The four calibration standards used are shielded open circuit, short circuit, a load and a thru. This model provides full error correction of directivity, source match, reflection and transmission signal path frequency response, load match and isolation for  $S_{11}$ ,  $S_{21}$ ,  $S_{12}$ , and  $S_{22}$ .

Our measurement also has an inherent calibration in that the procedure involves performing a 'free-space' reference measurement and a 'through wall' measurement using the exact setup. Any errors in the reference measurement will be cancelled by the second measurement.

### 3.2.3 The Sample Materials

Three typical building materials were used as wall sample for characterization. These are wood, gypsum and glass. Table 3.7 shows the materials and dimensions of each.

TABLE 3.7: Wall materials showing dimensions

<b>Material</b>	<b>Dimension (cm)</b>
<b>Wood</b>	<b>1.8×122×245</b>
<b>Glass</b>	<b>0.8×122×242</b>
<b>Gypsum Board</b>	<b>1.2×120×240</b>

### 3.3 Measurement Procedure

As mentioned earlier, the frequency domain technique was employed. This technique is described in section 2.3. For the purpose of wall characterization, a HP8510C Vector network analyzer with two-port S-parameter test set was used and each data point obtained from the measurement is in a complex form represented by a magnitude and a phase term. The maximum number of points obtained by the HP8510C VNA is 801.

The output of the network analyzer port 1 is fed through a 1.5 m cable to a wideband power amplifier; another 1.5 m cable is connected to the amplifier output to a wideband antenna mounted on a tripod. An identical antenna mounted on a similar tripod stand is used as a receiving antenna. The receive antenna output is fed through a 4.5 m cable to the network analyzer port 2.

The device under test (DUT) is the sample wall material and it was chosen to be quite large enough to cover beam footprint at any incident angle in order to avoid edge diffraction and scattering. Also its thickness was large enough to provide considerable delay, which should be greater than the incident pulse width, to enable distinguishing



between multiple reflections inside the wall. Time gating can further be used to extract the main required pulse, and eliminate all delayed pulses due to multiple reflections in the wall. On the other hand, if the wall is too thick, it can severely attenuate the signal.

To characterize the walls, transmission and reflection measurements are conducted to obtain the insertion loss function in terms of magnitude and phase. This information is further used to correct the position estimation of a target behind the wall as we will see later.

### **3.3.1 Transmission Measurements**

This method uses a wave that is sent by a transmitting antenna, propagates through a material of some thickness and is captured by a receiving antenna. The material under test is assumed to be the two-port device (DUT) with an overall transfer function which relates the output pulse to the input excitation pulse [Aur96]. The transmission measurement also allows for measuring both the attenuation and dispersion through the wall samples.

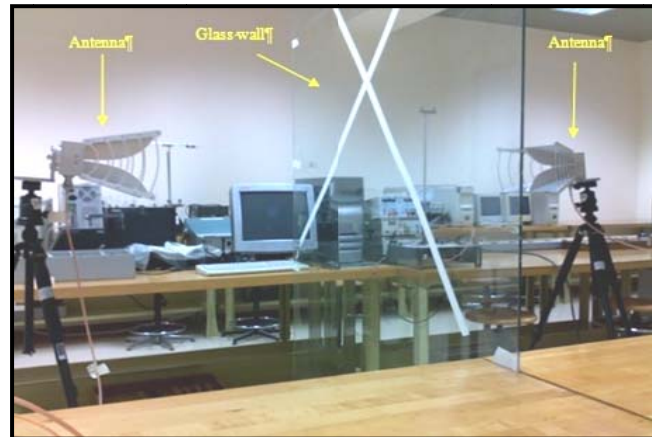
Two measurements are performed in this case. A ‘free-space’ measurement performed with empty space between transmitter and receiver, and a ‘through-wall’ measurement conducted with a ‘wall’ material inserted between the two antennas as depicted in Figure 3.3. The transmitter and receiver antennas are aligned for maximum signal reception. The wall material is placed at exactly midway between the antennas so that the wall is in the far-field region of each antenna, i.e. the separation distance between the antenna and the wall should be large enough to ensure far-field or Fraunhofer region

approximation where the antenna radiation pattern is independent of the separation distance, and the electromagnetic field incident on the wall is essentially a plane wave.

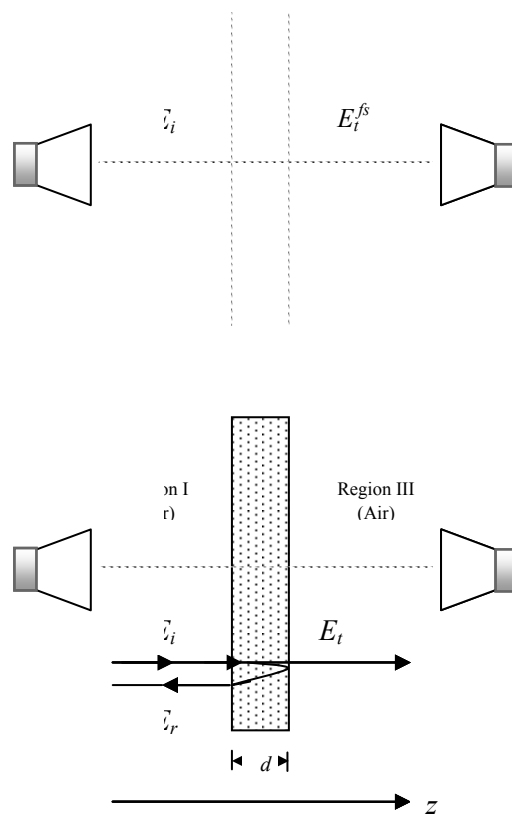
To achieve this, the Fraunhofer distance,  $d_f$  in this case, given as

$$d_f = \frac{2D_a^2}{\lambda}$$

must be much greater than both the largest physical linear antenna dimension  $D_a$ , and the wavelength  $\lambda$ . For the pair of antenna used,  $D_a$  is 0.241 m, and the corresponding far field distance at 18 GHz is 6.9 m. However, a few practical issues limited applying the far field approximation. First, at the time of performing these measurements, an anechoic chamber was not available, which would have allowed a considerable reduction of multipath effect. Therefore, the measurement was performed in a lab which contains fixed tables and other sources of multipath. Secondly, the available cables are a bit long and signal loss increases with distance and frequency, thus, amplifiers are needed on both the transmit and receive sides of the setup. However, the available amplifier has 30 dB gain and the maximum input power the ports of the HP8510C VNA system is +17 dB. So as not to damage the VNA, only one amplifier was used, which is on the transmitter side as mentioned earlier. In order to compensate for a weak received signal and stay clear of multipath, while ensuring the accuracy of the results, two actions were carried out. First, the distance to wall from the antenna was reduced to less than the far field approximation such that received signal strength is increased and edge diffraction from the wall is reduced. Next, time gating is performed to remove the effect of reflections from the floor



(a)



(b)

Figure 3.3: Transmission measurements, (a) Picture, (b) Schematic

and tables around.

The wall effect is based on extracting the complex dielectric constant from the measured insertion transfer function obtained as the ratio of two transmit signals given as [Muq03a]

$$H(j\omega) = \frac{\frac{E_t(j\omega)}{E_i(j\omega)}}{\frac{E_t^{fs}(j\omega)}{E_i(j\omega)}} = \frac{E_t(j\omega)}{E_t^{fs}(j\omega)} = \frac{X_t(j\omega)}{X_t^{fs}(j\omega)} \quad (3.2)$$

where  $E_i(j\omega)$  is the incident wave,  $E_t(j\omega)$  is the transmitted wave through the wall, and  $E_t^{fs}(j\omega)$  is the free space transmitted wave. The scattering parameter related to the insertion transfer function in this case is given as

$$S_{21}(j\omega) = H(j\omega)e^{-j\omega\tau_0} \quad (3.3)$$

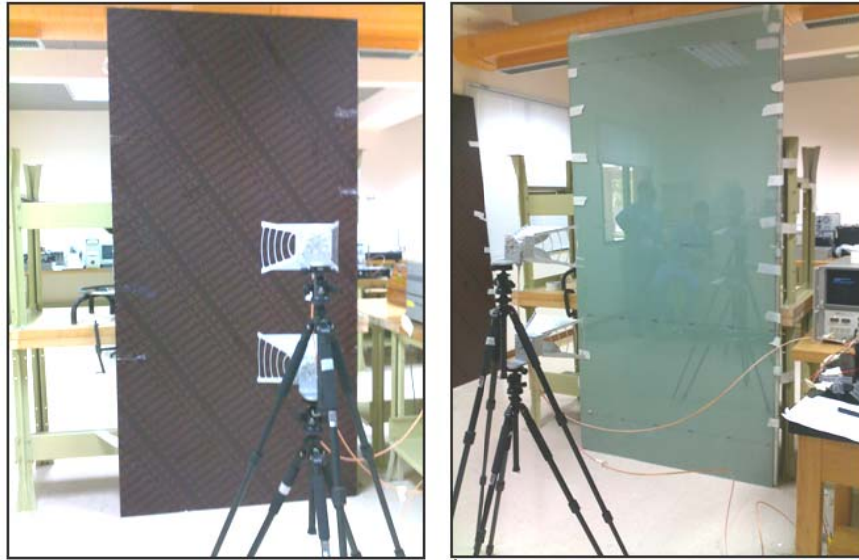
The terms  $X_t^{fs}(j\omega)$  and  $X_t(j\omega)$  are ‘free-space’ reference and ‘through-wall’ frequency domain signals obtained in the absence and presence of the wall respectively. The ‘free-space’ measurement is used as reference to take care of the effects of components other than the wall. Assuming a fictitious layer of free-space of the same thickness as the wall, then the propagation delay through this layer is  $\tau_0 \equiv d/c$  where  $d$  is the layer thickness and  $c$  is the speed of light in free space. Extra caution should be taken to make sure that exact setup is used to perform both experiments in order to avoid measurement inconsistencies.

### 3.3.2 Reflection Measurements

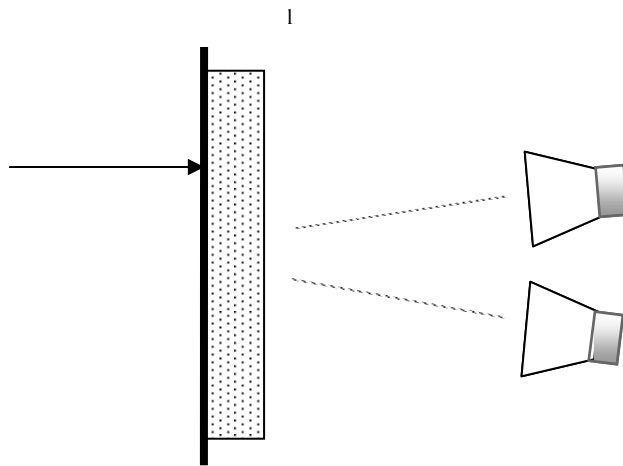
In reflection experiments, a metallic reflector, aluminum whose reflection coefficient is close to unity was used for reference measurements. Two measurements are conducted here also as with the transmission measurements, but in this case, both antennas are positioned on the same side of the wall as shown in Figure 3.4. The reference signal is obtained with only the aluminum plate in place. While the second is performed with the wall pressed against the aluminum sheet. To enable us use the same model with that of the transmission measurements in computing the dielectric constant, the wall thickness is assumed to be twice the original size. This is because in the reflection experiment, the signal propagates through the wall twice before arriving at the receiver, i.e., when it goes from transmitter through the wall to the aluminum sheet and when it is reflected by the aluminum sheet goes through the wall to the receiver. In addition, for the model to work for reflection, we considered only normal signal incidence on the wall. The reflected wave only changes its polarity undergoing a  $180^\circ$  phase change. Care was taken to ensure that there are minimum air gaps between the aluminum sheet and the wall samples. The antennas were arranged one above the other with receiver being above at a distance of 1 m from the floor, and are conveniently spaced apart to reduce coupling. A separation distance of 0.26 m was found to be convenient and the received signal was good.

### 3.4 Analysis Method

The free-space and through-the-wall measurements would be most accurate if performed inside an anechoic chamber, which absorbs all multipath components and reflections from



(a)



(b)

Figure 3.4: Reflection measurements, (a) Picture, (b) Schematic

the floor and the ceiling. Ideally, to avoid scattering from the edges, the sample wall to be measured should be infinitely wide. Also, samples under test have to be in the far-field regions of transmit and receive antennas, typically several meters for the frequency range of interest and dimensions of the antennas used. Maintaining these requirements is not a convenient task, keeping in mind that absorbers and chamber environment do not allow easy movement of large samples. Fortunately, time gating can be used to significantly reduce the undesired effects such as scattering from edges and reflections from surrounding walls. For time gating to be efficiently implemented, three conditions have to be met. First, the transmit and the receive antennas should be positioned away from the reflecting surfaces. Second, samples should have relatively large surface dimensions in order to minimize the edge effects. Finally, there should be flexibility in adjusting the distance between the antennas and the sample.

Time gating can also be used to isolate a desired portion of the received signal; namely, the first single-pass of the signal transmitted through the wall. In this application, the sample thickness should be large enough to yield sufficient delay. Thus, the first pulse can easily be extracted, and all delayed pulses due to multiple reflections inside the wall can be removed.

### **3.4.1 Single-Pass Technique**

The single-pass technique can be used if the portions of the signal due to multiple reflections inside the wall are either negligible or can be eliminated by means of time gating. We assume that the wave is normally incident on the material surface and the duration of the pulse is smaller than the pulse travel time through the material. The

derivations pertaining to the single-path propagation analysis are available in the appendix of [Muq03b]. Assuming low loss, the resulting dielectric constant becomes real-valued.

The results are summarized below:

$$\varepsilon'_r(f) \cong \left[ 1 + \frac{\Delta\tau(f)}{\tau_0} \right]^2 = \left[ 1 - \frac{1}{2\pi\tau_0} \frac{d\Phi_{sp}(f)}{df} \right]^2 \quad (3.4)$$

$$\tan \delta \cong -\frac{1}{\pi f \tau_0 \sqrt{\varepsilon'_r(f)}} \ln \left[ \frac{\left[ 1 + \sqrt{\varepsilon'_r(f)} \right]^2}{4\sqrt{\varepsilon'_r(f)}} |H_{sp}(f)| \right] \quad (3.5)$$

where  $H_{sp}(f) = |H_{sp}(f)| \exp[j\Phi_{sp}(f)]$  is the single-pass insertion transfer function. It is the ratio of the Fourier transform of the single-pass received signal when the slab is in place to the Fourier transform of the received signal in the absence of the wall. It should be noted that the derivative term  $d\Phi_{sp}(f)/df$  in (3.4) is based on the assumption that the phase varies linearly with frequency. The advantage of using the derivative of the phase is to avoid tracking the unwrapped phase function. As a function of the unwrapped phase, the dielectric constant is given by

$$\varepsilon'_r(f) \cong \left[ 1 + \frac{\Delta\tau(f)}{\tau_0} \right]^2 = \left[ 1 - \frac{\Phi_{sp}(f)}{2\pi\tau_0 f} \right]^2 \quad (3.6)$$

### 3.4.2 Multiple-Pass Technique

If the single-pass signal cannot be gated out satisfactorily, multiple reflections from the wall interior that constitute part of the received signal must be considered. This situation



particularly arises when the transit time through the thickness of the wall is small compared to the pulse duration. In this case, an insertion transfer function that accounts for multiple reflections of a homogenous wall is needed. The model to be presented can be used to determine the complex dielectric constant from the measured insertion transfer function.

To obtain an expression for the insertion transfer function  $H(j\omega)$ , we assume a plane wave normally incident on a dielectric wall of thickness  $d$  and permittivity  $\epsilon_r = \epsilon_r' - j\epsilon_r''$ , as depicted in Figure 3.3(b), establishes a reflected wave in region I (air), a set of forward and backward-traveling waves in region II (wall), and a transmitted wave in region III (air). Using electric and magnetic field expressions and boundary conditions for the electric and the magnetic fields at the wall – air interfaces, the transmission coefficient which is equivalent to  $S_{21}$  in scattering parameter terminology is readily obtained as [Muq03a].

$$T = \frac{4}{e^{\gamma d} \left( 2 + \frac{\eta_o}{\eta} + \frac{\eta}{\eta_o} \right) + e^{-\gamma d} \left( 2 - \frac{\eta_o}{\eta} - \frac{\eta}{\eta_o} \right)} \quad (3.7)$$

Based on the definition of insertion transfer function given in (3.2),

$$\frac{\frac{E_t}{E_i}}{\frac{E_t^{fs}}{E_i}} = \frac{T}{e^{-j\beta_0 d}} = T e^{j\beta_0 d} = H(j\omega) \quad (3.8)$$

Thus,

$$H(j\omega) = \frac{4e^{j\beta_0 d}}{e^{\gamma d} \left( 2 + \frac{\eta_o}{\eta} + \frac{\eta}{\eta_o} \right) + e^{-\gamma d} \left( 2 - \frac{\eta_o}{\eta} - \frac{\eta}{\eta_o} \right)} \quad (3.9)$$

where

$$\beta_o = \omega \sqrt{\mu_o \varepsilon_o},$$

$$\gamma = \alpha + j\beta = j\omega \sqrt{\mu_o \varepsilon_o (\varepsilon_r' - j\varepsilon_r'')}$$

$$\eta_o = \sqrt{\mu_o / \varepsilon_o}$$

$$\eta = \eta_o / \sqrt{\varepsilon_r' - j\varepsilon_r''}$$

A *multi-pass* transfer function is obtained that accounts for all the transmitted waves including the ones resulting from multiple reflections within the wall. Equation (3.9) can be solved for the dielectric constant when the insertion transfer function  $H(j\omega)$  is obtained by measurements as described in Section 3.3. It should be noted that equation (3.9) is a complex equation and its numerical solution requires two-dimensional root search algorithms.

Assuming the wall occupying region II is low loss, the relation  $\varepsilon_r'' / \varepsilon_r' \ll 1$  is satisfied, allowing considerable simplifications to be made, and  $\varepsilon_r'$  and  $\varepsilon_r''$  to be obtained from separate real expressions. The benefit of the simplified solution is that, instead of

time-consuming two-dimensional root search techniques, only a one-dimensional root search needs to be implemented. The following approximations can be made [Muq03a]

$$\begin{aligned}
 \gamma &= \alpha + j\beta \\
 &= j\omega\sqrt{\mu_0\varepsilon_0(\varepsilon_r' - j\varepsilon_r'')} \\
 &\cong j\omega\sqrt{\mu_0\varepsilon_0}\sqrt{\varepsilon_r'}\left(1 - j\frac{1}{2}\frac{\varepsilon_r''}{\varepsilon_r'}\right) \\
 &\cong j\beta_0\sqrt{\varepsilon_r'}\left(1 - j\frac{1}{2}\frac{\varepsilon_r''}{\varepsilon_r'}\right)
 \end{aligned}$$

and

$$\eta = \sqrt{\frac{\mu_0}{\varepsilon_0(\varepsilon_r' - j\varepsilon_r'')}} \cong \sqrt{\frac{\mu_0}{\varepsilon_0\varepsilon_r'}} = \frac{\eta_o}{\sqrt{\varepsilon_r'}}$$

Then,

$$\frac{\eta_o}{\eta} + \frac{\eta}{\eta_o} \cong \sqrt{\varepsilon_r'} + \frac{1}{\sqrt{\varepsilon_r'}} = \frac{\varepsilon_r' + 1}{\sqrt{\varepsilon_r'}}$$

and (3.9) becomes

$$H(j\omega) = \frac{4e^{j\beta_0 d}}{e^{(\alpha+j\beta)d}\left(2 + \frac{\varepsilon_r' + 1}{\sqrt{\varepsilon_r'}}\right) + e^{-(\alpha+j\beta)d}\left(2 - \frac{\varepsilon_r' + 1}{\sqrt{\varepsilon_r'}}\right)} \quad (3.10)$$

Rewriting the transfer function in terms of magnitude and phase, we get

$$|H(j\omega)| = \left[ \frac{16}{e^{2\alpha d} \left( 2 + \frac{\varepsilon_r' + 1}{\sqrt{\varepsilon_r'}} \right)^2 + e^{-2\alpha d} \left( 2 - \frac{\varepsilon_r' + 1}{\sqrt{\varepsilon_r'}} \right)^2 + 2 \cos(2\beta d) \left( 4 - \left( \frac{\varepsilon_r' + 1}{\sqrt{\varepsilon_r'}} \right)^2 \right)} \right]^{\frac{1}{2}} \quad (3.11)$$

and

$$\angle H(j\omega) = \beta_0 d - \phi \quad (3.12)$$

Where

$$\phi = \tan^{-1} \left\{ \frac{\left[ \frac{e^{\alpha d} \left( 2 + \frac{\varepsilon_r' + 1}{\sqrt{\varepsilon_r'}} \right) - e^{-\alpha d} \left( 2 - \frac{\varepsilon_r' + 1}{\sqrt{\varepsilon_r'}} \right)}{e^{\alpha d} \left( 2 + \frac{\varepsilon_r' + 1}{\sqrt{\varepsilon_r'}} \right) + e^{-\alpha d} \left( 2 - \frac{\varepsilon_r' + 1}{\sqrt{\varepsilon_r'}} \right)} \right] \cdot \tan(\beta d)} \right\} \quad (3.13)$$

In a compact form, (3.13) can be put as

$$\phi = \tan^{-1} \left\{ \left[ \frac{1 - e^{-2\alpha d} Q}{1 + e^{-2\alpha d} Q} \right] \cdot \tan(\beta d) \right\} \quad (3.14)$$

where

$$Q = \frac{2 - \frac{\varepsilon_r' + 1}{\sqrt{\varepsilon_r'}}}{2 + \frac{\varepsilon_r' + 1}{\sqrt{\varepsilon_r'}}} = \frac{2\sqrt{\varepsilon_r'} - \varepsilon_r' - 1}{2\sqrt{\varepsilon_r'} + \varepsilon_r' + 1} = \frac{-(\sqrt{\varepsilon_r'} - 1)^2}{(\sqrt{\varepsilon_r'} + 1)^2} = - \left( \frac{\sqrt{\varepsilon_r'} - 1}{\sqrt{\varepsilon_r'} + 1} \right)^2 \quad (3.15)$$

when  $e^{-2\alpha d} = X$ , then

$$|H(j\omega)|^2 = \frac{16\varepsilon_r'}{\frac{1}{X}(\sqrt{\varepsilon_r'} + 1)^4 + X(\sqrt{\varepsilon_r'} - 1)^4 - 2\cos(2\beta d)(\varepsilon_r' - 1)^2}, \quad (3.16)$$

or

$$X^2(\sqrt{\varepsilon_r'} - 1)^4 - 2\left[\cos(2\beta d)(\varepsilon_r' - 1)^2 + \frac{8\varepsilon_r'}{|H(j\omega)|^2}\right]X + (\sqrt{\varepsilon_r'} + 1)^4 = 0$$

which is a quadratic equation in  $X$ . Solving the equation for  $X$ , we have

$$X = e^{-2\alpha d} = \frac{\left[\cos(2\beta d)(\varepsilon_r' - 1)^2 + \frac{8\varepsilon_r'}{|H(j\omega)|^2}\right] \pm \sqrt{\left[\cos(2\beta d)(\varepsilon_r' - 1)^2 + \frac{8\varepsilon_r'}{|H(j\omega)|^2}\right]^2 - (\varepsilon_r' - 1)^4}}{(\sqrt{\varepsilon_r'} - 1)^4} \quad (3.17)$$

Only the solution with the negative sign is valid. Substituting for  $X$  from (3.17) into (3.14)

we get an equation which is only in terms of  $\varepsilon_r'$ .

$$\tan[\beta_0 d - \angle H(j\omega)] + \frac{1 - QX}{1 + QX} \tan(\beta d) = 0 \quad (3.18)$$

Solving this equation numerically,  $\varepsilon_r'$  is readily determined.  $X$  and  $\alpha$  are then found from

(3.17). Finally,  $\varepsilon_r''$  is calculated using

$$\varepsilon_r'' = \frac{2c\alpha\sqrt{\varepsilon_r'}}{\omega} \quad (3.19)$$

## **3.5 Wall Parameter Calculation**

This section details the signal processing procedures used to extract the wall parameters from the measurements. Recall that two measurements are carried out in each experiment; a ‘reference’ measurement and a ‘through’ measurement. Figure 3.5 summarizes these procedures.

### **3.5.1 Data Acquisition**

Using the frequency domain technique, 801 complex data points representing magnitude and phase information are obtained over a frequency range of 1 – 18 GHz. This is the maximum number of data points that can be obtained over a given frequency range on the HP8510C network analyzer. This data is acquired and converted to files readable by MATLAB.

### **3.5.2 Un-gated Insertion Transfer Function, Time delay and Initial guess of permittivity**

The un-gated insertion transfer function is obtained by dividing the through wall data by the reference data. A finite impulse response filter of order 100 is then used to remove the noise at the low frequencies and those beyond the antenna bandwidth. The frequency domain signals are then converted to time domain using inverse fast fourier transform to get the impulse responses. Zeros are padded for higher time domain resolution. Figure 3.6 shows the magnitude, phase, un-gated insertion transfer function, and the impulse responses for the ‘reference’ and ‘through’ signals.

The impulse responses obtained from frequency-domain measurements are correlated using a sliding correlator to obtain the first guess on the delay and effective dielectric constant. An estimate of the average dielectric constant could also be obtained through peak-to-peak impulse time delay,  $\Delta\tau$ . This average dielectric constant, which does not reflect the frequency dependence, is given by

$$\varepsilon_r' \cong \left[ 1 + \frac{\Delta\tau}{d/c} \right]^2 \quad (3.20)$$

where  $d$  is the wall thickness and  $c$  is the speed of light in free-space.

### 3.5.3 Time Gating

In the absence of an anechoic chamber, multipath components, multiple reflections in the wall, and reflections from the floor, ceiling and other structures become a threat to the measurement accuracy. In order to reduce this effect of multipath, time gating is used to selectively remove or include the undesired responses in time. The remaining time domain responses can then be transformed back to the frequency domain with the effect of the ‘gated-out’ responses being removed. The delayed signals can be filtered out by imposing a window function over the dominating signal that is identified to be the desired one. In our case, this window is based on the modified Kaiser window [Muq03b] where the parameter  $\beta$  controls the amount of roll-off of the window function. Note however that, wall parameters are independent of the type of window used. We used a  $\beta$  of 20 and adjusted the window parameters (rise time, fall time and width) in order to obtain accurate values for the wall parameters.

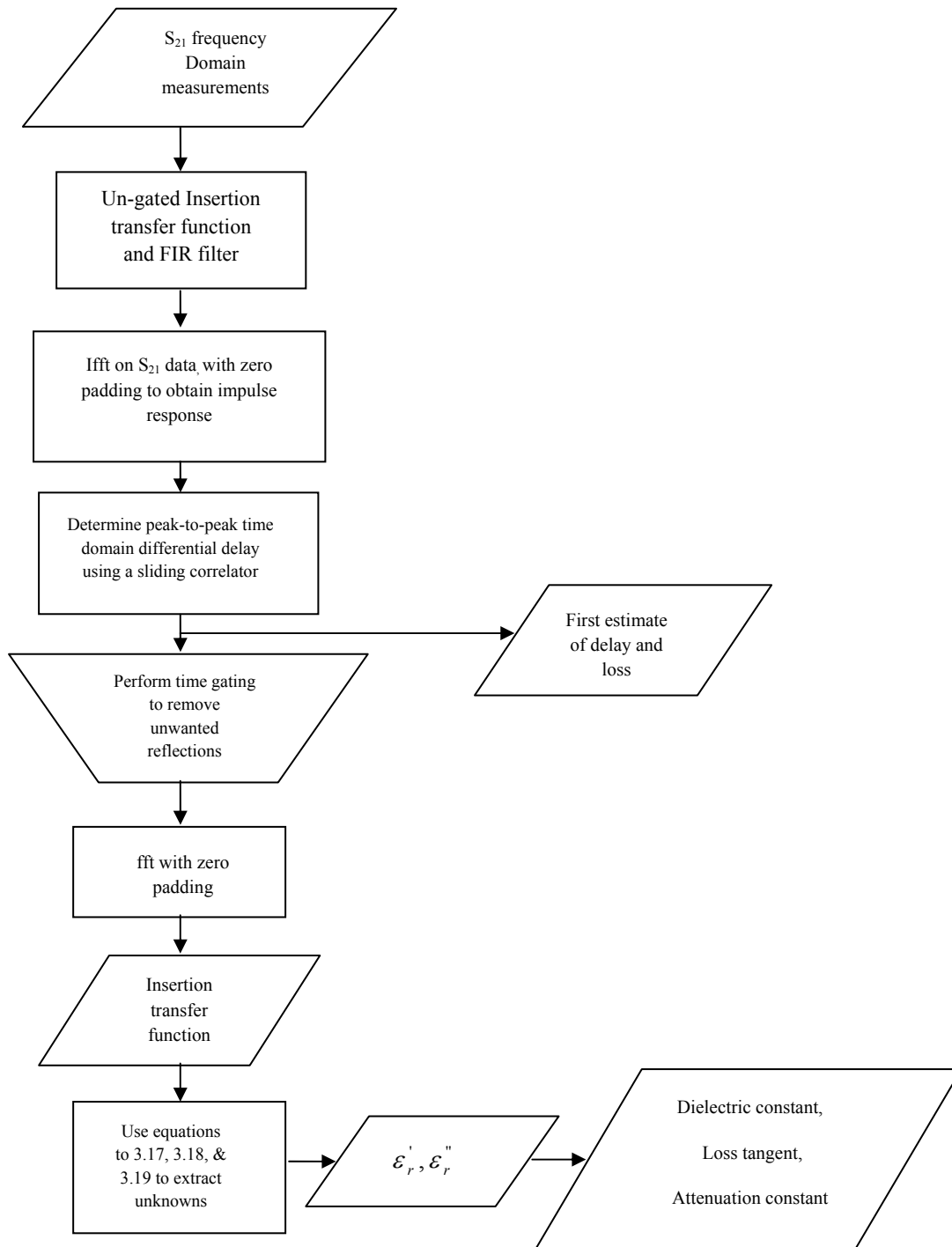


Figure 3.5: Chart for characterizing obstructed measurements



The associated 'reference' and 'through wall' frequency domain signals are then recovered using fast fourier transform and equation (3.2) is used to obtain the insertion transfer function. Figure 3.7 shows the window, and in Figure 3.8 an un-gated time domain waveform with a window, and time domain gated waveform after applying the window are shown.

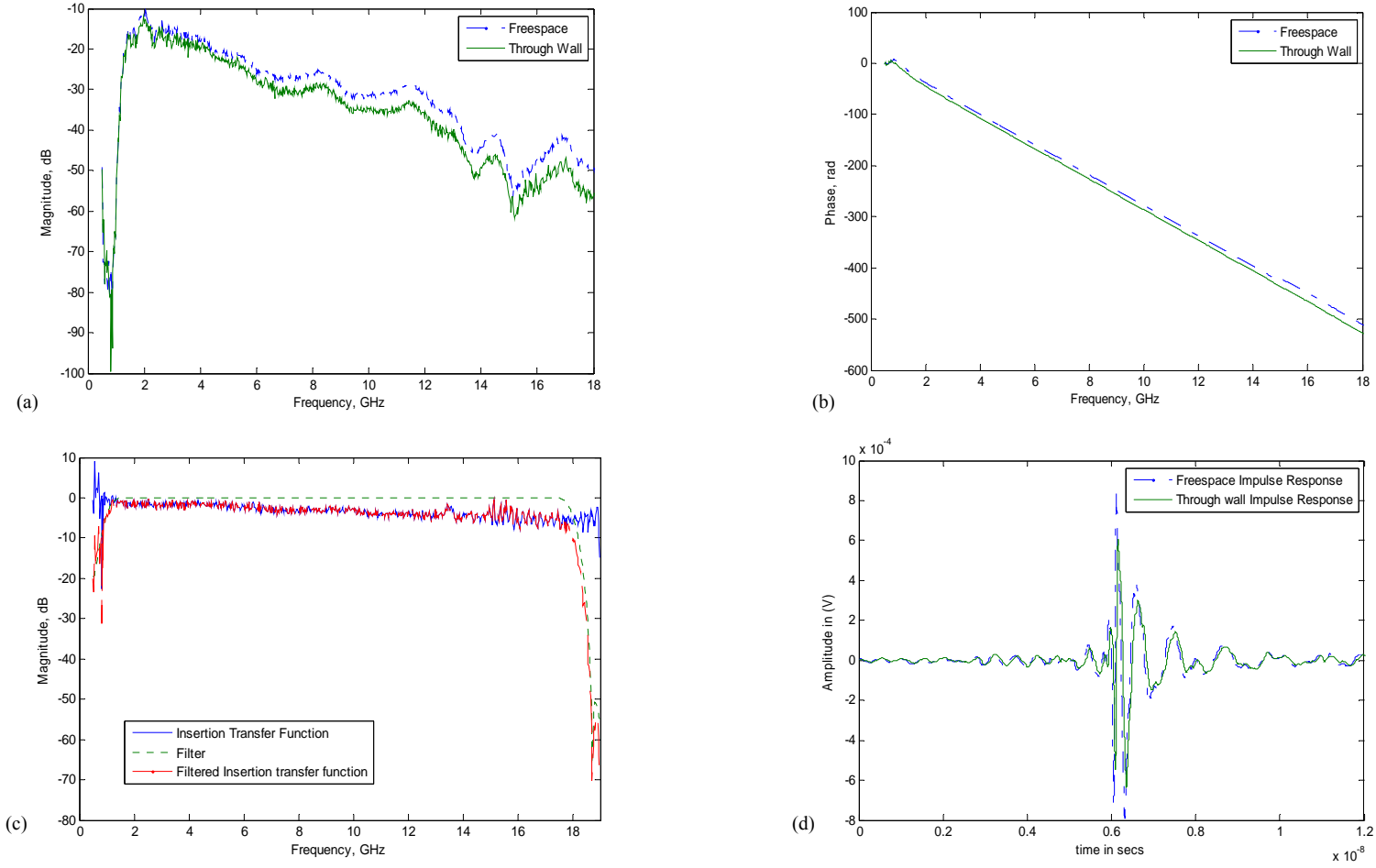


Figure 3.6: Frequency domain measurements (a) measured magnitude, (b) measured Phase, (c) filter and filtered un-gated insertion transfer function, (d) impulse responses.

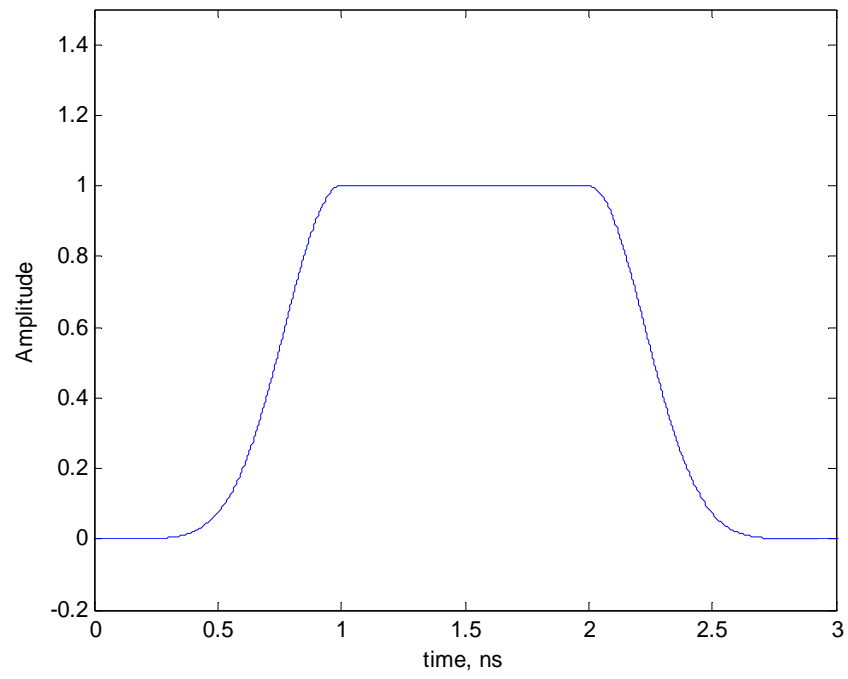
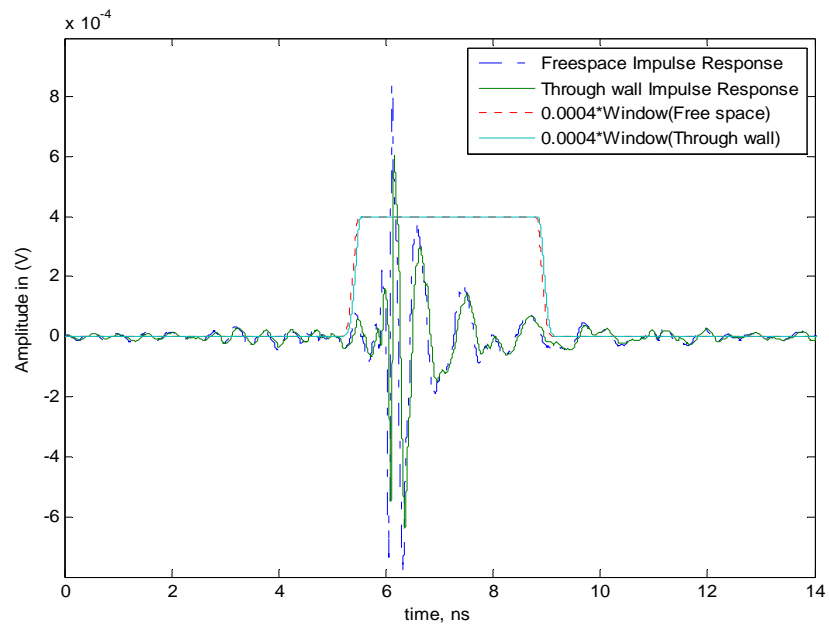
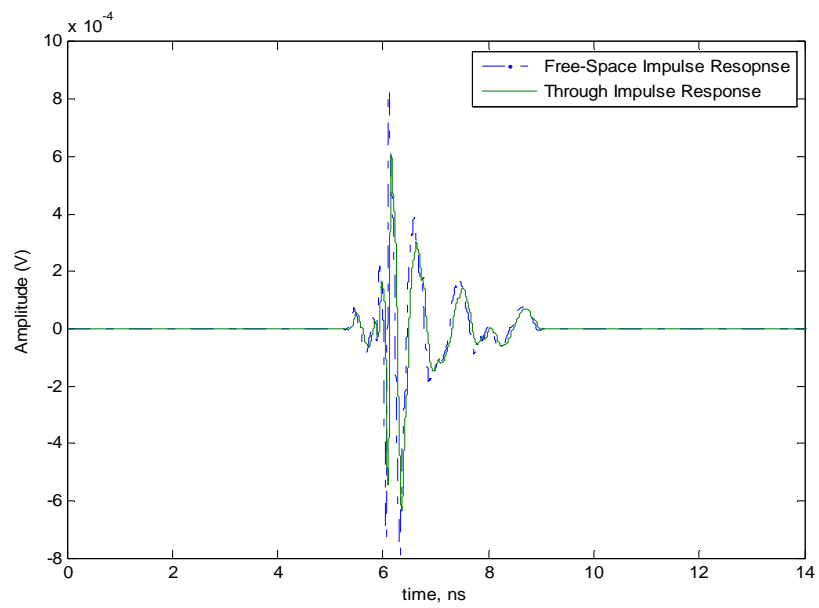


Figure 3.7: The gating window



(a)



(b)

Figure 3.8: (a) Un-gated time domain signal with window, (b) gated time domain signal

### **3.5.4 Wall (material) Parameters**

Both magnitude and phase information are needed for accurate characterization of walls. The dielectric constant, loss tangent and attenuation constant for the sample materials are calculated. The multiple-pass technique from [Muq03a] using the one-dimensional search is employed. The dielectric constant and loss tangent are obtained from the insertion transfer function (See equations 3.17, 3.18, & 3.19).

## **3.6 Measurement Results**

This part of the work presents and discusses the results for the wall characterization experiments. As mentioned earlier, transmission and reflection measurements were conducted on three different wall materials including wood, glass and gypsum. Wall parameters namely, dielectric constant, insertion loss, attenuation constant and loss tangent were extracted for the given materials. Results for both transmission and reflection measurements indicate a close agreement with each other, and also with results found in the literature.

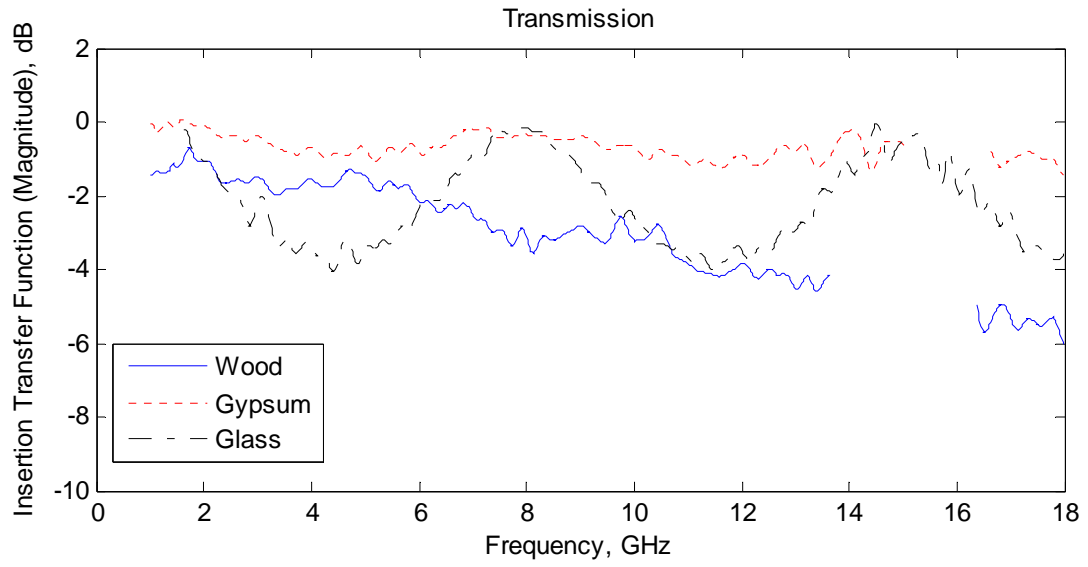
We further considered effect of multiple walls, including double walls, when we have air gap between the walls, and the effect of varying the thickness of this air gap. Triple wall scenarios were also investigated. Repeatability and variability analysis were conducted to evaluate the measurement precision.

### **3.6.1 Transmission Measurements Results**

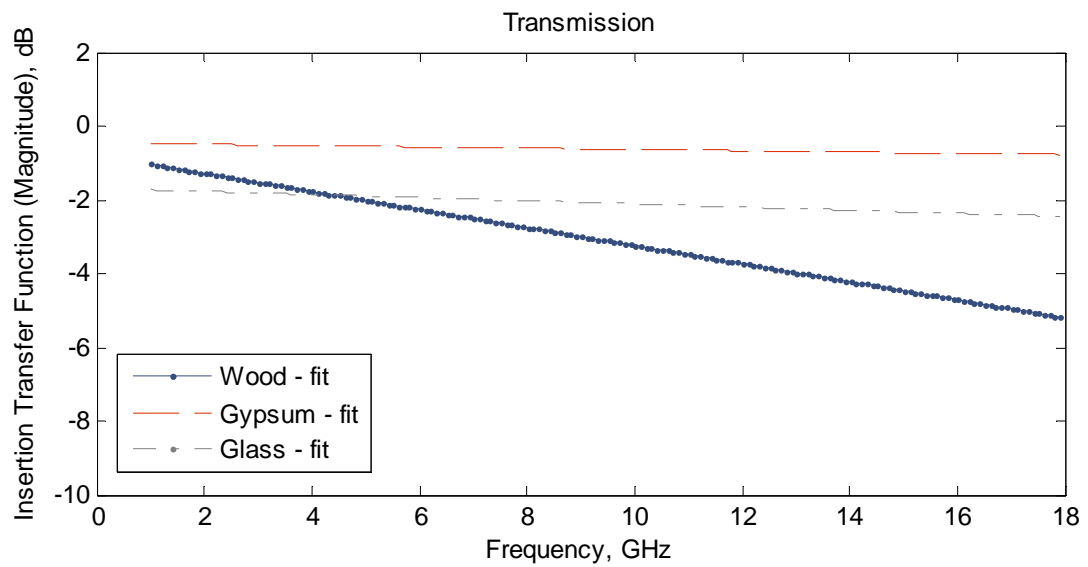
Results obtained from transmission measurements for the magnitude of the insertion transfer function calculated from equation (3.2) are shown in Figure 3.9 for the three

materials. Both the measured raw data of the transfer function and their fits are shown in Figure 3.9 (a) and (b) respectively. Wood shows a higher loss as expected with up to 6 dB loss at 18 GHz attributed to its composition and thickness. We also can observe the ‘wiggling’ in the glass curve which is related to its small thickness; therefore errors are bound to occur.

In Figure 3.10, the extracted dielectric constants are given for each material. Erroneous data have been removed from the results as seen at around 16 GHz (see Figure 3.13 for erroneous data). We relate this issue to the spectral limits of the antenna as indicated by the null at around 15.5 GHz – 16 GHz in Figure 3.6(a) and is more pronounced for reflection-type measurements as will be seen later in Figure 4.5(a). This means that, at that frequency, very little signal is transmitted. This problem is also reflected in the antenna test results (see Figure A2) by the numerous large side lobes in the antenna pattern starting from around 15 GHz. The results for the antenna gain also showed a loss of 4 dB from 14 dB at 13 GHz to 10 dB at 16 GHz. This has manifested on most of the results including those from reflection measurements if we observe. Because of the presence of noise in the data, the one-dimensional algorithm uses a search that is bounded (minimum constrained search) to enable it converge. An initial guess is taken for the dielectric constant from equation (3.20) and the solution obtained is used as an initial guess for the next point till all frequency points are solved. Figure 3.10(b) also shows quadratic fits for the dielectric constants. The coefficients for these fits can be found in Table 3.8. All three materials have uniform structure, therefore, examining Figure 3.10, we see that the dielectric constants, in the average sense; exhibit a decreasing trend with



(a)



(b)

Figure 3.9: Transmission insertion transfer function versus frequency for different walls, (a) Measured, (b) Fits to measured data

frequency. Glass shows a slightly more negative slope and this is because dielectric constants tend to be higher at low frequencies.

As mentioned earlier, the loss tangent and dielectric constant were derived from the insertion transfer function using the low-loss analysis method (one-dimensional root search). In Figure 3.11, the loss tangents are shown. It is worthy of note that for most materials, measuring the loss is more difficult than measuring the real part of the complex permittivity [Gey90].

The attenuation constant in dB/m, is calculated from equation (2.14) where the unit is in Nepers/m (Np/m) using the following,

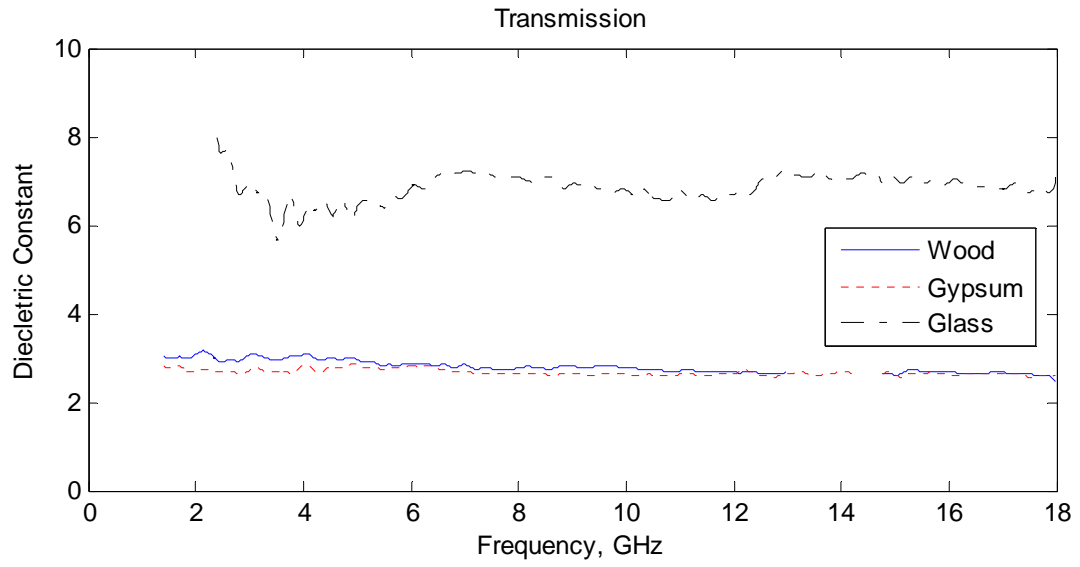
$$\alpha(\text{dB} / \text{m}) = 20 \log(e) \times \alpha(\text{Np} / \text{m}) = 8.686\alpha(\text{Np} / \text{m}) \quad (3.21)$$

Figure 3.12 shows the attenuation constants for wood, glass and gypsum board. This indicates the attenuation of the field strength as it passes through the media. The attenuation constant for wood increases roughly linearly with frequency, from around 60 dB/m at 4 GHz, to 250 dB/m at 16 GHz.

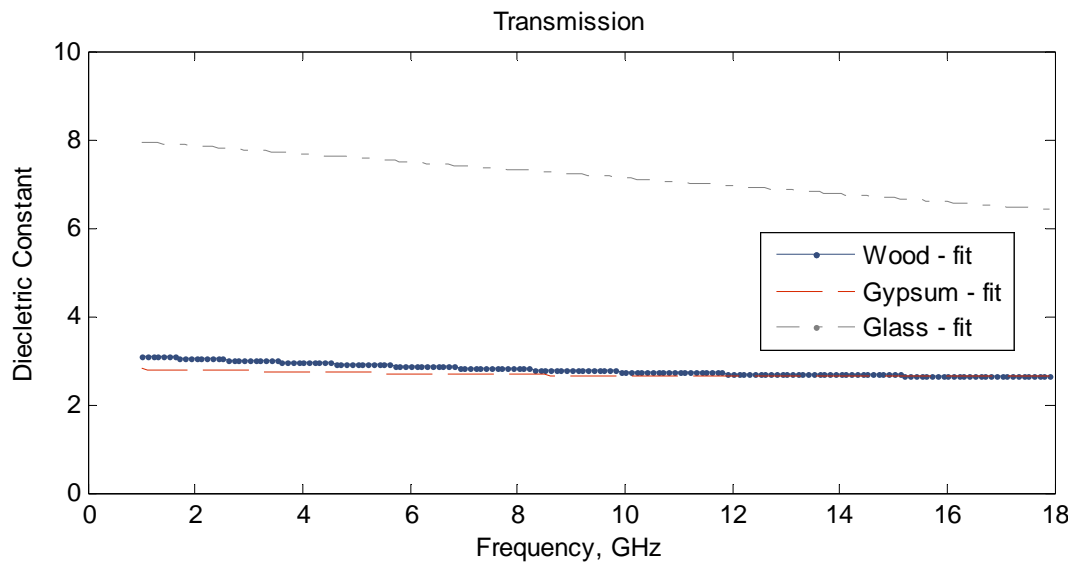
TABLE 3.8: Coefficients of linear and quadratic fit for the extracted parameters

	Coefficients of linear (Figures 3.8(b), 3.10(b), 3.11(b)) or quadratic fits (Figures 3.9(b), 3.13(b)) to extracted the parameters $-af + b$ or $af^2 + bf + c$ , $f(\text{GHz})$								
	Wood			Glass			Gypsum		
	a	b	c	a	b	c	a	b	c
<b>Insertion transfer function</b>	-0.245	-0.785	--	-0.0424	-1.687	--	-0.0175	-0.4615	--
<b>Dielectric constant (transmission)</b>	0.0016	-0.056	3.1565	-0.910	8.0396	--	0.00081	-0.0257	2.827
<b>Dielectric constant (reflection)</b>	-0.000945	-0.091	4.1995	-0.0066	-0.028	7.4192	-0.0013	-0.009	3.422
<b>Loss tangent</b>	-0.000906	0.119	--	-0.000903	0.0273	--	0.007+0.0003i	-0.093-0.002i	--
<b>Attenuation constant</b>	14.91	12.78	--	3.3662	16.774	--	3.589-0.7i	11.4+4.1i	--



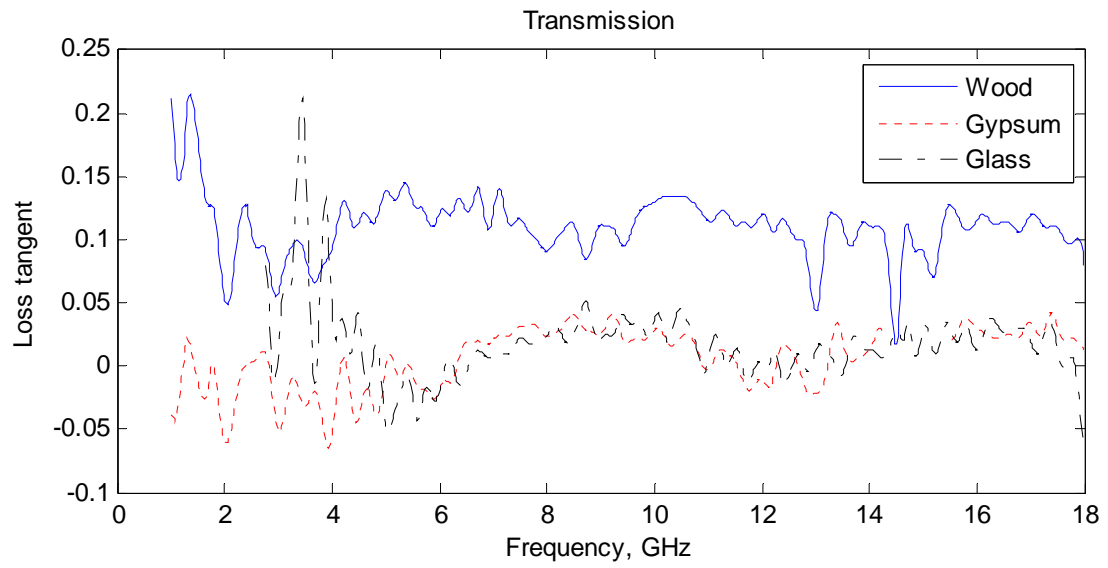


(a)

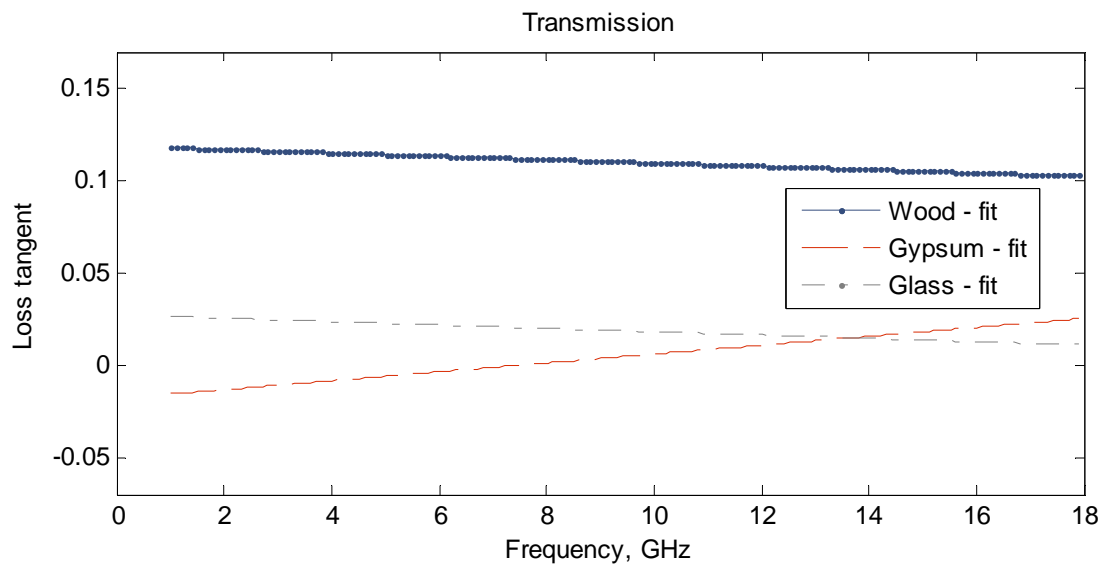


(b)

Figure 3.10: Transmission: dielectric constant versus frequency for different walls

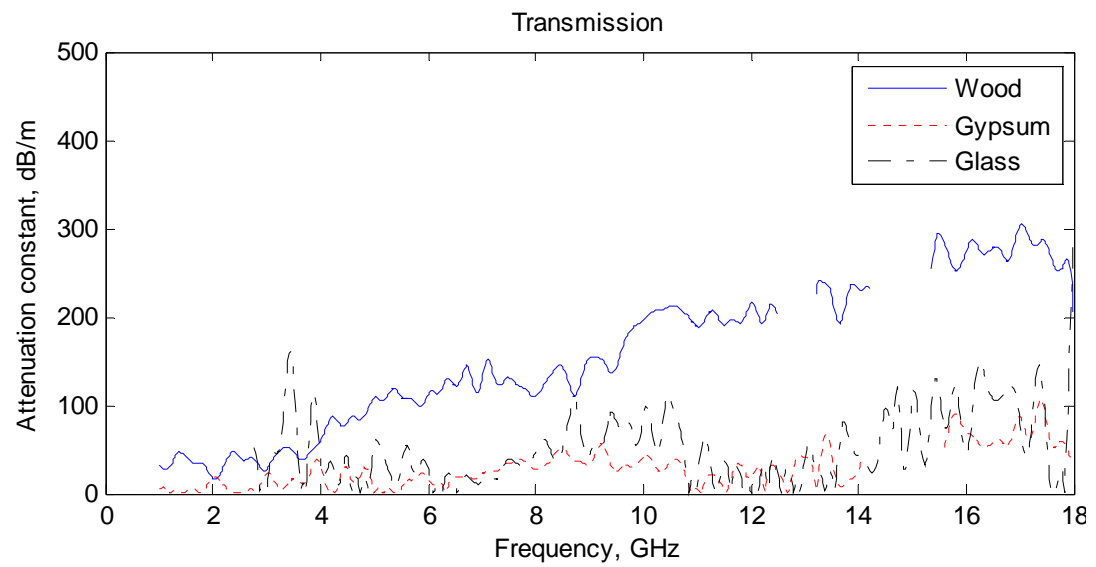


(a)

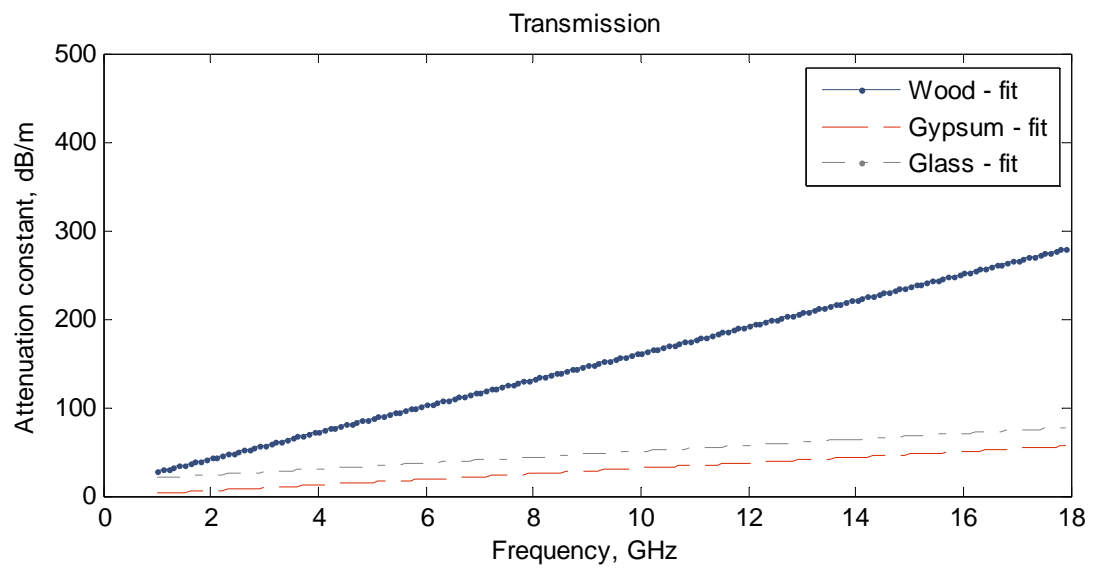


(b)

Figure 3.11: Transmission: Loss tangents versus frequency for various walls

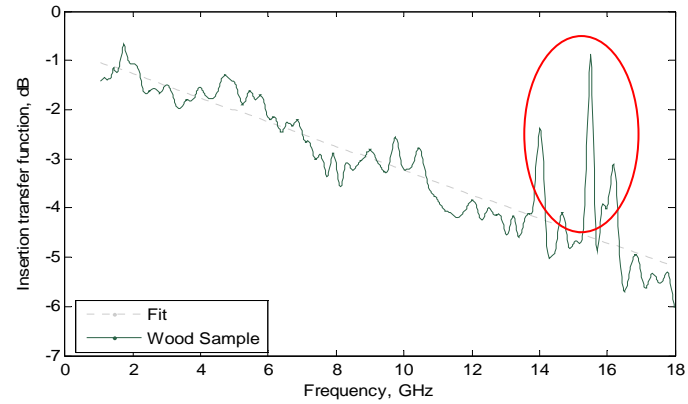


(a)

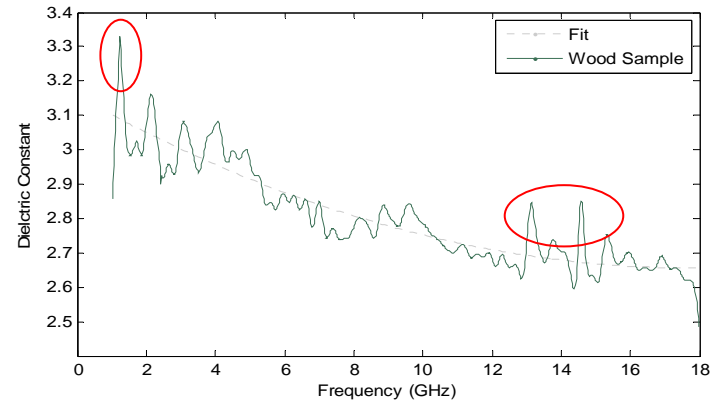


(b)

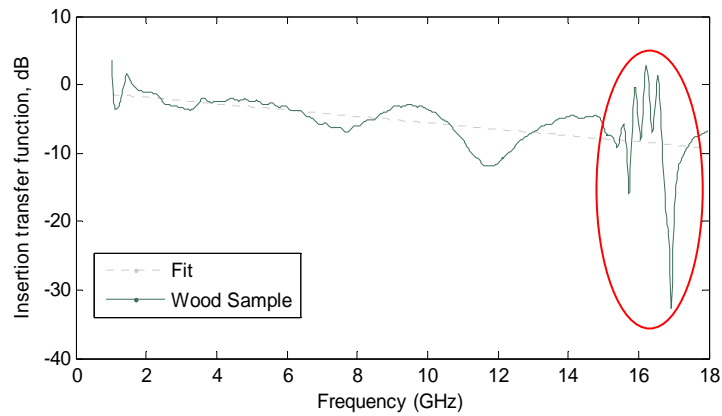
Figure 3.12: Transmission: attenuation constant for the different walls



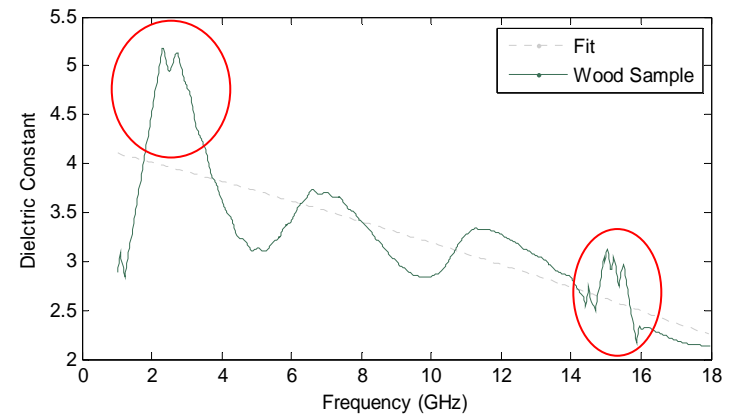
(a)



(b)



(c)



(d)

Figure 3.13: Showing Erroneous data points for; (a) Transmission-insertion transfer function, (b) Transmission-dielectric constant, (c) Reflection-insertion transfer function, (d) Reflection-dielectric constant

### 3.6.2 Reflection Measurements Results

The same model was used to compute the wall parameters for the reflection measurements. In section 3.3, we indicated that the procedure for carrying out the reflection experiments was slightly different from that of transmission because both antennas are collocated on the same side of the wall, and to enable the use of the same model for characterization, the wall thickness is assumed to be twice the original size. This is because the signal has to propagate twice through the wall before arriving at the receiver.

The dielectric constant is shown for wood, glass and gypsum, in Figure 3.14. Calculating the dielectric constant and hence, the loss tangent for glass from the reflection measurements was difficult because of the multiple reflections arriving at the receiver at the same time from the glass surface, the aluminum sheet behind it, and from internal slab reflections making time gating difficult. In particular, a large part of the signal is reflected from the glass surface even before passing through the wall. This has also made getting the first estimate of the dielectric constant from equation (3.20) using peak-to-peak delay difficult. Thus, the root search algorithm will not converge properly leading to false solutions as indicated by the peaks in the dielectric constant for glass given in Figure 3.14(a). Consequently, the attenuation constant and loss tangent are also affected as shown in Figure 3.16(c) and (d) respectively.

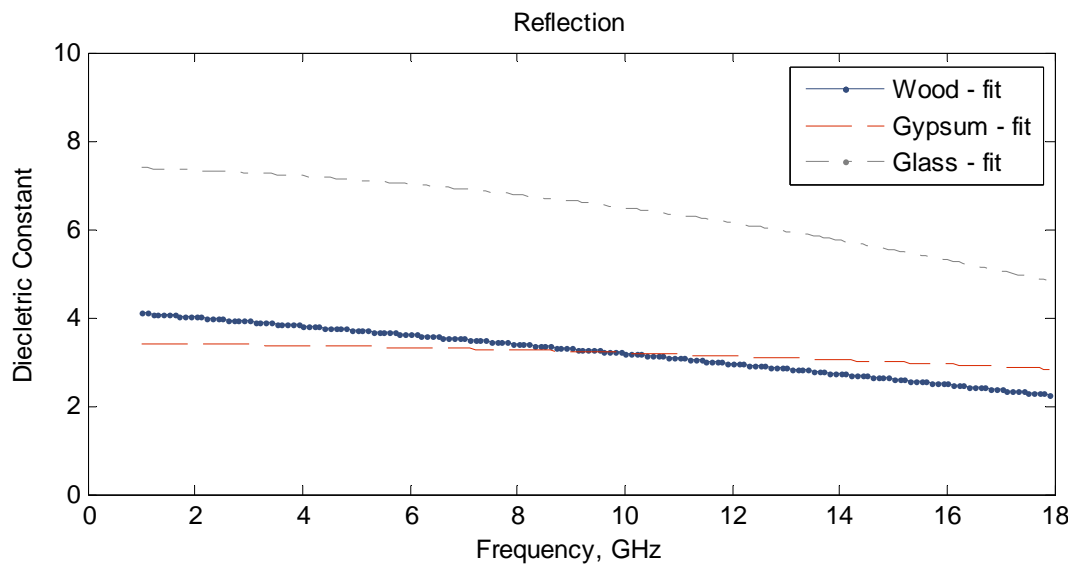
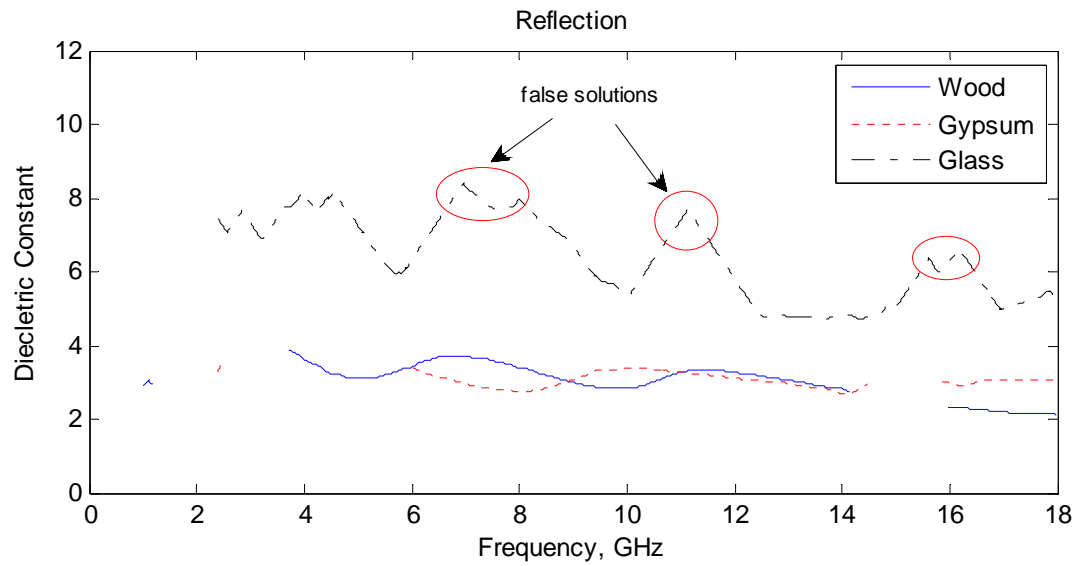


Figure 3.14: Reflection: Dielectric constant versus frequency for the three materials

### 3.6.3 Between Transmission and Reflection

Having mentioned that the same model was used in calculating the dielectric constant for both transmission and reflection measurements, it should be noted that in both cases only normal incidence was considered. In reflection however, the phase of the signal is shifted 180°. In Figure 3.15, results for transmission and reflection obtained for wood sample are shown. We can observe a close agreement between the results for the two methods. Some of the inconsistencies are as a result of sources of errors like the far-field (see section 3.9) or remaining air-gap between aluminum and wall sample. Figures 3.16 and 3.17 shows result comparison for glass and gypsum respectively. Plots for insertion transfer function are showing its magnitude in dB.

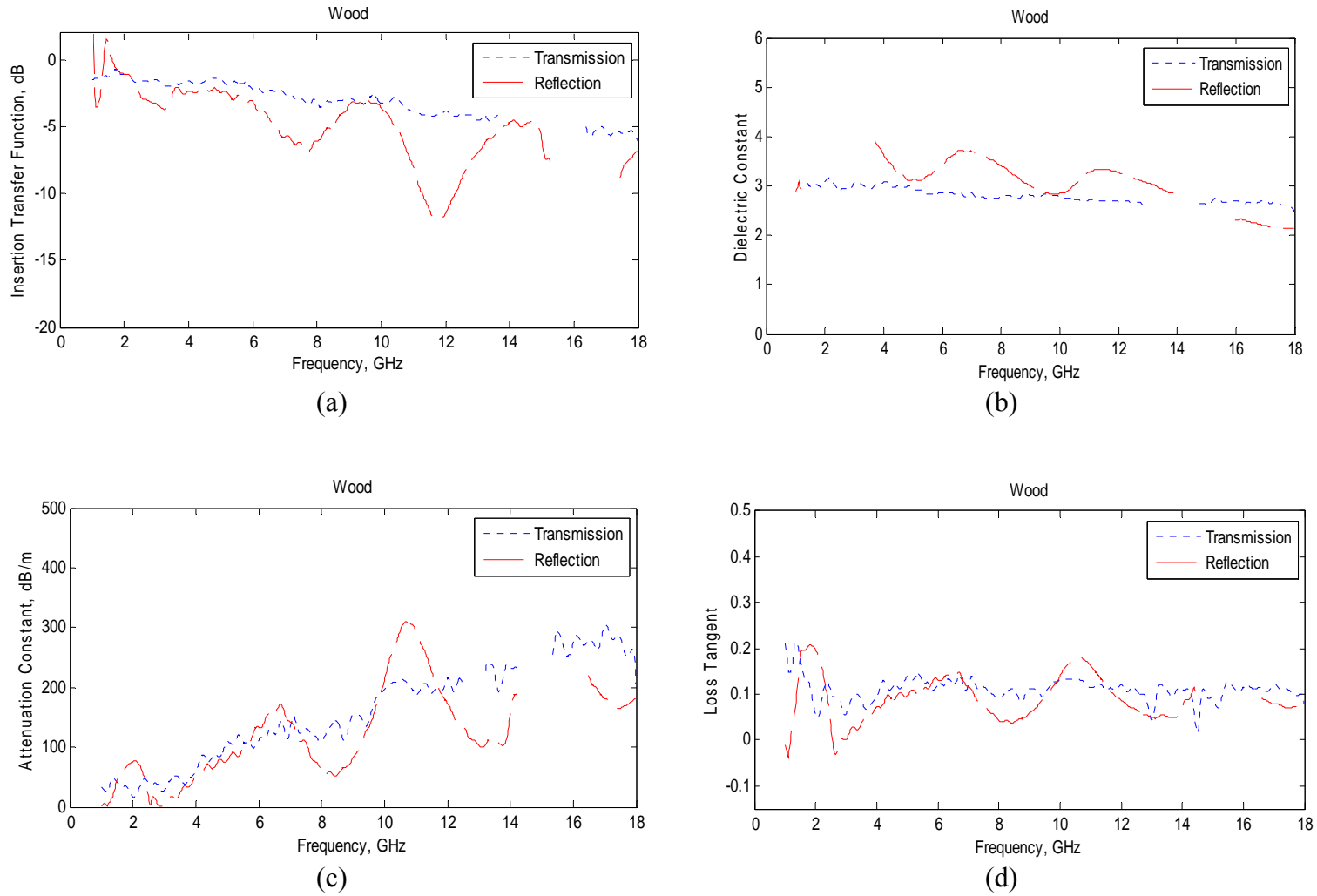


Figure 3.15: Comparing transmission and reflection results for wood; (a) insertion transfer function, (b) dielectric constant, (c) attenuation constant, (d) loss tangent



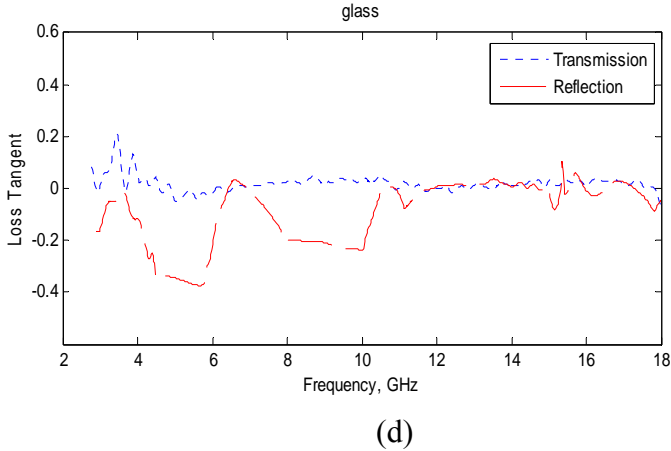
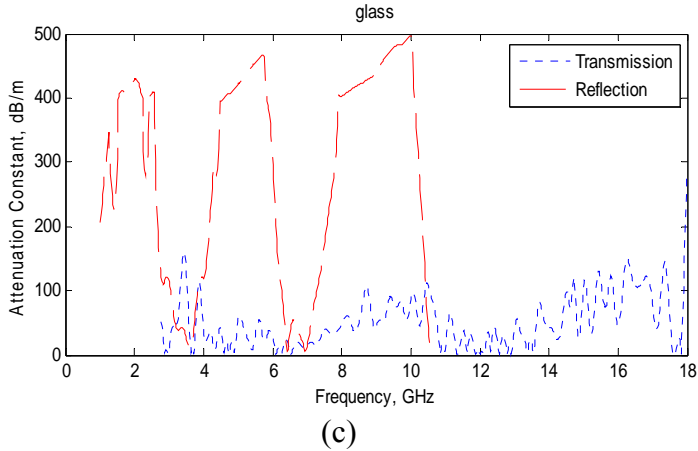
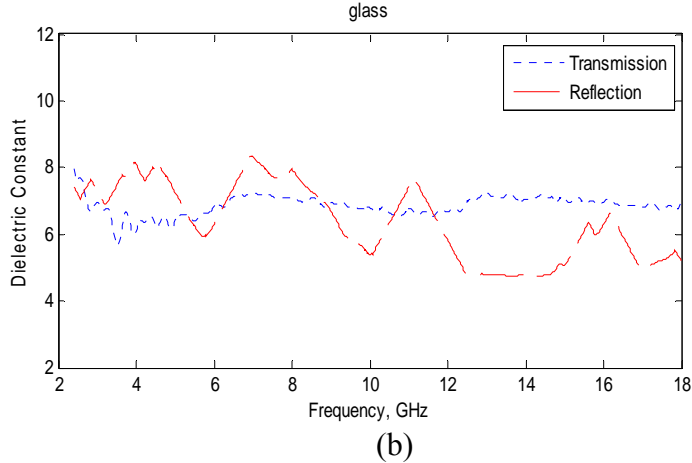
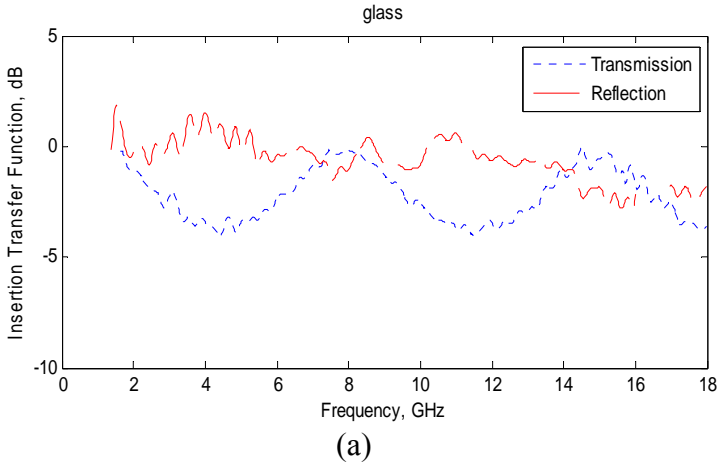


Figure 3.16: Comparing transmission and reflection results for glass; (a) insertion transfer function, (b) dielectric constant, (c) attenuation constant, (d) loss tangent

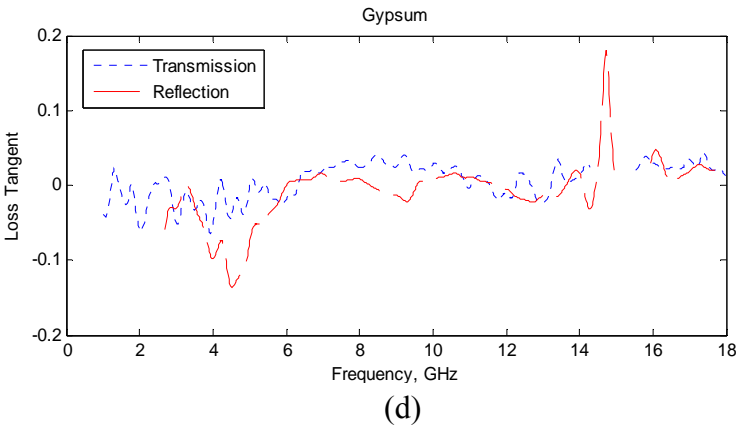
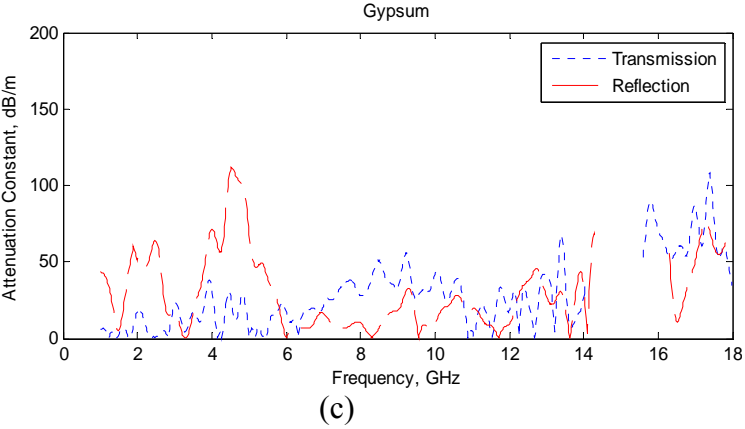
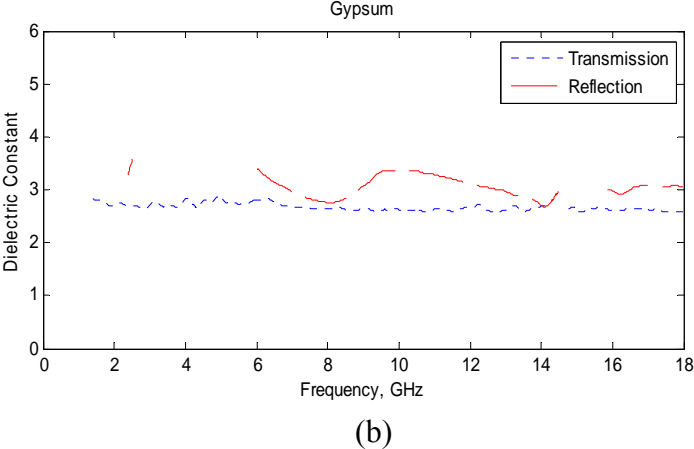
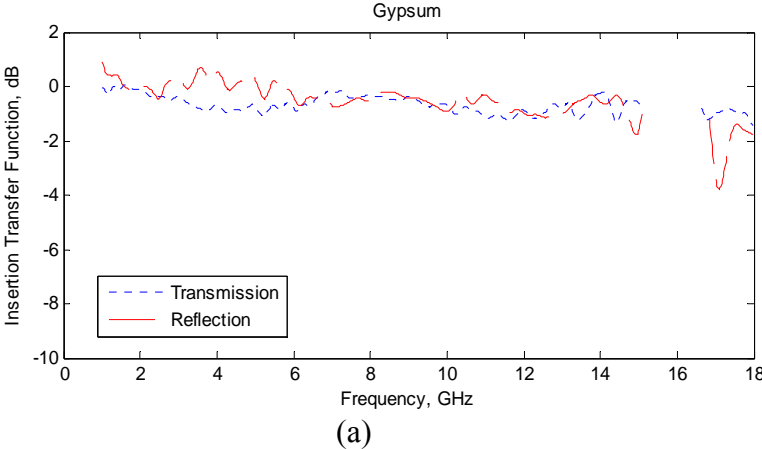


Figure 3.17: Comparing transmission and reflection results for a gypsum (a) insertion transfer function, (b) dielectric constant, (c) attenuation constant, (d) loss tangent

### 3.7 Comparison with Literature

To measure the accuracy of the results, we compare them to what is obtained in the literature. Table 3.9 summarizes comparison between our data and published results. These comparisons clearly indicate that the results for the dielectric constant of materials tested are relatively accurate. However, the accuracy of loss tangent, conductivity or  $\epsilon_r''$  is less certain. This uncertainty is also widely reflected in reported data. For instance [Sag04] reported a mean dielectric constant of 4.45 for gypsum which is entirely different from 2.42, 2.4, and 2.25 reported by [Cui01], [Muq05], and [Tes07a] respectively. Also, [Cui01] gave a conductivity of 0.35 S/m for glass, which is significantly different from  $10^{-12}$  ohm<sup>-1</sup>m<sup>-1</sup> given in [Vae88]. (Note that conductivity and loss tangent are related by the expression  $\sigma = \omega \epsilon_0 \epsilon_r' \tan \delta$  where  $\tan \delta = \epsilon_r'' / \epsilon_r'$ ). We should however, understand that the same materials used by different researchers may vary in composition and sizes, and therefore differences in the results are expected. In general, we believe our results are relatively accurate even with presence of certain limitations (see sources of error in section 3.9) to our measurements. It should also be noted that in many cases the insertion loss of a wall is largely due to reflection and much less due to absorption of the signal, so inaccuracies in the loss tangent does not have a major impact on path loss evaluation [Muq05].

TABLE 3.9: Results comparison with literature

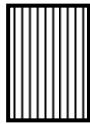
Wall	Results	
Wood	Literature	[Sag04], [Sag05] reported a mean value of $\epsilon_r' = 3.22$ for dielectric constant at 8 – 12 GHz and $\epsilon_r'' = 0.31$ for imaginary part of complex permittivity corresponding to loss tangent of 0.096. [Vae88] calculated dielectric constant for X- Band frequency to be between 3 and 7. Also reported a $\sigma = 10^{-12}$ ohm <sup>-1</sup> /m.
	Our Findings	From Figure 3.10, we read an average value of $\epsilon_r' = 3.0$ at 8 – 12 GHz for transmission measurements and an average of 3.2 from Figure 3.14 for reflection measurements. Figure 3.11 shows a loss tangent of 0.11 at that frequency range. In Figure 3.14, our result for dielectric constant using reflection measurements lie within 3 – 7 at a mean of 3.5.
Glass	Literature	[Cui01] measured and reported a mean value of $\epsilon_r' = 6.06$ at 5.8 GHz with a max value of 6.31 for the dielectric constant. They also measured conductivity to be 0.35 S/m. [Muq05] results showed $\epsilon_r'$ value of 6.7 at 5 GHz for dielectric constant. [Ber00] provided a range for $\epsilon_r'$ from 3.8 – 8 at 3 GHz. [Tes07a] reported an average of 6.6 for dielectric constant and $\epsilon_r''$ of 0.5005 corresponding to a loss tangent of 0.075 in the X – Band range. [Vae88] reported a range of 5 -10 for dielectric constant of glass and a $\sigma = 10^{-12}$ ohm <sup>-1</sup> /m. [Wil02] reported $\epsilon_r'$ of 6.38 for frequency range of 2 – 7 GHz and loss tangent of 0.026
	Our Findings	At 5.8 GHz, Figure 3.16(b) reads a value of $\epsilon_r' = 6.5$ and 6.3 for transmission and reflection measurements respectively and we have a loss tangent of about 0.01 from Figure 3.11(a). Figure 3.10(a) reads a value of 6.2 for dielectric constant at 5 GHz. Our result for $\epsilon_r'$ of glass at 3 GHz in Figure 3.14 is 7, which lies in the range 3 – 8. We have an average of 6.8 for dielectric constant in the X-Band from Figure 3.10(a). And in Figure 3.14(a) an average $\epsilon_r' = 6.6$ in the range of 9 – 11 GHz. Figure 3.16(d) shows an average loss tangent of 0.09 for transmission. Transmission measurements results in Figure 3.10(a) indicate a value between 6.6 – 7.0 in the range 2 – 7 GHz.
Gypsum	Literature	In [Cui01], results show mean $\epsilon_r' = 2.02$ with a max value of 2.42 for the dielectric constant. [Ali03] reported a value of $\epsilon_r' = 2.3$ for dielectric constant and $\sigma = 0.03$ S/m. [Muq05] reported $\epsilon_r' = 2.4$ for dielectric constant at 5 GHz and a loss tangent of 0.005. [Tes07a] also reported $\epsilon_r' = 2.41$ and a corresponding loss tangent of 0.01.
	Our Findings	In Figure 3.10(a) a value of 2.7 can be read for dielectric constant using transmission measurement at 5.8 GHz. We also have between 4 GHz and 6 GHz an average value of 0.006 for the loss tangent from Figure 3.11. Again, Figure 3.10 shows $\epsilon_r' = 2.6$ at 5 GHz and Figure 3.11 shows an average loss tangent of 0.025 in the X-Band frequency range.

### **3.8 Multiple Walls**

The main idea behind considering multiple wall characterization was to investigate how effects such as the penetration loss compare with that of a single wall. Since we are analyzing the wall transfer function, our experiments cascading two(three) different(same) wall materials together (to make one wall) gives us an insight on whether having information on a single wall will enable us predict and make decisions about the multiple walls. In this part of the work, we deal only with the insertion transfer function, so we are able to say how much loss, over the wide frequency band, is there in a single wood wall compared to that of double its size. Furthermore, in the multiple layer configurations, we compare the product of the single layer transfer functions to the transfer function of the cascaded multiple layers (overall transfer function). This arrangement is illustrated in Figure 3.21. Another arrangement investigated is when the double walls are spaced by an air-gap of varying sizes. The insertion loss through double walls spaced 5 cm and 10 cm apart were investigated.

#### **3.8.1 Double Layer**

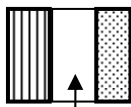
A section of single wood and double glass walls are shown in Figure 3.18, Figure 3.18(c) shows a spaced double wall, while Figure 3.19 shows magnitude of the received signal, insertion transfer function and impulse response for single and double wood walls obtained from transmission measurements. The loss is higher at higher frequencies with up to 4.5 dB difference between single and double walls. For the effect of inter-wall spacing, no significant difference was observed for all the wall materials. Figure 3.20 presents the results for wood.



(b) Single wood wall

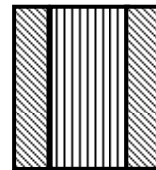
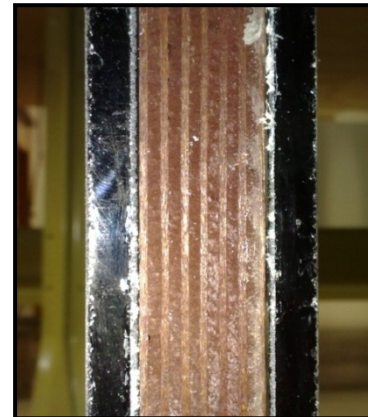


(a) Double glass wall



air gap

(c) spaced wall: wood and gypsum



(d) Three layer: glass-wood-glass

Figure 3.18: Wall configurations

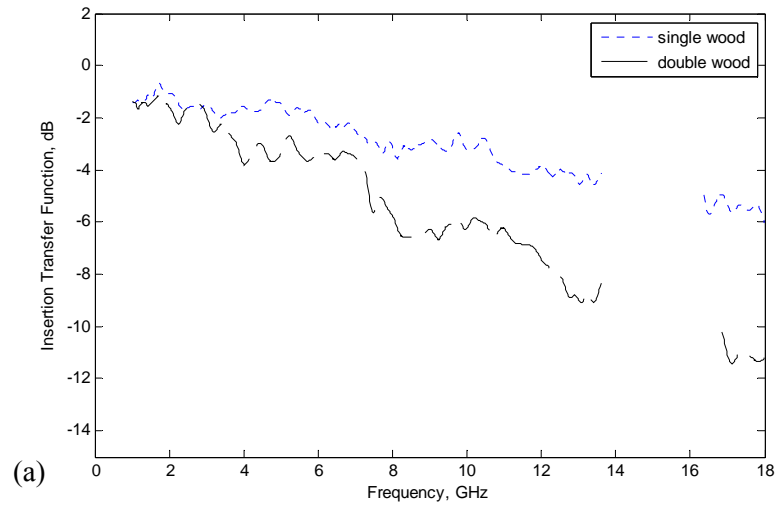
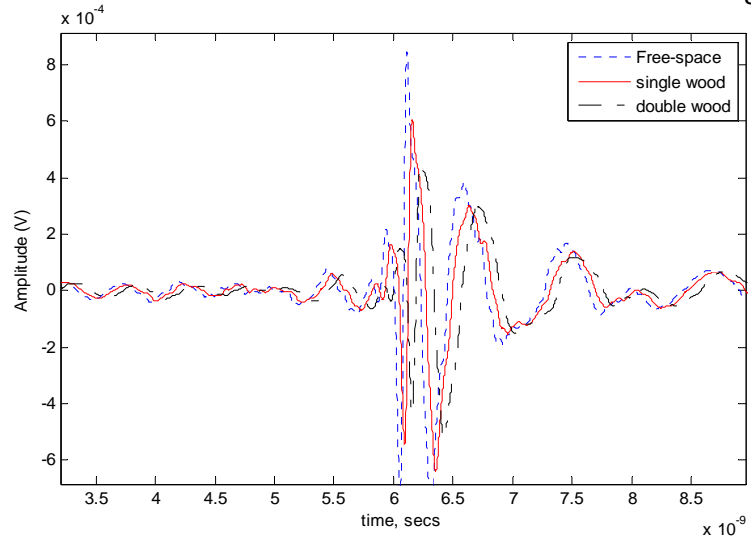
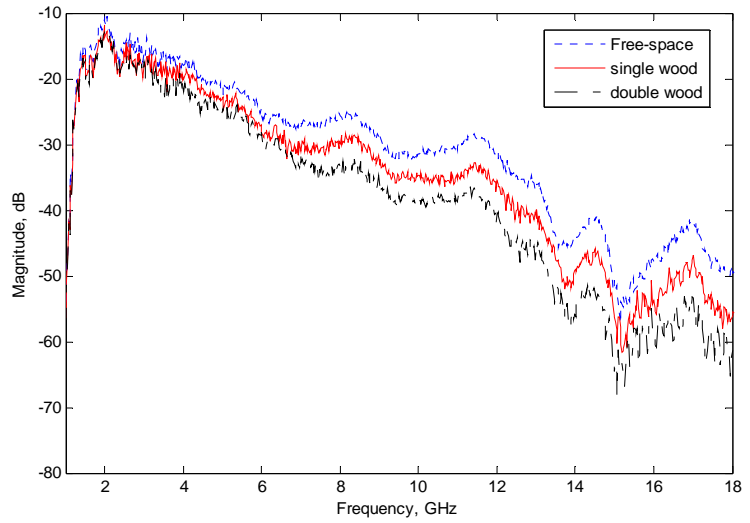
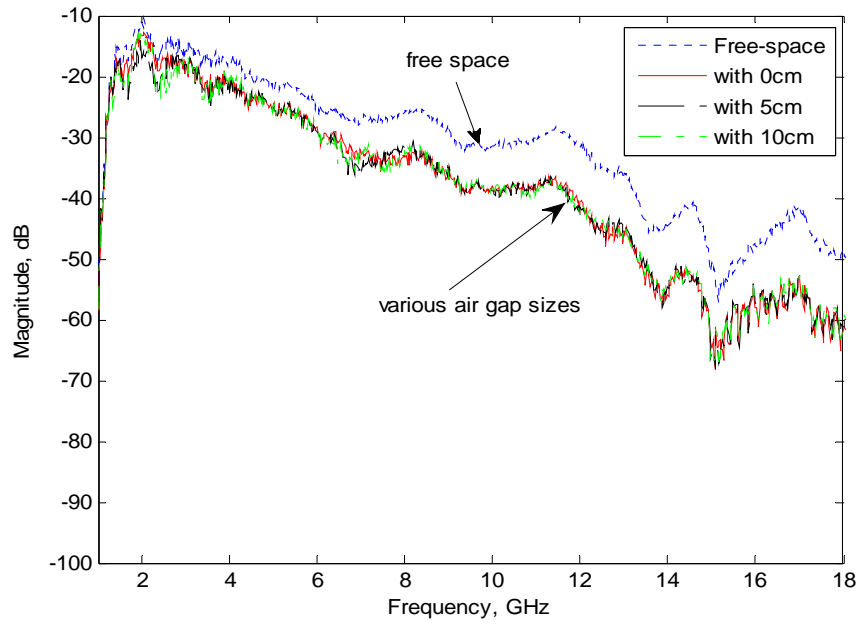


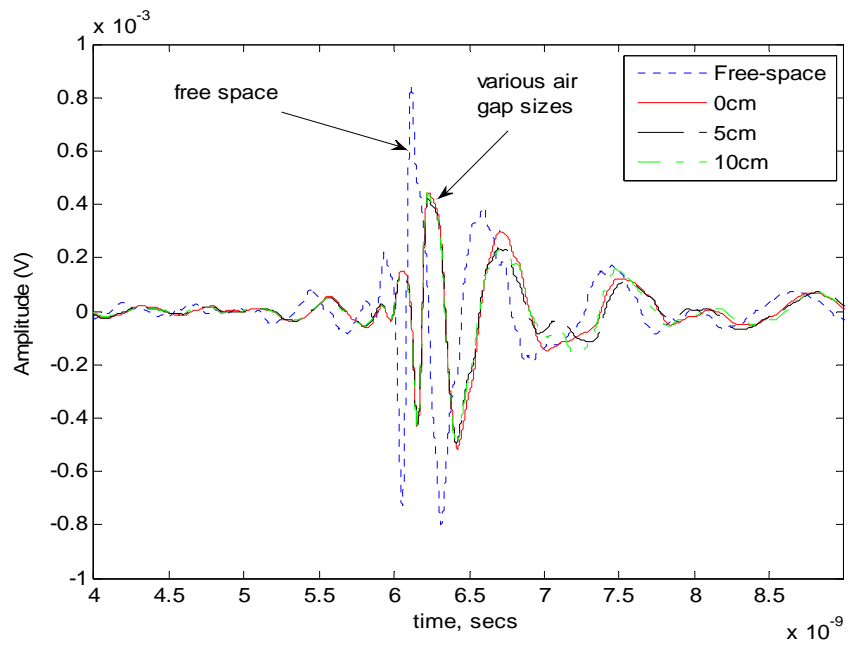
Figure 3.19: Results for double walls showing (a) magnitude of received signal (b) impulse response and (c) insertion transfer function for wood relative to free-space

(a)

(b)



(a)



(b)

Figure 3.20: Effect of inter-wall spacing – (a) magnitude, (b) impulse response for wood



### 3.8.2 Three Layer

The three layer configuration for glass-wood-glass is shown in Figure 3.18(d). Figure 3.22 shows products of single layer un-gated insertion transfer functions plotted versus frequency compared with transfer function of cascaded three layers for wood-glass-wood and wood-gypsum-glass (see Figure 3.21 for illustration). Close examination of these plots shows that at frequencies from 5 - 10 GHz and from 12 – 18 GHz, they are in good agreement with each other. This will make us conclude that with information on a single wall, we can be able to predict that of multiple walls.

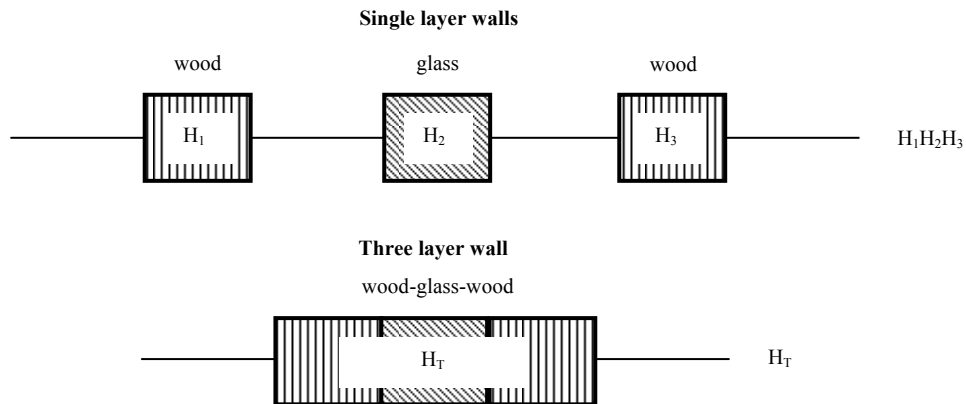
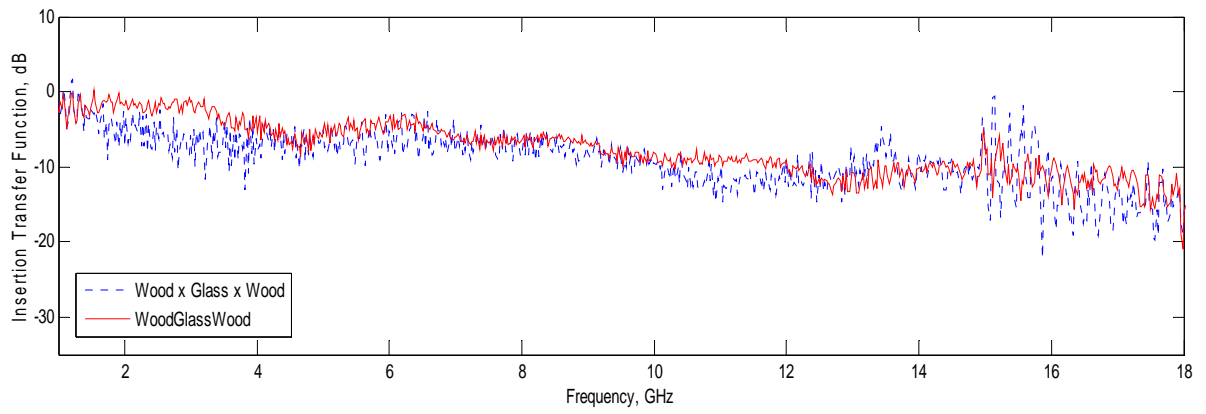
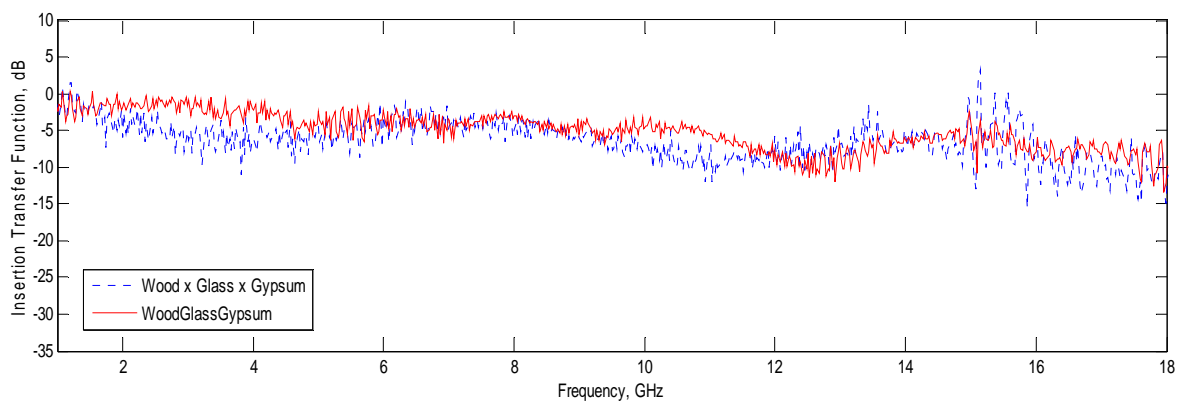


Figure 3.21: Block diagram of single layer and three layer insertion transfer functions



(a)



(b)

Figure 3.22: Three layer measurements

### 3.9 Accuracy Related Issues

In this section, issues related to the outcome of the measurements such as sources of errors, and those concerning the validity of measurements like repeatability and variability analysis, are discussed.

#### 3.9.1 Sources of Error

*Antennas:* The first major effect on the measurement is contributed by the antennas. This results from the inherent spectral limitations of the antenna as seen from Figure A2 in appendix A where several side lobes appear from around 15.5 GHz. We have also seen a direct consequence of this, where erroneous data points had to be removed from our results for the wall parameters. Another form of errors due to antennas is antenna alignment errors between free space and through wall measurements. An angular error in antenna pointing results in an error in the relative spectral content between the two setups and a corresponding error in the magnitude of the transfer function. That would then primarily affect the accuracy of the computed loss tangent versus frequency. In the low-loss analysis method (Equation 3.17 – 3.19), an error in the computed dielectric constant will propagate into an error in obtained loss tangent because the loss tangent depends on both the insertion transfer function and  $\epsilon_r'$ . This means also that the loss tangent error will be cumulative and more than in the dielectric constant or insertion transfer function. A related form of error is antenna – wall separation. Usually, a plane wave assumption is made in computing the wall parameters whereas, practical and physical limitations do not allow for far field approximation. The spherical-wave spreading error is minimized by moving the wall away from the antenna, but this reduces the signal strength and in turn

reduces the spectral content necessary for reliable characterization. It also increases the error due to wall edge effects.

*Cables and Connectors:* As discussed in section 3.2, one of the cables (Cable C) available for our use was 4.5 m long. This constituted a major source of signal loss particularly at high frequencies (see Figure 3.2). Connector mismatch is also a major issue. Figure 3.23 shows the effect (nulls at 2, 6.5 and 9.5 GHz) of connectors when Cable A, Cable B and Cable C are connected together using N – type to N – type female adapters to make one single Cable ABC.

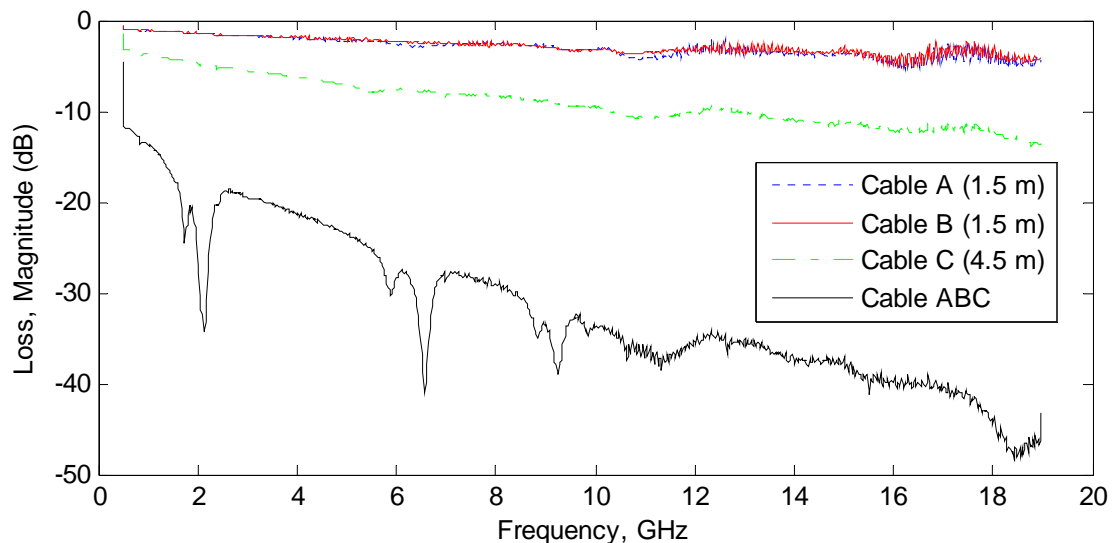


Figure 3.23: Effect of distance and connector mismatch

*Measurement setup and Lab environment:* The arrangement of the wall setup particularly for reflection experiments also contributed significantly to the outcome of the experiments. Air gaps might have existed between the sample material and the aluminum

reference plate causing reflections that affect the pulse shape. Edge effect as a result of diffraction at the sides of the wall is also another issue. Ideally, the measurements should be carried out in an anechoic chamber where reflections from the ceiling and the floor are absorbed. However, our measurements were carried out in a lab with many reflectors such as tables, metal cupboards and drawers, chairs, and lab materials like antennas, power meters etc. Though most of the effect of these items can be removed through calibration, others constitute series of random errors which cannot be easily removed by calibration.

### 3.9.2 Repeatability and Variability Analysis

**Repeatability** of measurements allows us obtain the same results for measurements taken at different instances of time for the same wall sample. This helps in evaluating the precision of the measurements. Measurements with high precision are said to be repeatable [Muq03b]. Figure 3.24 shows repeatability for a sample of wood (Wood 2). For this case, measurements were taken two times at different intervals. Observing the plots of the insertion transfer function and dielectric constant, we see that there are negligible differences between them. We can therefore conclude that the measurements are repeatable.

Measurements are said to have low **variability** if they yield approximately the same results for different samples of the same material (Wood 1 & Wood 2). Here two different samples of wood are measured and the results are shown in Figure 3.24. On close examination of these plots, we will note that though there is some degree of variability between the two samples, the differences are quite minor. For wood, it could be attributed to moisture content of the samples.

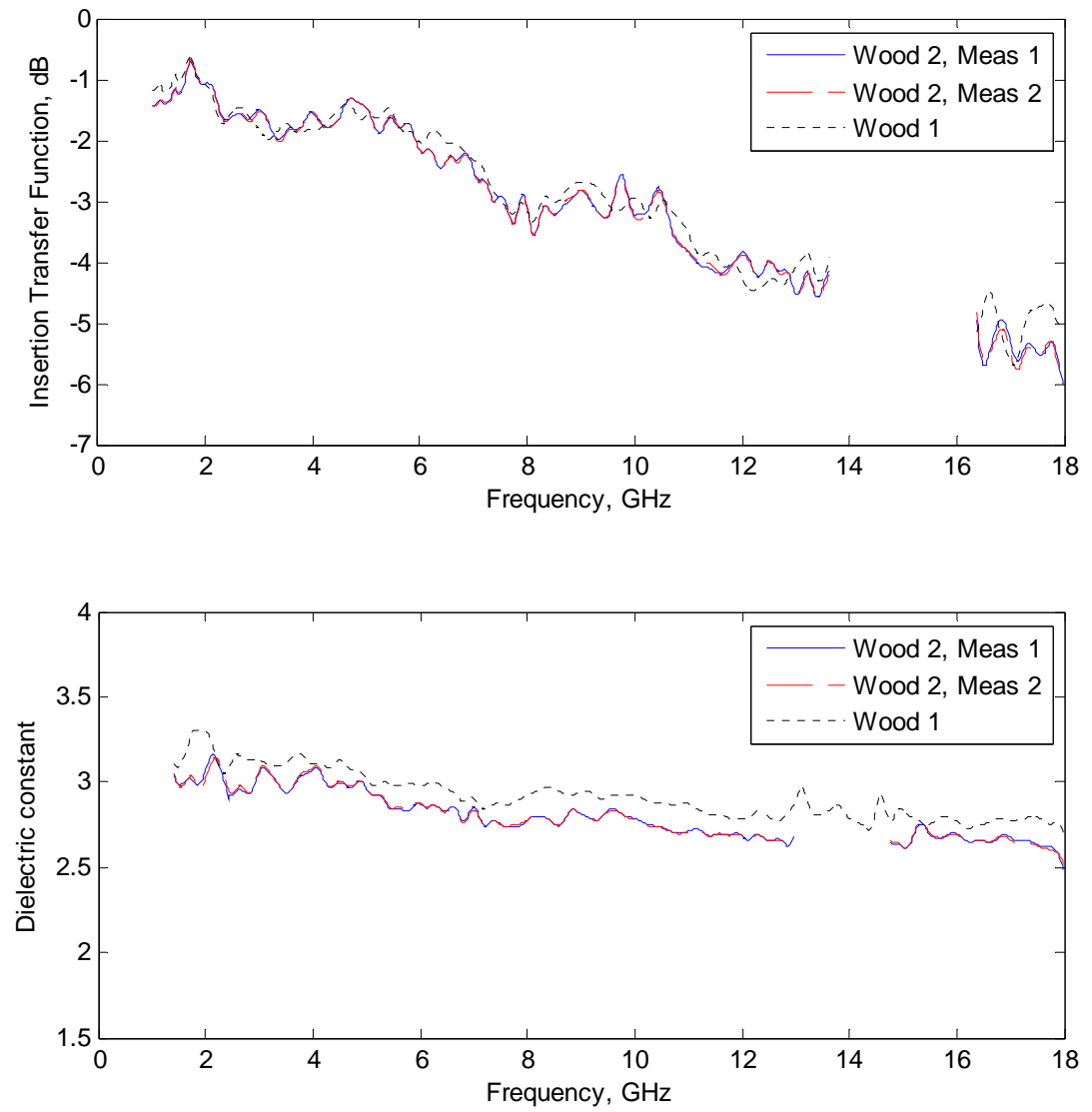


Figure 3.24: Repeatability and variability analysis

# CHAPTER 4

## 4 WALL COMPENSATION

### 4.1 Introduction

UWB through wall radars have been of long-standing interest, as they have been used in military applications for several decades. Their large absolute bandwidth offers high resolution with improved ranging accuracy. They found applications in rescue missions, behind-the-wall targets detection, surveillance and reconnaissance, and a host of other applications.

While penetrating through a material, an electromagnetic wave for through wall imaging and detection may change its speed significantly. This is closely related to the wall thickness and composition, its dielectric constant, and the angle of incidence of the wave. In addition to slowing down, the signal gets attenuated and undergoes refraction as it passes through the wall. It defocuses target image and displaces the target from its true position. False targets can also be present in the radar images. These effects are more pronounced for walls with higher dielectric constants or in presence of multiple walls between target and radar [Ahm07]. Wall compensation therefore, is when effort is being

made to correct the adverse effect of the wall on the outcome of the detection process so that the true target position can be obtained.

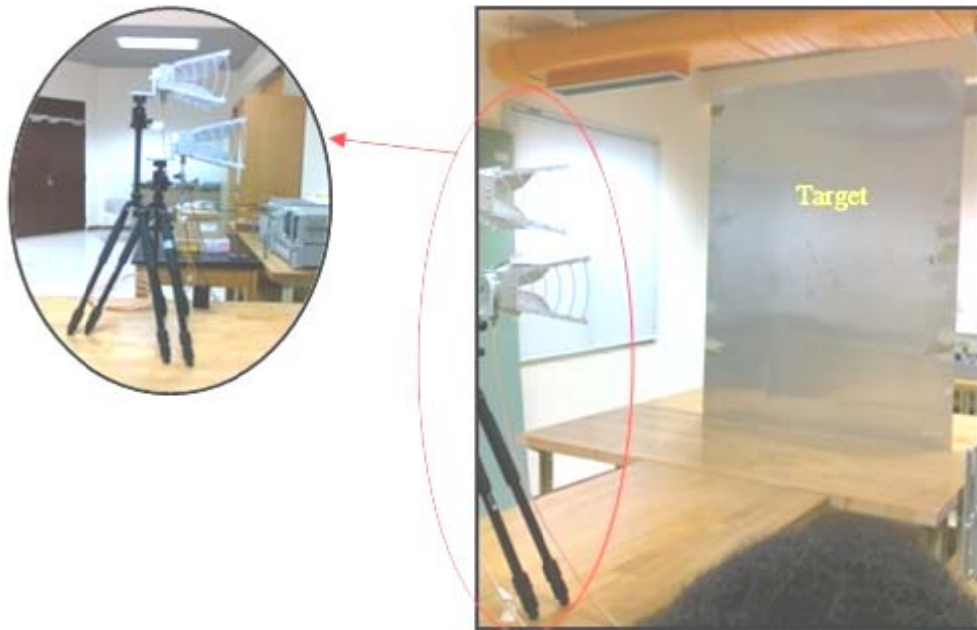
In this chapter, we demonstrate wall compensation by using wall information obtained from the wall characterization to correct the position estimation of the target object. This is achieved through conducting some experiments. This work is not performing imaging of objects behind walls, but rather performing compensation for localization applications and demonstrates the advantage of wall compensation to reduce the positioning error.

## **4.2 Measurement Setup and Procedure**

The experiments were performed using the same set of equipments used for wall characterization mentioned in chapter 3 including component connections and calibration. An aluminum sheet is used as the target object because it approximately reflects all the energy impinging on its surface. The procedure is described below:

1. The aluminum sheet (target) is put in front of both antennas (collocated on the same side) at a given distance (See Figure 4.1(a)). A transmitted signal from the transmitter is reflected by the aluminum and received by the receiving antenna. This is the reference measurement. (Note that throughout this chapter; we refer to measurements carried out without wall as ‘Target Only’.
2. A wall is then inserted between the antennas and the target with some distance on both sides (Figure 4.1(b)). Another measurement is carried out.
3. Steps 1 and 2 above were repeated for wood, glass, gypsum, and some multiple wall combinations. In each case, frequency domain responses are acquired.





(a)



(b)

Figure 4.1: Target measurements - (a) 'Target Only' (No Wall) (b) 'Target + Wall'

### 4.3 Wall Compensation Methods

Figure 4.2 shows the processed bandlimited time-domain impulse response from the target both with and without a wood wall. There are two main reflections in the case of the target behind the wall. The first (early) response (solid line) indicates a reflection from the wall surface. We can clearly see a delayed and attenuated response from the target when it is behind the wall represented by the second reflection. This delay translated into distance, corresponds to shift in the actual position of the target behind the wall. The dotted line represents the ‘Target Only’ measurement.

Our task is therefore to compensate for this displacement by removing the effect of the wall on the response obtained from the target. This is achieved in three different methods: (1) Using constant amplitude and delay (CDL), (2) Using full frequency dependent raw data (FFD), and (3) Using fitted dielectric constant and fits to the magnitude of frequency dependent data (FIT).

#### 4.3.1 Constant Amplitude and Delay Compensation

In constant amplitude and delay compensation, it is assumed that there is a constant amplitude attenuation due to the wall. It is also assumed that the delay is constant and thus, there is no frequency dependence. For **each** wall, we use the amplitude attenuation **it** incurred during wall characterization as ‘constant amplitude’ to compensate for the amplitude loss the same wall suffered in the target measurements. A similar approach is performed on the delay, and the time is corrected by a value equal to the delay the wall offered during the wall characterization measurements. Table 4.1 shows the constant values used for amplitude and delay. Figure 4.3 shows the compensated signal using this

approach compared with the response obtained without a wall for the case of wood, glass, and gypsum. The constant amplitude used information from transmission measurements, while the constant delay used is twice the value of the delay from transmission measurements. This is because the target measurement requires the signal to propagate twice through the wall. Delay from reflection measurements can also be used; however, the one from transmission gives better compensation.

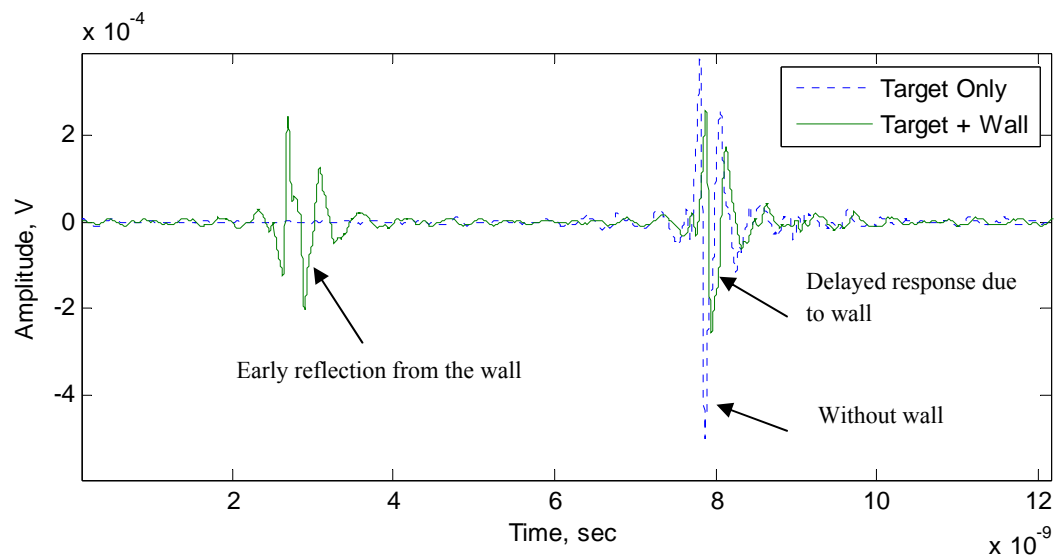
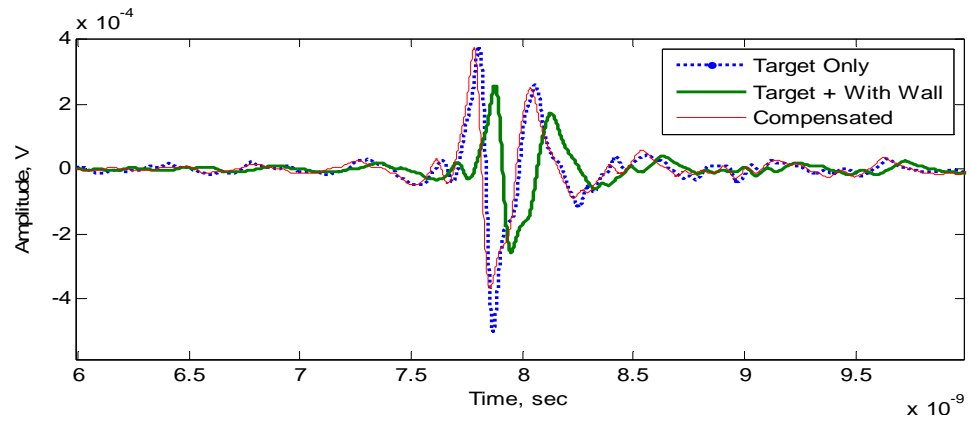
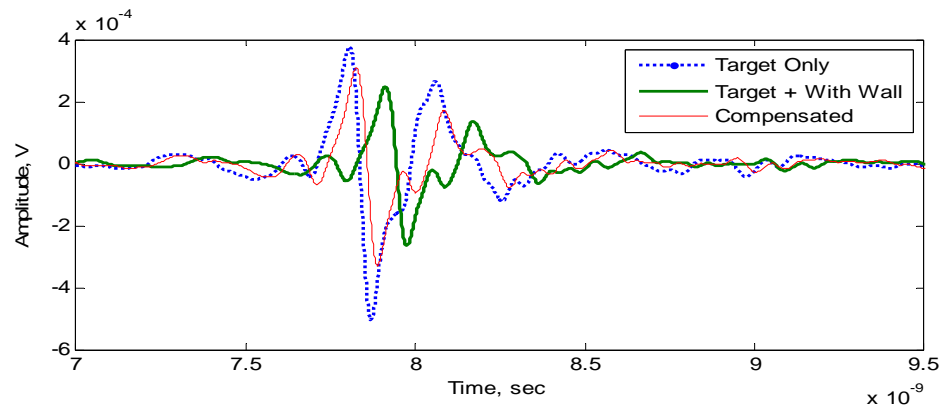


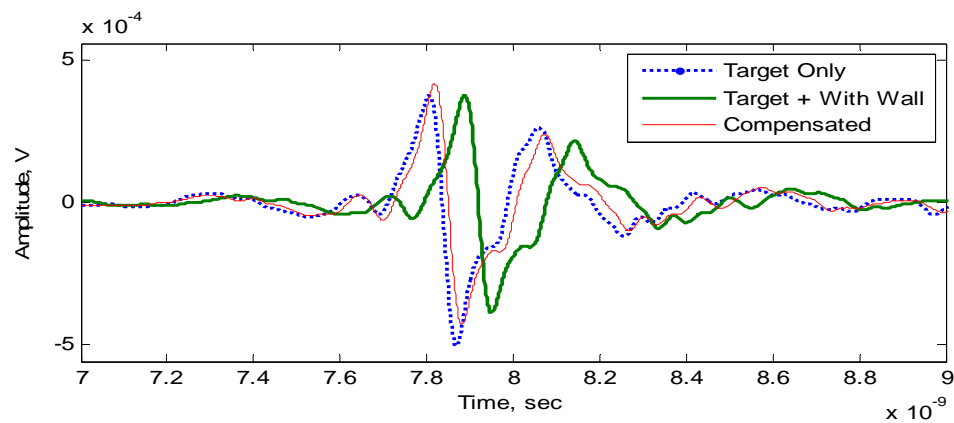
Figure 4.2: Reflections from target object with and without obstruction



(a)



(b)



(c)

Figure 4.3: Illustrating compensation using constant amplitude and constant delay, (a) wood, (b) glass, (c) gypsum

TABLE 4.1: Showing constant amplitude and constant delay values used

Wall	Constant amplitude (scale)	Constant delay (ns)
Wood	1.44	0.08513
Glass	1.24	0.0864
Gypsum	1.104	0.0690

### 4.3.2 Frequency Dependent Data Method

In real life localization situations, the obstruction is usually there. What we have between the localization device and the target can be modeled as a cascade of components including the wall, free-space, target, etc (everything except the wall). Figure 4.4 shows this model. We can assume a total transfer function for this model to be given as

$$H_{WE} = H_W H_E \quad (4.1)$$

where

$H_{WE}$  is transfer function of everything *including* the wall

$H_W$  is insertion transfer function of the wall

$H_E$  is the transfer function of everything *except* the effect of inserting the wall

In order to be able to accurately determine the target's position, the effect of the wall has to be removed by de-embedding the wall it from equation (4.1) by simply dividing the

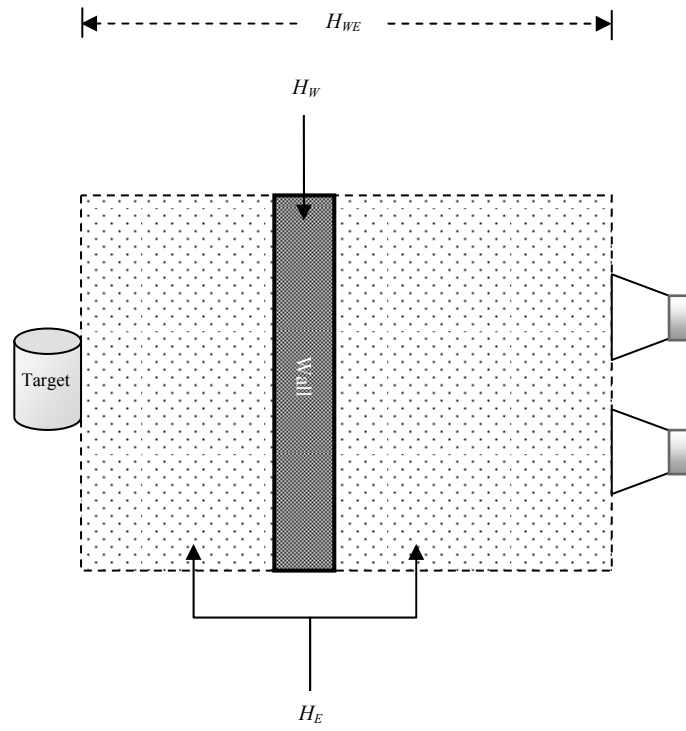


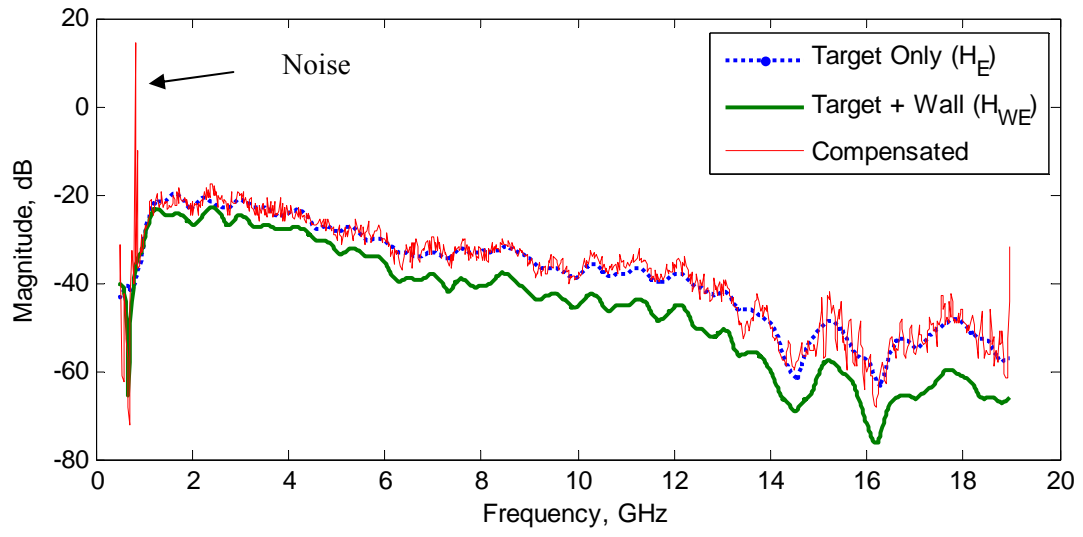
Figure 4.4: Transfer function of the localization scene

total transfer function by that of the wall. This is achieved using our previous knowledge of the wall obtained from wall characterization. The steps used in achieving this are summarized below:

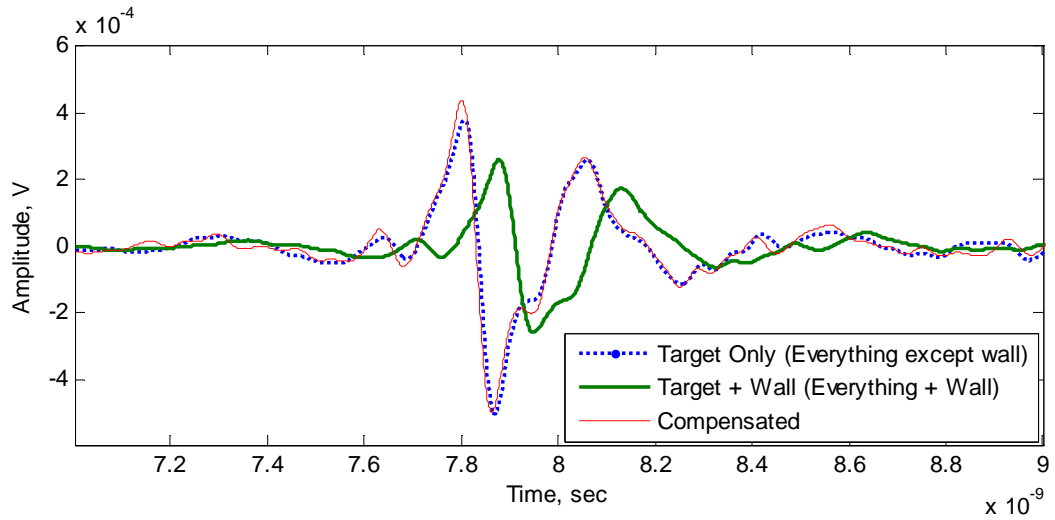
1. Perform frequency domain measurements with and without wall as described in section 4.2, steps 1 & 2, to get response from: (a) target only (with no wall) and from (b) target behind the wall. The later scenario gives us the transfer function  $H_{wE}$  of everything *including* the wall.
2. Use the insertion transfer function of the wall  $H_w$  obtained from previous knowledge (wall characterization) to divide  $H_{wE}$ . This step de-embeds the wall from  $H_{wE}$  resulting in  $H_E$  (transfer function of everything *except* the effect of inserting the wall). This  $H_E$  is a compensated version of the first scenario (a) in Step 1 above.

Figures 4.5 – 4.7 shows the result of using this method to perform wall compensation for our wood, glass, and gypsum walls respectively, both in frequency and time domain.

It should be noted that because of the raw frequency domain data directly obtained from measurements, the presence of noise is major concern. Noise clearly manifests in the time domain after inverse Fourier transform is applied on the frequency domain data. Therefore, noise reduction is performed by filtering the noisy regions around 1 GHz and 15.5 GHz in Figures 4.5(a) and 4.6(a) in the frequency domain before converting to time domain. Another point of emphasis is that, when using  $H_w$  from transmission measurements in performing compensation, the division is made twice, i.e.  $H_{wE}$  is



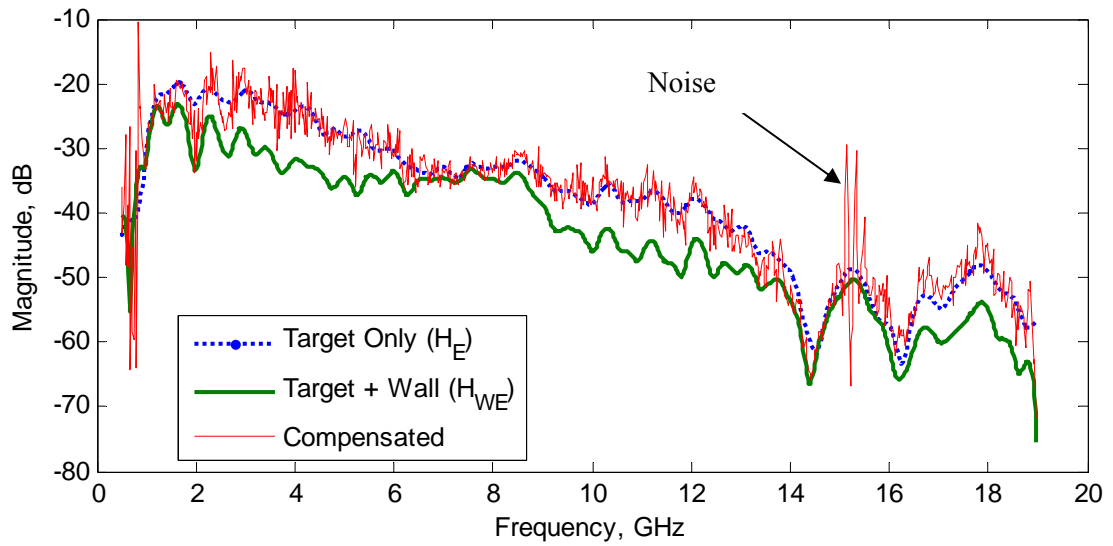
(a)



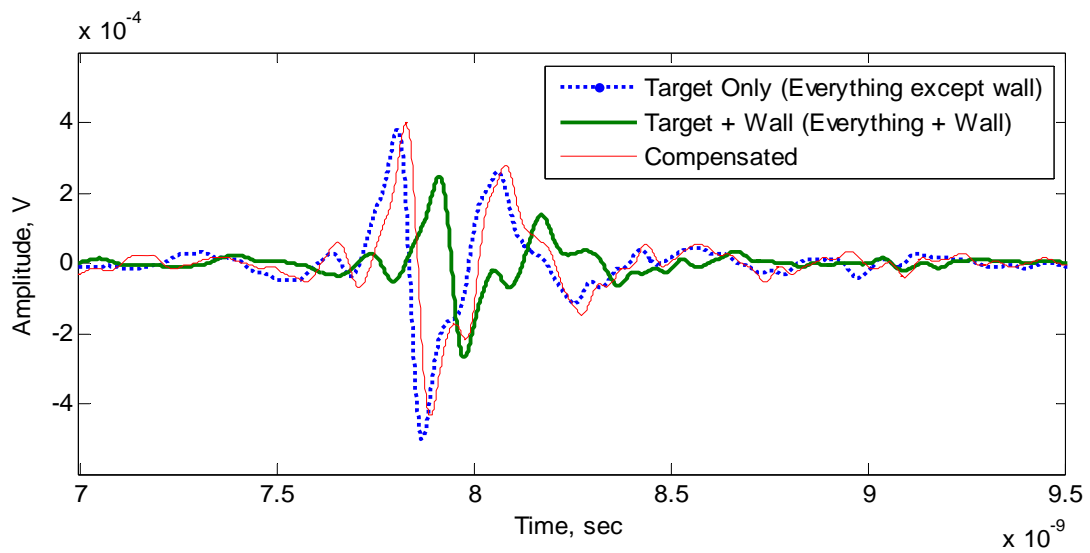
(b)

Figure 4.5: Wall compensation using raw data for **wood** sample in (a) frequency domain, (b) time domain



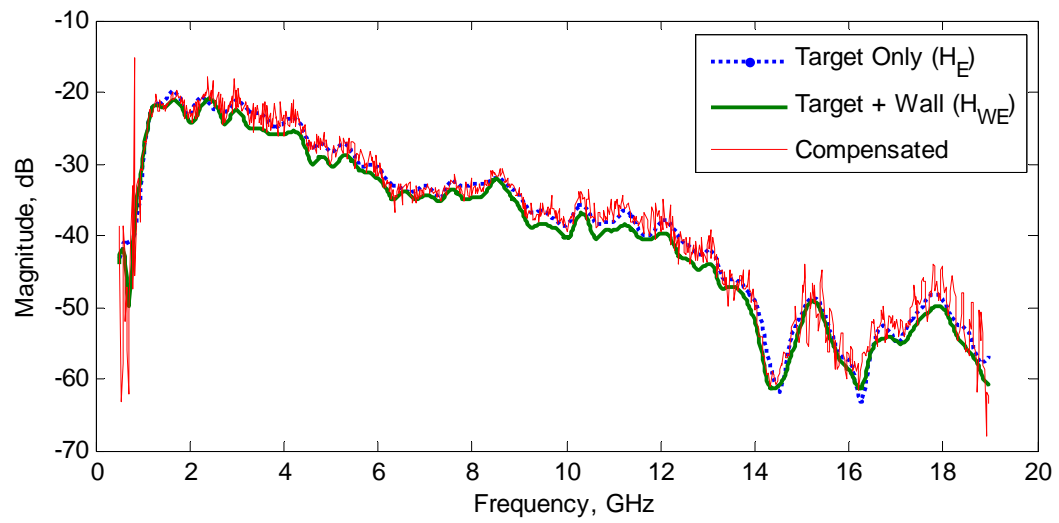


(a)

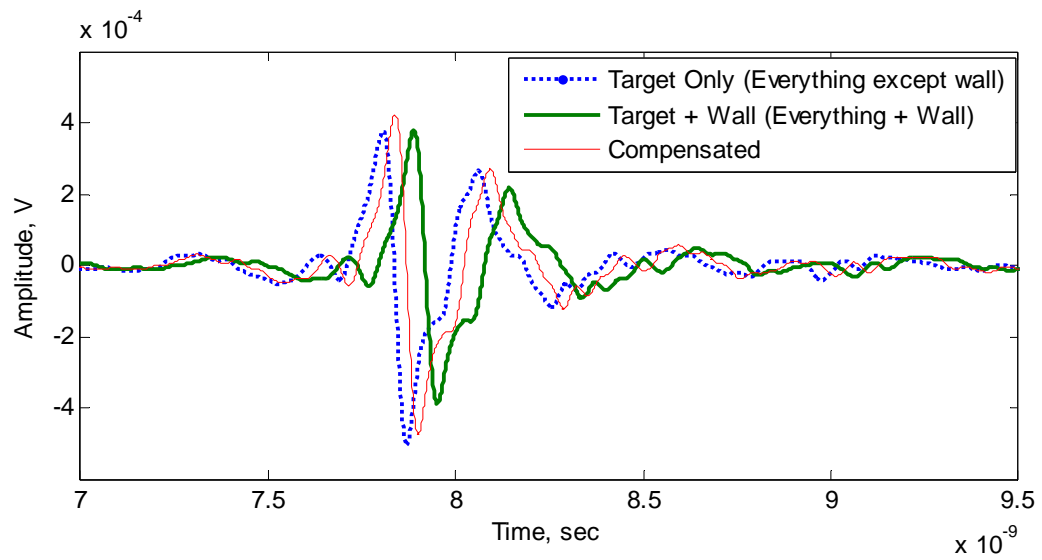


(b)

Figure 4.6: Wall compensation using raw data for **glass** sample in (a) frequency domain, (b) time domain



(a)



(b)

Figure 4.7: Wall compensation using raw data for **gypsum** sample in (a) frequency domain, (b) time domain

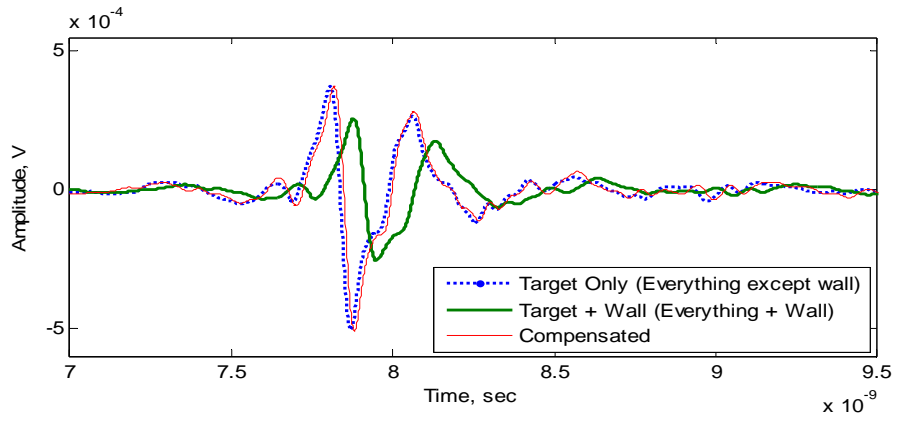
divided by  $H_w^2$ , and when using the transfer function from reflection measurements,  $H_{wE}$  is divided by  $H_w$ .

We can see from all the Figures that there is a close agreement between the compensated responses and the responses obtained from measurements performed without the wall. The advantage of this method over compensating with a constant delay and amplitude is that the pulse shape is corrected. In application like matched filter reception or correlation, pulse shape correction is very important. The advantage can be numerically illustrated using the energy capture.

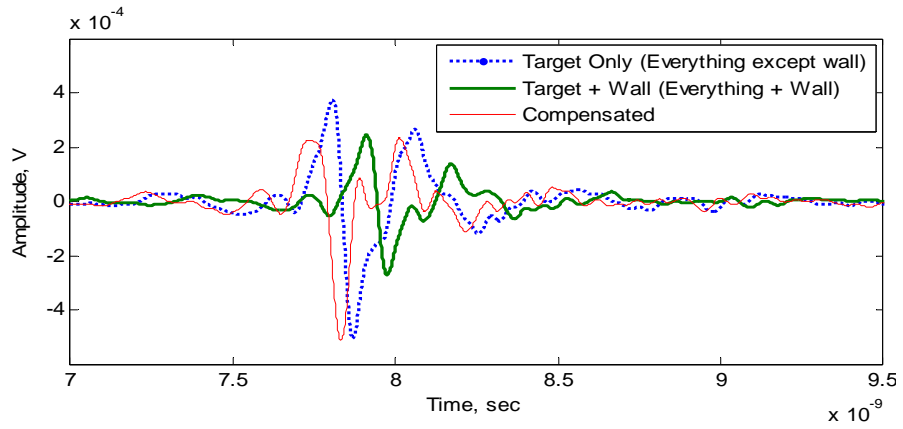
### 4.3.3 Data Fitting Method

As a tradeoff between the above two methods, one can provide the parameters that model the magnitude of the insertion loss of the wall using a linear equation to reflect the frequency dependence of the magnitude of the transfer function. Higher order fits are also possible but not needed especially if the walls used are having some variability.

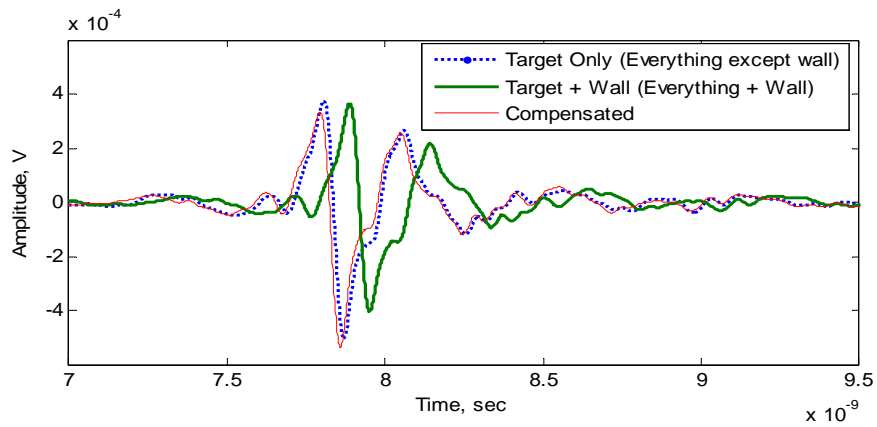
In this method, a fit to dielectric constant whose coefficients are given Table 3.8 in chapter 3 is used to obtain an un-wrapped phase  $\Phi_w$  from equation (3.6). The delay  $\tau_o$  in (3.6) is still modeled with a constant value as in the case with Constant amplitude and delay method. The phase obtained is then used together with the fit to the magnitude of insertion transfer function (having coefficients in Table 3.8), to calculate a complex insertion transfer function  $H_w(f) = |H_w(f)| \exp[j\Phi_w(f)]$  representing the wall. We further use  $H_w(f)$  to divide  $H_{wE}$  (transfer function of *everything including* the wall) as in



(a)



(b)



(c)

Figure 4.8: Wall Compensation using fit to data for (a) wood, (b) glass, and (c) gypsum

equation (4.1) and Step 2 in sub-section 4.3.2 (Frequency Dependent Data Method). The result for compensation using this method is shown in Figure 4.8. Wood and gypsum show good wall compensation indicated by the similarity between the ‘Target Only’ and ‘Compensated’ responses.

In order to assess the accuracy of the methods mentioned above in achieving wall compensation, we will make comparison between results for ‘No Wall’ and that of ‘Compensated’ (estimate) in order to get a measure of similarity between the two results for the methods. We also compare these results with the case where there is no compensation. The comparison will be in terms of the quantities *delay (peak-to-peak)* and *energy capture (waveform shape)*.

#### *Peak-to-peak Delay*

This quantity is useful in positioning applications and can be used to give approximate errors in the true position of detected objects. Since time and distance are related by the expression

$$s = v\Delta\tau \quad (4.2)$$

where  $v = c/\sqrt{\epsilon_r'}$  is the velocity of the wave through the wall of dielectric constant  $\epsilon_r'$ , the speed of light,  $c = 3.0 \times 10^8$  and  $\Delta\tau$  is the peak-to-peak time delay incurred by the signal passing through the wall. The dielectric constant  $\epsilon_r'$  can be a value chosen at the mid-frequency range for the wall material under consideration. Table 4.2 provides

approximate errors in the position of the target due to the three different walls. It also shows approximate errors after compensation has been done for the three methods. For the purpose of Table 4.2, we refer to the three methods with the following abbreviations in parenthesis: Constant Amplitude and Delay (CDL), Frequency Dependent Data (FFD), Fitted Dielectric constants and Fits to Magnitude of Frequency Dependent Data (FIT), and ‘No Compensation’ as (NC).

Since time domain responses are used to demonstrate wall compensation, the peak-to-peak delay was used to find the error due to the wall by comparing the ‘Target Only’ and ‘Target +Wall’ responses. Similarly, the peak-to-peak delay for the ‘Target Only’ and ‘Compensated’ responses are used to get the error after compensating for the wall. An equivalent error in displacement is also obtained. The negative sign in the errors indicate instances where we have ‘over-compensation’; therefore, the peak-to-peak difference will be negative. Note that these figures depend on the dielectric constant and thickness of the walls.

TABLE 4.2: Target position errors due to the walls

			Peak-to-peak error (ns)				Equivalent position error (cm)			
			Due to wall	After compensation			Due to wall	After compensation		
Wall	Thickness (cm)	Assumed $\epsilon_r$	NC	CDL	FFD	FIT	NC	CDL	FFD	FIT
Wood	1.8	3.0	0.07094	-0.01489	-0.006449	0.01161	1.23	-0.25	-0.1	0.2
Glass	0.8	6.5	0.10577	0.01936	0.02193	-0.0606	1.24	0.23	0.26	-0.71
Gypsum	1.2	2.4	0.08126	0.01225	0.03224	-0.0116	1.57	0.24	0.6	-0.22

Studying Table 4.2 closely, we can see that relative to no compensation at all (NC), wood perform better after FFD compensation as indicated by 0.0064 ns error in delay compared to 0.0148 ns and 0.0116 ns for CDL and FIT respectively. CDL gives 0.0193 ns error after compensation for glass which is less compared to that of FFD and FIT. Because peak-to-peak delay is used, changes in pulse shapes of the compensated responses for FFD and FIT will affect the amount of error both in time and space. We also attribute this to the high dielectric constant of glass, even though the thickness of our glass wall is 0.8 cm. Recall that walls with higher dielectric constant tend to defocus target images introducing errors in target positions [Ahm07]. Consequently, up to 0.71 cm error is seen after FIT compensation. For gypsum, FFD has the highest amount of error after compensation with 0.03224 ns corresponding to 0.6 cm error in displacement relative to NC, followed by CDL with 0.01225 ns (0.24 cm error). FIT gives the least. Overall, CDL compensation seems to give less error for the three walls and wood gives a better error performance for all three methods.

### *Energy Capture*

This quantity is useful analysis of signal waveforms. For our purpose, we employ the energy capture equation described in [Win97] to be

$$EC = \left\{ 1 - \frac{\|r(t) - r_c(t)\|^2}{\|r(t)\|^2} \right\} \times 100\% \quad (4.3)$$

where  $r(t)$  is the ‘Target Only’ signal called the ‘true signal’, and  $r_c(t)$  is the ‘Compensated’ signal and it is called the ‘estimate of the true signal’. We take window size of 1 ns around the main pulses (see Figures 4.5 – 4.7(b) and Figure 4.8 (a – c)) for this analysis. To achieve full comparison between the shapes of the waveforms, they are first synchronized with each other, and then the estimate is subtracted from the true signal to get an error as given by the numerator in equation (4.1). If the error is greater than the true signal  $r(t)$ , the percentage energy capture will be negative. Table 4.3 shows how similar, in percentage, the wall compensation results are to the results obtained from measurements without the wall for wood, glass and gypsum, using, Constant Amplitude and Delay Method, Frequency Dependent Data Method, and Data Fitting Method. We have added a column representing when there is no compensation (between ‘Target Only’ and ‘Target + Wall’). It should be noted that the accuracy of these figures depends on the size of the window around the main pulse over which the comparison is made. Wood and gypsum showed good compensation particularly in the data fitting method. This is indicated by the 99.32% similarity to the ‘No Wall’ case for wood and 98.70% for gypsum. For glass, we have up to 16% improvement in the results from the frequency dependent data method (96.45%) over constant amplitude and delay’s 80.68%. However, in the data fitting method, compensated waveform for glass suffered considerable distortion. As a fit to insertion transfer function for glass, the line in Figure 3.9(b) does not represent full information about the frequency dependence of its ‘wiggling’ curve in Figure 3.9(a) as compared to the other two methods. This led to the change in the compensated waveform shape in Figure 4.8(b), and hence 76.82% energy capture for



glass. This is not much of an improvement over the no compensation's 71.52%, let alone for the other methods. Overall, the results for energy capture in frequency dependent data method show relatively better similarity between 'Target Only' and 'Compensated' responses.

Generally, the basis of comparison depends on how the receiver is interested in the signal (time, energy, etc). Figure 4.9 shows the three different methods compared for our wood wall. As with the matched filter system, the use of pulse peak-to-peak delay to measure the correlation between the two results might be an easier approach to

TABLE 4.3: Percentage similarity of wall compensation results to 'No Wall' results

Wall	Method			
	No Compensation	Constant Amplitude and Delay	Frequency Dependent Data	Data Fitting
Wood	83.94 %	93.52 %	95.61 %	99.32 %
Glass	71.52 %	80.68 %	96.45 %	76.82 %
Gypsum	94.85 %	96.27 %	98.98 %	98.70 %

take, however; in this case the shape of the waveform is affected during the compensation process. Therefore, finding the correct peak of the signal will not be easy and the peak-to-peak delay will yield an unreliable outcome which cannot represent correlation or similarity. Consequently, wall compensation for double and triple walls suffered severe change in waveform, thus, no reliable results were obtained for them. Figure 4.10 shows an example for the case of double wall: wood-gypsum.

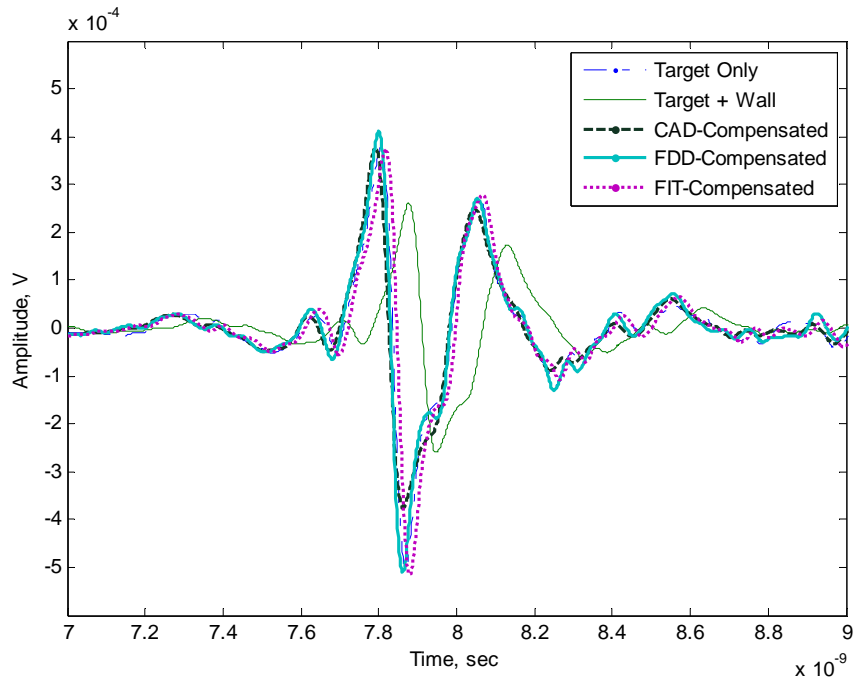
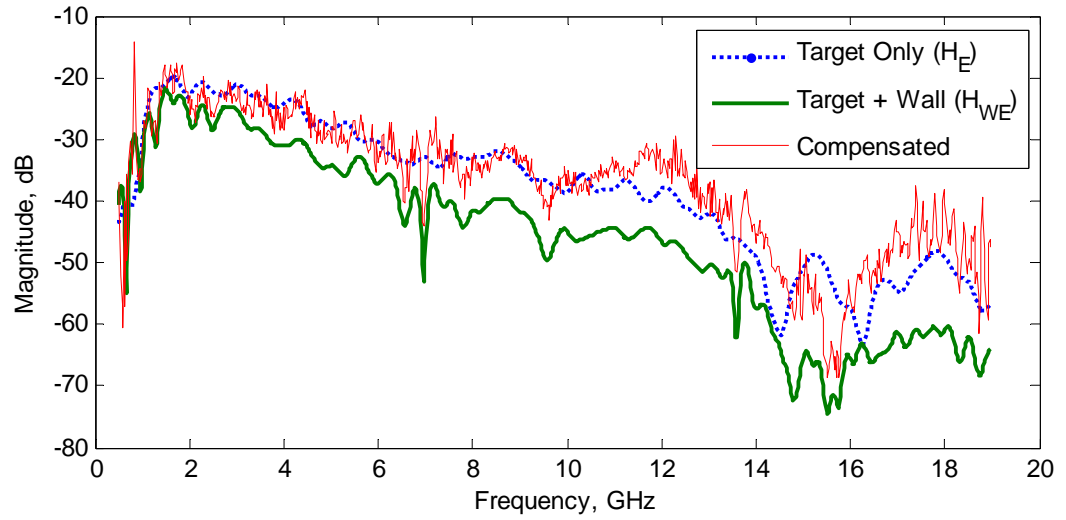
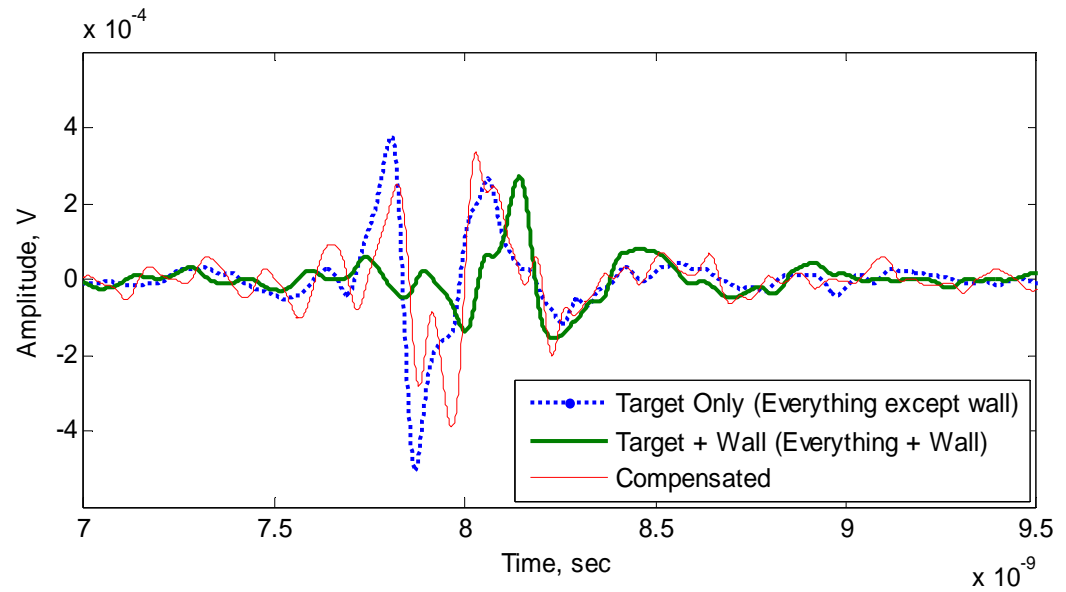


Figure 4.9: Compensation using the three methods for wood wall



(a)



(b)

Figure 4.10: Wall compensation for double wall (wood-gypsum)

#### **4.4 Conclusion**

This chapter proposes a way of compensating for the effect the obstruction has on the true position of a target in through wall detection applications. Three methods for wall compensation were discussed. The first one used estimated constant amplitude loss and delay values suffered by the walls in the previous wall characterization experiments to perform compensation, while the second uses full frequency dependent data from previous knowledge of the wall. The third uses a quadratic and linear fit to previously obtained dielectric constant and magnitude of insertion loss respectively, while assuming a constant delay. Results obtained show a good level of wall compensation for the different walls used. With the first method, up to 93.52% similarity was recorded between compensated and no wall responses for wood. Similarly, 98.70% similarity was obtained with the third method for gypsum wall.

# CHAPTER 5

## 5 CONCLUSIONS AND RECOMMENDATIONS

### 5.1 Summary and Conclusions

In this research, the adverse effect an obstruction has on the detection of an object behind it was investigated and methods were proposed to compensate for it. This was achieved by first performing a wideband electromagnetic characterization of typical building wall materials and assessing their impacts on localization.

An experimental campaign was employed in extracting wall parameters of three different materials namely; wood, glass and gypsum through measuring an insertion transfer function for each material. The insertion transfer function was obtained through frequency-domain measurements using a vector network analyzer. Transmission and Reflection measurements were carried out to measure the loss and the dielectric constant of the selected materials over a frequency range of 1 GHz to 18 GHz. A formulation by [Muq03] using one-dimensional root search for low-loss materials was used in evaluating the dielectric constant. The results for transmission and reflection measurements are in good agreement with each other and with published data. The results can serve as basis for further studies in developing applications for through wall imaging and localization. They can also be useful in link budget analysis and channel modeling.

Multiple walls were also considered and the obtained results indicate that with knowledge about a single wall of certain thickness, we can predict, to an appreciable level of accuracy, information about another wall double or triple its size (ignoring effect of the air-gap between walls).

The work further attempted to demonstrate wall compensation to correct the position estimation of an object located behind the wall. Measurements were carried out with a given target object, and information about the wall obtained from previous measurements for wall characterization was used in de-embedding the effect of the wall from the measurements. Three methods were proposed for achieving wall compensation namely; constant amplitude and delay, frequency dependent data, and data fitting methods. Our results show that we were able to achieve a reasonable measure of compensation for the three wall materials when we compared the ‘Compensated’ and ‘Target Only’ (No Wall) results. We used two measures, correction in delay and energy capture to assess the accuracy of the three methods. Delay uses the peak-to-peak time difference of the ‘Target Only’ and ‘Compensated’ responses to find the error after compensation relative to ‘Target + wall’ (no compensation). With constant amplitude and delay, glass indicated a 0.0025 ns (0.03 cm) error improvement over frequency dependent data method. This is also a 0.04124 ns (0.48 cm) improvement over the data fitting method. The energy capture takes 1 ns around the main pulse of ‘Target Only’ and ‘Compensated’ responses, compares them and give outcome as a percentage of similarity between the two. Data Fit method showed higher percentage similarity for wood with 99.32% over constant amplitude and delay’s 93.52% and frequency dependent data

method's 95.61%. On the other hand, glass, using frequency dependent data method showed significant improvement over the other two methods with 96.45% similarity.

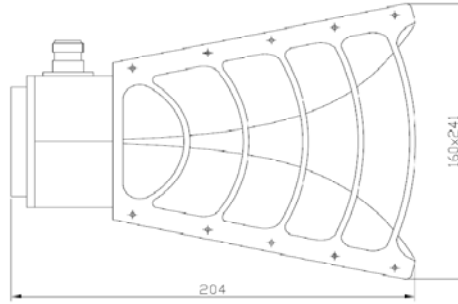
## **5.2 Recommendations for future research**

For further research, we recommend extensions along the following directions:

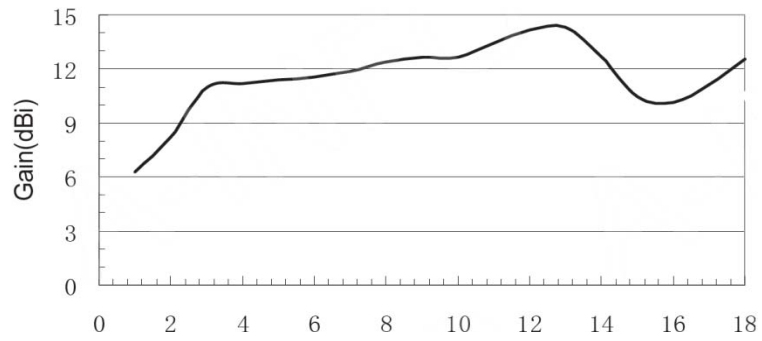
- 1 Characterization should involve more wall types as found in real life like concrete and brick.
- 2 The impact of oblique incidence and different distances between antennas and walls for both transmission and reflection should be considered. Results can be improved by performing experiments in an anechoic chamber.
- 3 Using time-domain measurement setup and comparing the result with frequency domain measurements.
- 4 Demonstrate position correction and image focusing using signals received with antenna arrays rather than single antenna.
- 5 Experiment with practical targets which are small and mobile.
- 6 Use multiple antennas with different characteristics to improve the obtained results.
- 7 Using simulation tools to augment experimental measurements

# A APPENDIX A

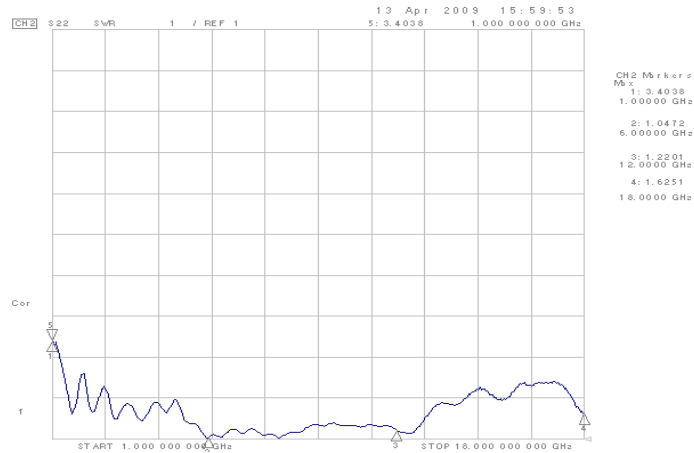
## I. Antenna Test Results



(a) Physical Dimensions



(b) Antenna gain



(c) Antenna VSWR

Figure A.1: Antenna physical dimensions, gain and VSWR



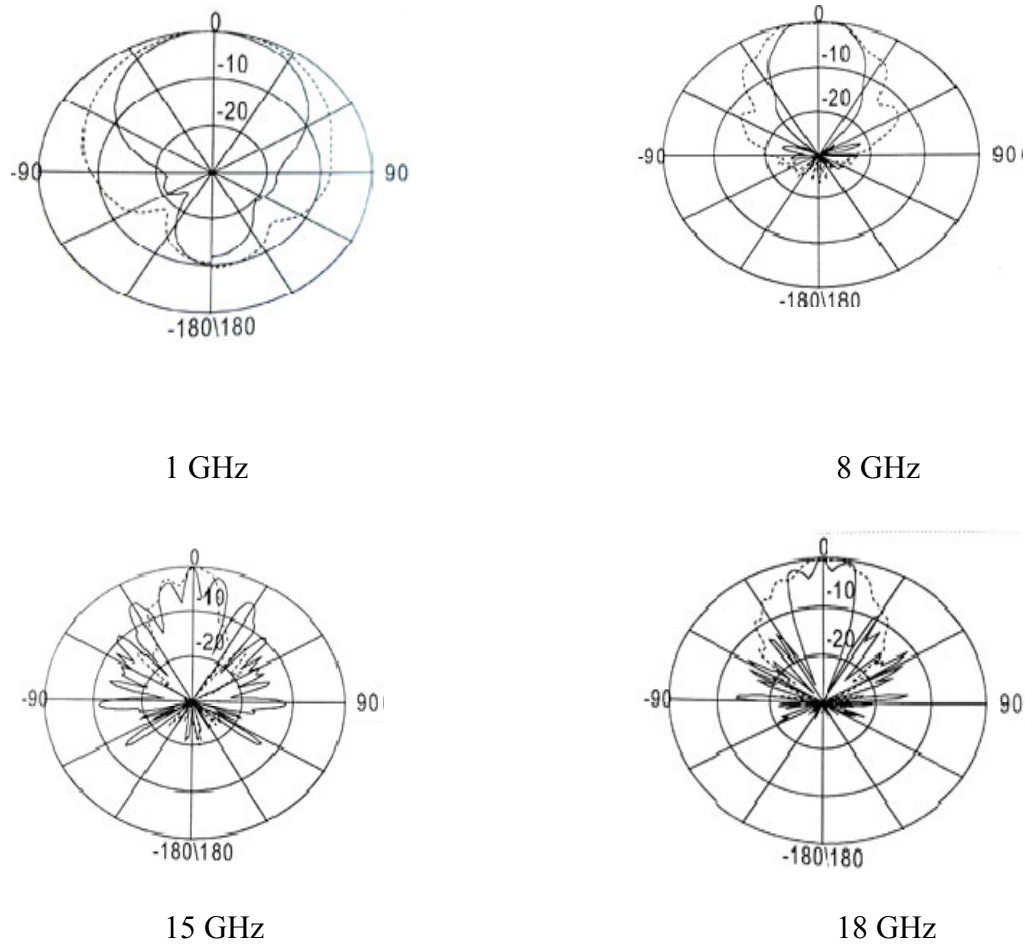


Figure A.2: Antenna pattern at various frequencies

TABLE A.1: Antenna test results

	<b>3 dB Beamwidth (degrees)</b>			
<b>Frequency</b>	1 GHz	8 GHz	15 GHz	18 GHz
<b>E-Plane (dotted line)</b>	90.08	40.25	14.47	30.04
<b>H-Plane (solid line)</b>	63.54	33.27	5.81	17.52

## NOMENCLATURE

### English Symbols

$c$	Speed of light = $3.0 \times 10^8$
$D$	Electric flux density in material
$d$	Wall thickness
$d_f$	Fraunhofer distance or Far field distance
$D_a$	Largest physical linear dimension of antenna
$D_o$	Free space electric flux density
$E$	Electric field
$E_o$	Amplitude of applied Electric field
$E_i$	Incident electric field on wall surface
$E_t$	Through wall transmitted electric field
$E_i^{fs}$	Free space transmitted electric field
$E_r$	Reflected electric field from wall
$f$	Frequency
$H_1$	Single layer transfer function of 1 <sup>st</sup> wood as used in Figure 3.21
$H_2$	Single layer transfer function of glass as used in Figure 3.21

$H_3$	Single layer transfer function of 2 <sup>st</sup> wood as used in Figure 3.21
$H_E$	Transfer function of everything except the wall
$H(j\omega)$	Insertion transfer function
$H_{sp}$	Single-pass insertion transfer function
$H_T$	Total transfer function of three layer wood-glass-wood as used in Figure 3.21
$h(t)$	Impulse response
$H_W$	Transfer function of wall only
$H_{WE}$	Total transfer function of everything including wall and free space
$J$	Electric current density
$k$	Damping coefficient of friction
$m$	Mass of dipole
$N$	Number of electric dipoles
$P$	Molecular Polarization in material structure
$q$	Electric charge of dipole
$R$	Antenna separation
$r$	Pearson's correlation coefficient
$r(t)$	'Target Only' signal (true signal)
$r_c(t)$	'Compensated' signal (estimate of the true signal)

$s$	Used as Tension parameter (spring) in Chapter 2, and in Chapter 4 it denotes Target distance
$S_{21}$	Scattering parameter (forward transmission coefficient-gain)
$T$	Transmission coefficient
$X_i(j\omega)$	Through wall transmitted signal
$X_i^{fs}$	Free space transmitted signal

## Greek Symbols

$\alpha$	Attenuation constant
$\beta$	Phase constant
$\varepsilon$	Permittivity of a material
$\varepsilon_o$	Permittivity of free space (vacuum)
$\varepsilon_r$	Relative permittivity of material
$\varepsilon_r'$	Dielectric constant (real part of relative permittivity)
$\varepsilon_r''$	Imaginary part of relative permittivity
$\varepsilon_\infty$	Optical dielectric constant
$\varepsilon_s$	Static dielectric constant
$\ell$	Displacement of electric dipole
$\Gamma$	Damping factor

$\lambda$	Wavelength
$\sigma$	Conductivity
$\sigma_e$	Effective conductivity
$\sigma_s$	Static conductivity
$\sigma_a$	Alternating current field conductivity
$\Phi_{sp}$	Single-pass phase
$\tan \delta$	Loss tangent
$\tau$	Material relaxation time
$\tau_o$	Propagation delay through wall
$\Delta\tau$	Peak – peak impulse time delay
$\mu$	Permeability
$v_g$	Group velocity
$v_p$	Phase velocity
$\omega$	Angular frequency
$\omega_o$	Material resonance frequency
$\gamma$	Complex propagation constant

## REFERENCES

- [Ada08] G. Adamuik, M. Porebska, E. Pancera, C. Sturm, T. Zwick and W. Wiesbeck, "Influence of the Antennas and Propagation Effects on UWB Localization and Imaging Systems", *Proceedings of the German Microwave Conference, GeMIC*, pp. 310 – 313, December 2008.
- [Aft09] M. Aftanas, "Signal Processing Steps for Objects Imaging Through the Wall with UWB Radar", *9th Scientific Conference of Young Researchers, SCYR 2009*, Faculty of Electrical Engineering and Informatics, Technical University of Kosice, Slovak Republic, May 2009, pp. 14-17.
- [Agi00] Agilent Technologies, "Agilent 8510C Network Analyzer Data Sheet", pp. 4, printed in the USA, 2000.
- [Agi01] Agilent Technologies, "8510C Network Analyzer System, Operating and Programming Manual", Edition 3.0, printed in the USA, May 2001, chapter 8, pp.1.
- [Ahm07] F. Ahmad, M. G. Amin, and G. Mandapati, "Autofocusing of Through-the-Wall Radar Imagery Under Unknown Wall Characteristics", *IEEE Transactions on Image Processing*, Vol. 16, pp. 1785-1795, 2007.

- [Ali03] P. Ali-Rantala, L. Ukkonen, L. Sydanheimo, M. Keskilammi and M. Kivikoski “Different Kinds of Walls and there Effect on the Attenuation of Radiowaves Indoors”, *Proceedings of IEEE Antennas and Propagation society international Symposium* 2003, Vol. 3, pp. 1020 – 1023.
- [Aku04] B. Akuthota, R. Zoughi and K. E. Kurtis, “Determination of Dielectric Property Profile in Cement-Based Materials Using Microwave Reflection and Transmission Properties”, *Instrumentation and Measurement Technology Conference, IMTC*, pp. 327 – 332, 2004, Como, Italy.
- [Ant03] G. Antonini, A. Orlandi, and S. D’elia, “Shielding Effects of Reinforced Concrete Structures to Electromagnetic Fields due to GSM and UTMS Systems”, *IEEE Transactions on Magnetics*, Vol. 39, No. 3, pp. 1582-1585, 2003.
- [Aur96] F. J. Aurand, “Measurement of Transient Electromagnetic Propagation through Concrete and Sand”. Sandia National Laboratories, *Sandia Report SAND96-2254 UC-706*, Livermore, California 94550, Sept. 1996.
- [A-INF] A-INFO Test Report for Low Noise Amplifier LA1018N3209, Chengdu A-INFO Inc., China.
- [Bal89] C. A. Balanis, “Advanced Engineering Electromagnetics”, New York, Wiley, 1989.

- [Bar08] E. J. Baranoski, "Through-wall imaging: Historical perspective and future directions", *Journal of the Franklin Institute*, 345, 2008, pp. 556-569.
- [Bar06] E. J. Baranoski, "VisiBuilding: Sensing through Walls", *IEEE Sensor Array and Multichannel Workshop*, Winston & sons, Washington DC, 2006, pp. 1 – 22.
- [Ber00] H. L. Bertoni, "Radio propagation for modern wireless systems", *Prentice Hall PTR, NJ, USA*, p. 55.
- [Cam60] [http://www.cambridgeconsultants.com/prism\\_200.html](http://www.cambridgeconsultants.com/prism_200.html)
- [Cha08] R. Chandra, A. N. Gaikwad, D. Singh, and M. J. Nigam, "An approach to remove the clutter and detect the target for Ultra-wideband through-wall imaging," *Journal of Geophysics and Engineering*, Vol. 5, pp. 412-419, Oct. 2008.
- [Cui01] I. Cuinas and M. G. Sanchez, "Measuring, Modeling, and Characterizing of Indoor Radio Channel at 5.8 GHz", *IEEE Transactions on Vehicular Technology*, Vol. 50, No. 2, pp. 526 – 535, March 2001.
- [Deh08] M. Dehmollaian, K. Sarabandi, "Analytical, numerical and experimental methods for through-the-wall radar imaging", *IEEE International Conference on Acoustics, Speech and Signal Processing, ICASSP*, March 2008, pp. 5181 – 5184.



- [Dib06] M. Di Benedetto, T. Kaiser, A. F. Molisch, I. Opperman, C. Politano and D. Porcino, “UWB Communication Systems A Comprehensive Overview”, *EURASIP Book Series on Signal Processing and Communications, Vol. 5, Hindawi Publishing corporation*, 2006.
- [Dyn05] Dynawave Inc., “StripFlex Cable SF-142B Data Sheet”, Times Microwave Systems, 2005.
- [FCC02] Federal Communication Commission, “First Order and Report, Revision of Part 15 of the Commission’s Rules Regarding Ultra Wideband Transmission System, FCC 02-48, April 2002.
- [For07] A. Fort, “Body Area Communications: Channel Characterization and Ultra-wideband System-Level Approach for Low Power”, *PhD Dissertation Submitted to the Department ELEC, Vrije Universiteit Brussel, Belgie*, 2007.
- [Gre03] H. G. Schantz, “Introduction to Ultra-wideband Antennas”, *Proceedings of the IEEE UWBST Conference*, November 2003, pp. 1 – 9.
- [Gul05a] A. Gulck, O. Schimmer, F. Daschner, J. K. Piotrowski, and R. H. Knochel, “Noncontacting Determination of Moisture Content in Bulk Materials using Sub-nanosecond UWB pulses”, *IEEE Transactions on Microwave Theory and Techniques*, Vol. 53, pp. 2107-2113, 2005.

- [Gul05b] A. Gulck, T. Lehmann, R. Knochel, “Characterisation of Dielectric Obstacles Using Ultr-Wideband Techniques”, *Proceedings of the European Microwave Conference*, Vol. 3, pp. 259 – 262, October 2005.
- [Guo08] G. Cui, L. Kong, J. Yang, X. Wang, “A New Wall Compensation Algorithm for Through-the-wall Radar Imaging”, *1<sup>st</sup> Asian and Pacific Conference on Synthetic Aperture Radar, APSAR*, November 2007, pp. 393 – 396.
- [Han09] M. J. Hannon, P. Malloy, “Application Guide to RF Coaxial Connectors and Cables”, *AR/RF Microwave Instrumentation Application Note #51*, April 2009.
- [Har08] B. J. Harker, A. D. Chadwick, G. L. Harris, “Ultra-Wideband 3-D Imaging (UWB 3-D Imaging)”, 2008 Roke Manor Research Limited, UK
- [Has93] H. Hashemi, “The Indoor Propagation Channel”, *Proceedings of the IEEE*, Vol. 81, No. 7, pp. 943 – 968, July 1993.
- [Hay06] W. A. Hayt, Jr., J. A. Buck, “Engineering Electromagnetics, 7<sup>th</sup> Edition”, McGraw-Hill series in electrical engineering, 2006.
- [Hie08] M. Hiebel, “Vector Network Analyzer (VNA) Calibration: The Basics”, Rohde and Schwarz Vector Network Analysis Solutions, USA, 2008, pp. 3.

- [Hua96] H. Yi and D. Parsons, "A time domain approach for measuring the dielectric properties and thickness of walls of a building", *IEE Colloquium on Propagation aspects of Future Mobile Systems* (Digest No. 1996/220), pp. 7/1 – 7/7, 1996.
- [Jat05] P. Jaturatussanai, M. Chamchoy and S. Promwong, "Characteristics of UWB Propagation Through Building Materials", *Proceedings of the International Symposium on Communications and Information Technology*, Vol. 1, pp. 987 – 990, Beijing, October 2005.
- [Kra93] D. Kralj, L. Carin, "Ultra-wideband Characterization of Lossy Materials: Short-pulse Microwave Measurements", *IEEE MTT-S International Microwave Symposium Digest*, Vol. 3, June 1993, pp. 1239 – 1242.
- [Lai05] C. P. Lai, R. M. Narayanan, "Through-wall imaging and characterization of human activity using ultrawideband (UWB) random noise radar", *Sensors, and Command, Control, Communications, and Intelligence (C3I) Technologies for Homeland Security and Homeland Defense IV*, Vol. 5778, No. 1, pp. 186-195, 2005.
- [Lee04] J. Lee and S. Choi, "Through-Material Propagation Characteristic and Time resolution of UWB signal", *International Workshop on Ultra Wideband Systems Joint with Conference on Ultra Wideband Systems and Technologies (Joint UWBST & IWUWBS)* 2004, pp. 71-75.

- [Lem02] J. J. Lemmon, R. A. Dalke, “Analysis of the RF Threat to Telecommunications Switching Stations and Cellular Base Stations”, *National Telecommunications and Information Administration Report*, NTIA Report 02-391.
- [Liu07] C. Liu, C. Huang and C. Chiu, “Channel Capacity for Various Materials of Partitions in Indoor Ultra Wideband Communication System with Multiple Input Multiple Output”, *3<sup>rd</sup> IEEE UZ Regional chapter International Conference in Central Asia on Internet*, Taskent, Uzbekistan, September 2007, pp. 1 – 5.
- [Mah05] M. Mahfouz, A. Fathy, Y. Yungiang, E. E. Ali, and A. Badawi, “See-Through-Wall Imaging using Ultra Wideband Pulse Systems”, in *Proceedings of the 34<sup>th</sup> Applied Imagery and Pattern Recognition Workshop*, AIPR, October 2005
- [Muq03a] A. H. Muqaibel and Safaai-Jazi, “A New Formulation for Characterization of Materials Based on Measure Insertion Transfer Function”, *IEEE Transactions on Microwave Theory and Techniques*, Vol. 51, No. 8, pp. 1946 – 1951, August 2003.
- [Muq03b] A. H. Muqaibel, “Characterization of Ultra Wideband Communication Channels”, *Ph.D Dissertation Submitted to the Faculty of Bradley*

*Department of Electrical and Computer Engineering Virginia Polytechnic Institute and State University, March 2003.*

- [Muq05] A. H. Muqaibel, A. Safaai-Jazi, A. Bayram, A. M. Attiya and S. M. Riad, “Ultrawideband through-the-wall propagation”, *IEE Proceedings on Microwave Antennas Propagation*, Vol. 152, No.6, pp. 581 – 588, December 2005.
- [Muq08] A. H. Muqaibel and Safaai-Jazi, “Characterization of wall dispersive and attenuative effects on UWB radar signals”, *Journal of the Franklin Institute*, Vol. 345, Iss. 6, pp. 640 – 658, September 2008.
- [Nem06] Z. Nemeč, J. Mrkvica, V. Schejbal, D. Cermak, P. Bezousek, J. Jerabek and R. Sikl, “UWB Through-wall Propagation Measurements”, *Proceedings of the European Conference on Antennas and Propagation, EuCAP*, Nice, France, 2006, pp. 1 – 6.
- [Noo08] N. Noori, A. Abolghasemi and M. Fardis, “Modeling of Ultra Wideband Transmission through Building walls”, *Proceedings of International Conference on Microwave and Millimeter wave Technology, ICMMT*, Vol. 2, pp. 982 – 985, April 2008.
- [Oka09] H. Okamoto, K. Kitao, and S. Ichitsubo, “Outdoor-to-Indoor Propagation Loss Prediction in 800 MHz to 8 GHz Band for Urban Area”, *IEEE*

*Transactions on Vehicular Technology*, Vol. 58, No. 3, March 2009, pp. 1059 – 1067.

- [Ous05] H. H. Ouslimani, R. Abdeddaim, and A. Priou, “Free-Space Electromagnetic Characterization of Materials for Microwave and Radar Applications”, *Progress In Electromagnetics Research Symposium 2005*, Hangzhou, China, pp. 128 – 132.
- [Pac97] Hewlett Packard, “Exploring the Architectures of Network Analyzers” *Application Note 1287-2*, printed in the USA, 1997.
- [Pen03] D. Pena, R. Feick, H. D. Hristov, and W. Grote, “Measurement and Modelling of Propagation Losses in Brick and Concrete Walls for the 900-MHz Band”, *IEEE Transactions on Antennas and Propagation*, Vol. 51, No. 1, pp. 31 – 39, January 2003.
- [Rov09] J. Rovnakova, D. Kucor, “Compensation of Wall Effect for Through-wall Tracking of Moving Targets”, *Radioengineering*, Vol. 18, No. 2, June 2009, pp. 189 – 195.
- [Sac08] J. Sachs, M. Aftanas, S. Crabbe, M. Drutarovsky, R. Klukas, D. Kocur, T. T. Nguyen, p. Peyerl, J. Rovnakova, E. Zaikov, “Detection and Tracking of Moving or Trapped People Hidden by Obstacles Ultra-wideband Pseudo-Noise Radar” *European Radar Conference, EuRAD*, Amsterdam, The Netherlands, 2008.

- [Sag04] F. Sagnard, T. Quiniou, G. El Zein, “Wide-Band Characterization of Building Materials for Propagation Modeling: Analysis of Dispersion Phenomena”, *Proceedings of the IEEE 50<sup>th</sup> Vehicular Technology Conference* 2004, Milan, Italy, pp. 239 – 243.
- [Sag05] F. Sagnard and G. El Zein, “*In Situ* Characterization of Building Materials for Propagation Modeling: Frequency and Time Responses”, *IEEE Transactions on Antennas and Propagation*, Vol. 53, No. 10, pp. 3166 – 3173, October 2005.
- [Sch06] V. Schejbal, P. Bezousek, D. Cermak, Z. Nemecek, O. Fiser and M. Hajek, “UWB Propagation Through walls”, *The Radioengineering Journal*, Vol. 15, No. 1, pp. 17 – 24, April 2006.
- [Shi08] G. Shingu, K. Takizawa, and T. Ikegami, Human body detection using MIMO-UWB radar sensor in an indoor environment, in *Proceedings of the Ninth International Conference on Parallel and Distributed Computing, Applications and Technologies*, December 2008, pp. 437–442.
- [Sin07] S. Singh and J. J. Lee, “Using UWB Radio as Sensors in Disaster Recovery”, *IEEE International Conference on Ultra-wideband, ICUWB*, September 2007, pp. 311 – 315.
- [Tes07a] G. Tesserault, N. Malhouroux, P. Pajusco, “Multi-Frequencies Characterization of Buildings Materials: Angular and Polarization

Analysis”, *The Second European Conference on Antennas and Propagation, EuCAP*, November 2007, pp. 1-5.

- [Tes07b] G. Tesserault, N. Malhouroux, and P. Pajusco, “Determination of Material Characteristics for Optimizing WLAN Radio”, *Proceedings of the 10<sup>th</sup> European Conference on Wireless Technology*, pp. 225 – 228, October 2007, Munich, Germany.
- [TIA96] Federal Standard 1037C, “Glossary of Telecommunication Terms”, August 1996.
- [Vae88] W. T. E. Vaessen, J. Dyk, A. van der Vorst, “RF Shielding due to Building Structures Like Brick Walls, Wire Grid and Metal Coated Windows”, *Proceedings of the 18<sup>th</sup> European Microwave Conference*, Stockholm, 1988, pp. 625 – 631.
- [Vil08] I. Vilovic, R. Nad, Z. Sipus, and N. Burum, “A non-destructive approach for extracting the complex dielectric constant of the walls in building”, *50<sup>th</sup> International Symposium ELMAR 2008*, pp. 608 – 612, Zadar, Croatia.
- [Wan06] G. Wang, M. G. Amin, and Y. Zhang, “New approach for target location in the presence of wall ambiguities”, *IEEE Transactions on Aerospace and Electronic Systems*, Vol. 42, pp. 301-315, 2006.



- [Wen08] Z. Wenji, L. Lianlin, and L. Fang, “Autofocusing imaging through the unknown building walls”, *The Microwave Conference, AMPC*, pp. 1- 5, 2008, Asia Pacific, 2008.
- [Wil02] R. Wilson, “Propagation through Common Building Materials 2.4 GHz vs 5 GHz”, a Report prepared for James A. Crawford, CTO Magis Networks, Inc., San Diego, CA, August 2002.
- [Win97] M. Z. Win and R. A. Scholtz, “Energy capture vs correlator resources in ultra-wide bandwidth indoor wireless communications channels”, *MILCOM '97 Proceedings, vol. 3*, November 1997, pp 1277 – 1281.
- [Yan08] Y. Yang, Y. Wang and A. E Fathy, “Design of Compact Vivaldi Antenna Arrays for See-through wall Applications”, *Progress in Electromagnetic Research, PIER Vol. 82*, 2008, pp. 401 - 418.
- [Yaz04] K. Y. Yazdandoost and R. Kohno, “Complex Permittivity Determination of Material for Indoor Propagation in Ultra-Wideband Communication Frequency”, *International Symposium on Communications and Information Technologies, ISCIT*, pp. 1224 – 1227, 2004, Sapporo, Japan, October.
- [Yoo99] K.Y. Yoon, M. Tateiba, K. Uchida, “Analysis of Electromagnetic Wave Scattering from Building Walls with Periodic and random Surface”,

*International Symposium on Electromagnetic Compatibility*, Tokyo, May  
1999, pp. 284 – 287.

## VITA

### NURUDDEEN MOHAMMED IYA

Electrical Engineering Department, King Fahd University of Petroleum & Minerals, P. O. Box 8608, Dhahran, KSA • Email [nuruddeeniya@yahoo.com](mailto:nuruddeeniya@yahoo.com) • Telephone +966552973617

---

NATIONALITY  
Nigeria

PERMANENT ADDRESS  
Babankiwo lane, Farawa opp Legislator's Qtrs, Maiduguri road, Kano, Nigeria.

#### EDUCATION

- **M.Sc Telecommunications Engineering**, October 2008 – December 2010  
King Fahd University of Petroleum and Minerals, Dhahran, Saudi Arabia
- **B.Eng Electrical/Electronics Engineering**, January 2000 – September 2005  
Abubakar Tafawa Balewa University, Bauchi, Nigeria

#### WORK EXPERIENCE

- **Research Assistant**, October 2008 - Present  
King Fahd University of Petroleum and Minerals, Dhahran, Saudi Arabia
- **Tutor**, August 2007 – September 2008  
University of Maiduguri, Borno, Nigeria
- **Field Support Engineer**, March 2006 – August 2007  
Microaccess Limited, Abuja, Nigeria
- **Student Intern (Repair)**, February – July 2004  
Intercellular Nigeria Plc Maiduguri, Borno, Nigeria

#### SKILLS

- Cisco Certified Network Associate (2007)
- Computer and internet ability. Strong working knowledge of data transmission networks. MSOffice Suite, MATLAB.

#### PROFESSIONAL MEMBERSHIP/AFFILIATION

- Graduate Member Nigerian Society of Engineers

#### ACTIVITIES & INTERESTS

- Participant and Team Leader in a BCG vaccination exercise conducted in rural areas of Kano state, Nigeria
- Electoral committee member of Association of Electrical/Electronic Engineering Students 2001 - 2005
- President of Press Club and Literary and Debating Society 1998 - 1999
- Loves traveling to places which developed in me the ability to adapt to changing environments and be aware of diversity in culture
- Cycling, reading, and keeping abreast of emerging trends in technology

#### HONORS/AWARDS

- Mobil Producing Nigeria Unlimited Scholarship Award for Undergraduate Study
- Federal Government of Nigeria Merit Scholarship Award for Undergraduate Study
- Head Prefect, Federal Government College Sokoto 1999

#### PUBLICATIONS

- A. H. Muqaibel, M. Al-Sunaidi, **N. M. Iya** and A. Safaai-Jazi, "Chapter 1: *Wall Attenuation and Dispersion*", Book title: "*Through Wall Radar Imaging*". Publication Date, Dec 13 2010.